Intravenous anaesthetics inhibit nicotinic receptor-induced currents and Ca^{2+} transients in rat intracardiac neurons

Martin Weber

2003

Dissertation

submitted to the

Combined Faculties for the Natural Sciences and for Mathematics

of the Ruperto-Carola University of Heidelberg, Germany

for the degree of

Doctor of Natural Sciences

presented by

Diplom-Psychologe Martin Weber

born in: Schwäbisch-Hall

Oral examination:

Intravenous anaesthetics inhibit
nicotinic receptor-induced currents and Ca^{2+} transients
in rat intracardiac neurons

Referees: Prof. Dr. Rainer H.A. Fink
Prof. Dr. Michael Wink

SUMMARY

The effects of intravenous (i.v.) anaesthetics on nicotinic acetylcholine receptor (nAChR)-mediated transients in intracellular free Ca^{2+} concentration ($[Ca^{2+}]_i$) and currents were investigated in neonatal rat intracardiac neurons using fura-2 photometry and patch-clamp recordings. Extensive preliminary tests using fura-2 containing solutions in the presence or absence of the anaesthetics were carried out to detect any interference of these drugs with the fura-2 fluorescence signal: Using photospectrometry and a ratiometric photometry set-up to carry out a series of calibrations of the fura-2 signal revealed that ratiometric fura-2 recordings can faithfully be carried out in the presence of clinically relevant concentrations (clinical EC_{50}) of the i.v. anaesthetics studied. In fura-2 loaded neurons, nAChR activation evoked a transient increase in $[Ca^{2+}]_i$, which was reversibly inhibited by the clinical EC_{50} of the i.v. anaesthetic thiopental. The EC_{50} for thiopental inhibition of nAChR induced $[Ca^{2+}]_i$ transients was 28 μM, close to the estimated clinical EC_{50} of thiopental (25 μM). However, control experiments using Ca^{2+} -channel blockers showed that voltage-gated Ca^{2+} -channels (Ca_v) are activated by the depolarization following nAChR activation and thus indirectly contribute to increases in $[Ca^{2+}]_i$. When fura-2 loaded neurons were voltage-clamped at –60 mV to eliminate any contribution of voltage-gated Ca^{2+} channels, then thiopental simultaneously inhibited nAChR-induced increases in $[Ca^{2+}]_i$ and peak current amplitudes. Thiopental inhibited nAChR-induced peak current amplitudes in dialyzed whole cell recordings by ~ 40 % at –120, –80 and –40 mV holding potential suggesting that the inhibition is voltage independent. Thiopental did not inhibit caffeine-induced $[Ca^{2+}]_i$ transients, indicating that an inhibition of Ca^{2+} release from internal stores via ryanodine receptor (RyR) channels is unlikely. The barbiturate pentobarbital and the dissociative anaesthetic ketamine used at clinical EC_{50} concentrations were also shown to inhibit nAChR-induced increases in $[Ca^{2+}]_i$. In conclusion, thiopental and other i.v. anaesthetics may inhibit nAChR-induced currents and $[Ca^{2+}]_i$ transients in intracardiac neurons by binding to nAChR and thereby may contribute to changes in heart rate and cardiac output under clinical conditions.

Keywords: fura-2, intracardiac neurons, intracellular Ca^{2+}, intravenous anaesthetics, ketamine, nicotinic acetylcholine receptor, pentobarbital, ryanodine receptor, thiopental.

ZUSAMMENFASSUNG

In dieser Arbeit wurde die Wirkung intravenöser (i.v.) Anästhetika auf intrazelluläre Kalziumsignale und Membranströme, die durch die Aktivierung von nikotinergen Acetylcholin-Rezeptoren (nAChR) entstehen, an neonatalen Herzganglienneuronen untersucht. Als Untersuchungsmethoden wurden photometrische Messungen mit dem Kalziumindikator Fura-2, sowie Patch-Clamp Messungen, teils auch in Kombination, eingesetzt. In Voruntersuchungen mit Fura-2 -haltigen Lösungen wurde überprüft, ob i.v. Anästhetika mit dem Farbstoff Fura-2 selbst interagieren. Mittels Spektrophotometrie sowie einer Serie von Kalibrierungen des Fura-2 Signals am Fluoreszenzmikroskop konnte gezeigt werden, dass Fura-2 Messungen in der Anwesenheit klinisch relevanter effektiver Konzentrationen (klinische EK_{50}) der untersuchten Anästhetika zuverlässig durchgeführt werden können. In Fura-2 beladenen Neuronen führte die Aktivierung von nAChR zu einem vorübergehenden Anstieg der intrazellulären freien Kalziumkonzentration ($[Ca^{2+}]_i$), welcher durch die klinische EK_{50} von Thiopental reversibel gehemmt werden konnte. Die Erstellung der Dosis-Wirkungs-Beziehung von Thiopental auf die Hemmung nikotinerg induzierter $[Ca^{2+}]_i$ –Transienten ergab eine EK_{50} von 28 μM, die damit sehr nahe an der klinischen EK_{50} für Thiopental (25 μM) liegt. Weitere Kontrollexperimente unter Verwendung von Kalziumkanal-Blockern zeigten jedoch, dass spannungsgesteuerte Kalziumkanäle durch die Depolarisation, die durch die Aktivierung der nAChR entsteht, aktiviert werden und somit indirekt zu nikotinerg induzierten Anstiegen der $[Ca^{2+}]_i$ mit beitragen. Um diesen Beitrag der spannungsgesteuerten Ca^{2+} -Kanäle zu eliminieren wurden im Rahmen simultaner Fura-2 sowie Patch-Clamp Messungen Neurone mit einem Haltepotential von –60 mV „geklemmt“. Es ergab sich eine simultane, Thiopental-induzierte Hemmung der Amplituden von nikotinerg induzierten $[Ca^{2+}]_i$ –Transienten und Einwertsströmen. In („dialyzed“) Patch-Clamp Messungen wurden die Amplituden nikotinerg induzierter Einwertsströme bei –120, –80 und –40 mV Haltepotential jeweils um ca. 40 % erniedrigt, was auf eine spannungsunabhängige Hemmung hinweist. Thiopental hatte keine hemmende Wirkung auf Koffein-induzierte $[Ca^{2+}]_i$ -Anstiege, was eine Hemmung von Ryanodin-Rezeptoren (RyR) durch Thiopental unwahrscheinlich erscheinen lässt. Die klinische EK_{50} des Barbiturats Pentobarbital sowie des dissoziativen Anästhetikums Ketamin hatten ebenfalls hemmende Wirkung auf nikotinerg induzierte $[Ca^{2+}]_i$ –Transienten. Dies lässt darauf schließen, dass es durch

die Wirkung von Thiopental und anderer i.v. Anästhetika am nAChR zu einer Hemmung nikotinerg induzierter Ströme sowie intrazellulärer Kalziumsignale in Herzganglienneuronen kommen kann, was wiederum zu Veränderungen der Herzfrequenz sowie des Herzminutenvolumens, die bei der Verwendung dieser Medikamente im Rahmen der Anästhesie zu beobachten sind, mit beitragen kann.

Stichwörter: Fura-2, Herzganglienneurone, intravenöse Anästhetika, intrazelluläres Ca^{2+}, Ketamin, nikotinerger Acetylcholin-Rezeptor, Pentobarbital, Ryanodin-Rezeptor, Thiopental.

TABLE OF CONTENTS

LIST OF ABBREVIATIONS

A	=	Ampere
ACh	=	acetylcholine
ω-agatx IVA	=	ω-agatoxin IVA
ANS	=	autonomic nervous system
ATP	=	adenosine triphosphate
AV	=	atrioventricular
BAPTA	=	1,2-bis(2-aminophenoxy)ethane-*N*,*N*,*N'*,*N'*-tetraacetic acid
BPM	=	beats per minute
C	=	Coulomb(s)
$[Ca]_I$	=	free Ca^{2+} concentration (inside of the cell)
cAMP	=	cyclic adenosine monophosphate
$[Ca]_o$	=	free Ca^{2+} concentration (outside of the cell)
Ca_v	=	voltage-operated Ca^{2+} channel(s)
CBF	=	central blood flow
CICR	=	calcium-induced calcium-release
clinical EC_{50}	=	clinically relevant (half-maximal) effective concentration
C_m	=	cell membrane capacitance
CMR_{O2}	=	cerebral metabolic rate for oxygen
CNG	=	cyclic nucleotide gated channel(s)
CNS	=	central nervous system
CO	=	cardiac output
ω-ctx GVIA	=	ω-conotoxin GVIA
Da	=	Dalton
DAG	=	diacylglycerol
DHP	=	dihydropyridine(s)
DHPR	=	dihydropyridine receptor(s)
DS	=	dissection solution
ECG	=	electrocardiography
E_{ion}	=	equilibrium potential (for a particular type of ion)
ER	=	endoplasmic reticulum
F	=	Faraday's constant
FW	=	molecular weight

G	=	G –protein
h	=	hour(s)
HR	=	heart rate
HVA	=	high-voltage activated (calcium channel(s))
ICP	=	intracranial pressure
I_{CRAC}	=	calcium-release-activated current
IMM	=	inner mitochondrial membrane
Ins(1,4,5)P_3(R)	=	inositol-1,4,5-trisphosphate (receptor(s))
$[ion]_i$	=	free ion concentration (inside of the cell)
$[ion]_o$	=	free ion concentration (outside of the cell)
IP_3(R)	=	inositol-1,4,5-trisphosphate (receptor(s))
IR	=	immunoreactivity
i.v.	=	intravenous
I-V	=	current-voltage (relation)
I-V converter	=	current-to-voltage converter
K	=	Kelvin
ket	=	ketamine
kg	=	kilogram(s)
klinische EK_{50}	=	see clinical EC_{50}
l	=	litre(s)
LGIC	=	ligand-gated ion channel(s)
LWA	=	low-voltage activated (calcium channel(s))
M2	=	2nd transmembrane segment
mAChR	=	muscarinic acetylcholine receptor(s)
MAP	=	mean arterial pressure
MCU	=	mitochondrial Ca^{2+} uniporter
min	=	minute(s)
ml	=	millilitre(s)
MR	=	metabotropic receptor(s)
MYA	=	million years
NAADP	=	nicotinic acid adenine dinucleotide phosphate
nAChR	=	nicotinic acetylcholine receptor(s)
NCX	=	Na^+/Ca^{2+} exchanger(s)
NMDAR	=	N-methyl-D-aspartate receptor(s)

NPY	=	neuropeptide Y
OMM	=	outer mitochondrial membrane
OPA	=	operational amplifier
P2XR	=	inotropic purinoceptor(s)
P2YR	=	metabotropic purinoceptor(s)
PCR	=	polymerase chain reaction
Phe	=	phenylalanine
PIP_2	=	phosphatidylinositol-4,5-biphosphate
PLC	=	phospholipase C
PMCA	=	plasma membrane Ca^{2+} -ATPase
PSS	=	physiological salt solution
P_X	=	channel permeability (of an ion X)
R	=	gas constant
RespR	=	respiratory rate
ROC	=	receptor-operated (ion) channel(s)
RyR	=	ryanodine receptor(s)
S	=	Siemens
SA	=	sinuatrial
SD	=	standard deviation
SEM	=	standard error of mean
SERCA	=	sarco(endo)plasmatic reticulum Ca^{2+} -ATPase(s)
SIF (cells)	=	small, intensely fluorescent (cells)
SMOC	=	second messenger-operated channel(s)
SR	=	sarcoplasmic reticulum
STOC	=	store-operated channel(s)
SV	=	stroke volume
T	=	absolute temperature
TH	=	tyrosine hydroxylase
thio	=	thiopental
TRP	=	transient receptor potential channel(s)
TTX	=	tetrodotoxin
V	=	Volt(s)
Val	=	valine
VDAC	=	voltage-dependent anion channel(s)

V_E	=	minute ventilation
VIP	=	vasoactive intestinal polypeptide
VR	=	vanilloid receptor channel(s)
z_{ion}	=	charge (of a particular type of ion)

TABLE OF FIGURES

1 INTRODUCTION

The present study has examined the *effects of clinically relevant concentrations of intravenous (i.v.) anaesthetics* on *membrane currents* and *intracellular calcium signals* in *rat intracardiac neurons* following *nicotinic acetylcholine receptor* (nAChR) *activation.*

Clinically, *i.v. anaesthetics* are well known to *affect cardiac parameters* such as heart rate and cardiac output, and have been shown to alter cardiovascular functions in animal studies. On a *molecular level*, clinically relevant concentrations of i.v. anaesthetics are assumed to *target* a superfamily of ligand-gated-ion channels (LGIC) that includes the *nAChR channels.*

As intracardiac neurons are known to *contribute to the regulation of heart rate* and cardiac output, and *neurotransmission* to these neurons is *predominantly nicotinic*, it was hypothesized that *i.v. anaesthetics may contribute to the changes in cardiac parameters* observed under clinical conditions *by inhibiting nAChR channels* in intracardiac neurons.

This is a new aspect of heart rate regulation under i.v. anaesthesia, as *most studies* published to date dealing with the effects of i.v. anaesthetics on ion channels have only been carried out in *expression systems.* Yet, to relate studies of anaesthetic effects on ion channels in expression systems to physiological function, it is crucial to carry out studies in functionally relevant native cells. Thus, the present thesis is one of the first studies that examine the effects of clinically relevant anaesthetic concentrations on *native neuronal receptors in an anatomically relevant tissue.*

Furthermore, most studies to date have focused on electrophysiological effects of clinically relevant concentrations of anaesthetics. In contrast, *anaesthetic effects on* neuronal second-messenger systems such as *the Ca^{2+} signalling system* have hardly been examined - despite the well-known role of Ca^{2+} ions for various cellular functions, including excitability, neurotransmitter release, and gene transcription.

The present study is based on our previous study (Beker et al., 2003), which has shown that *nAChR activation* in these neurons involves the generation of *inward currents* concurrent with *intracellular Ca^{2+} transients.* Furthermore, we have shown that nAChR activation is followed by Ca^{2+} release from intracellular stores through *ryanodine receptor (RyR) channels.* As nAChR activation is likely to depolarize the cell, it can be reasoned that *voltage-gated Ca^{2+} channels* (Ca_v) are activated and may also contribute to the observed Ca^{2+} signals. Taken together, these data suggest that *nAChR activation* may play an *important role for intracellular Ca^{2+} signalling* in rat intracardiac neurons.

Based on these results, it was decided to study the effects of i.v. anaesthetics on membrane currents as well as intracellular Ca^{2+} transients following nAChR activation in rat intracardiac neurons.

1.1 Autonomic control of the heart

The *autonomic nervous system (ANS)* is a *neuronal control system* that helps to maintain the inner *homeostasis* of the body. Regarding the *cardiovascular system*, it contributes to the adjustment of the blood circulation to various internal as well as external stimuli such as the need to fight or flight, physical work, food digestion etc. This is achieved by regulating the *resistance of the vessels to blood flow* and the *cardiac output* (CO). The CO is the blood volume that the heart pumps in a minute, which is the *stroke volume* (SV) multiplied by the *heart rate* (HR).

1.1.1 Innervation of cardiac pacemaker centres

As intracardiac neurons contribute to the autonomic innervation of the heart, this chapter begins with a brief *overview of the cardiac pacemaker system* and subsequently describes the *traditional concept of the autonomic innervation of the heart*. Chapter 1.1.2 then focuses on *intracardiac neurons* and describes recent findings that challenge these traditional concepts.

Neuronal control of CO is obtained through both branches of the ANS by innervation of specific *target regions* within the heart, namely the *myocardium* and the *pacemaker-* and *conductile-system*, which is illustrated in figure 1B. The latter can be subdivided into three *pacemaker centres* that are able to *generate spontaneous* and *rhythmic action potentials*:

The *sinuatrial* (SA) *node* is the *primary pacemaker* of the heart. It is located in the right atria close to the entry point of the vena cava superior. The spontaneously arising action potentials in its pacemaker cells initiate a frequency of 60 to 80 beats per minute (BPM) in resting human adults. The generated activity spreads through the myocardial cells of the atria to the *atrioventricular (AV) node* as the *secondary pacemaker* of the heart. It is located in the posterior part of the right atria at the interatrial and interventricular septum and represents the only excitable spot between the atria and the ventricle. From the AV bundle, activation spreads through a specialized conduction system that forms the *tertiary pacemaker system*, which includes the *bundle of His,* the *bundle branches* and the

Purkinje fibres. The latter innervate the working myocardium of the ventricles (see: Berne & Levy, 1998; Thews & Vaupel, 1997; Vander et al., 1987).

Increased sympathetic activity yields to *cardioaugmentation* by *positive chronotropic, dromotropic* and *inotropic effects*, i.e. increases in heart rate, conduction velocity of innervation within the heart, and myocardial contractile force, respectively. Increased parasympathetic activity yields to *cardiodepression* by the opposing negative chronotropic, dromotropic and inotropic effects: *Chronotropic effects* are mainly obtained by modulation of the SA node. The SA node is targeted by a greater number of parasympathetic than sympathetic nerve endings, and *parasympathetic tone* also appears to outrank sympathetic tone *on heart rate:* This became apparent in experiments where *both branches of the autonomic system* were *blocked* and heart rate was found to rise from the resting heart rate of typically ~ 70 BPM up to ~ 100 BPM in humans. *Dromotropic effects* are mainly obtained by modulation of the AV node. *Inotropic effects* are obtained by modulating the myocardial contractile force (Berne & Levy, 1998; Thews & Vaupel, 1997).

The two branches of the ANS also differ in the more upstream segments of their innervation pathways: *Sympathetic preganglionic neurons* involved in the regulation of the heart are located in the intermediolateral columns of the lower cervical and upper thoraic segments of the spinal cord. Their relatively short axons synapse with *sympathetic postganglionic neurons* located in nearby paravertebral ganglia of the sympathetic chain and the longer axons of the latter project to the heart. *Neurotransmission between pre- and postganglionic neurons is primarily nicotinic*, while *neurotransmission between postganglionic neurons* and the target tissue is mainly *noradrenergic*.

Parasympathetic preganglionic "cardiac" neurons are located in the nucleus ambiguous and the dorsal motor nucleus of the vagus in the medulla oblongata. Their relatively long preganglionic axons join the *vagus nerve* and synapse with *postganglionic parasympathetic neurons*, i.e. *intracardiac neurons* that are located in parasympathetic ganglia in the heart. The relatively short axons of intracardiac neurons connect with the cardiac target tissues. *Neurotransmission between pre- and postganglionic neurons* is also primarily *nicotinic*. Neurotransmission between postganglionic neurons and the target tissues is mainly mediated by type two muscarinic AChR (mAChR; summarized in: Antoni, 1996; Iversen et al., 2000; Powley, 1999; Sved, 1999, Vander et al., 1987).

Figure 1 illustrates the parasympathetic innervation of the heart.

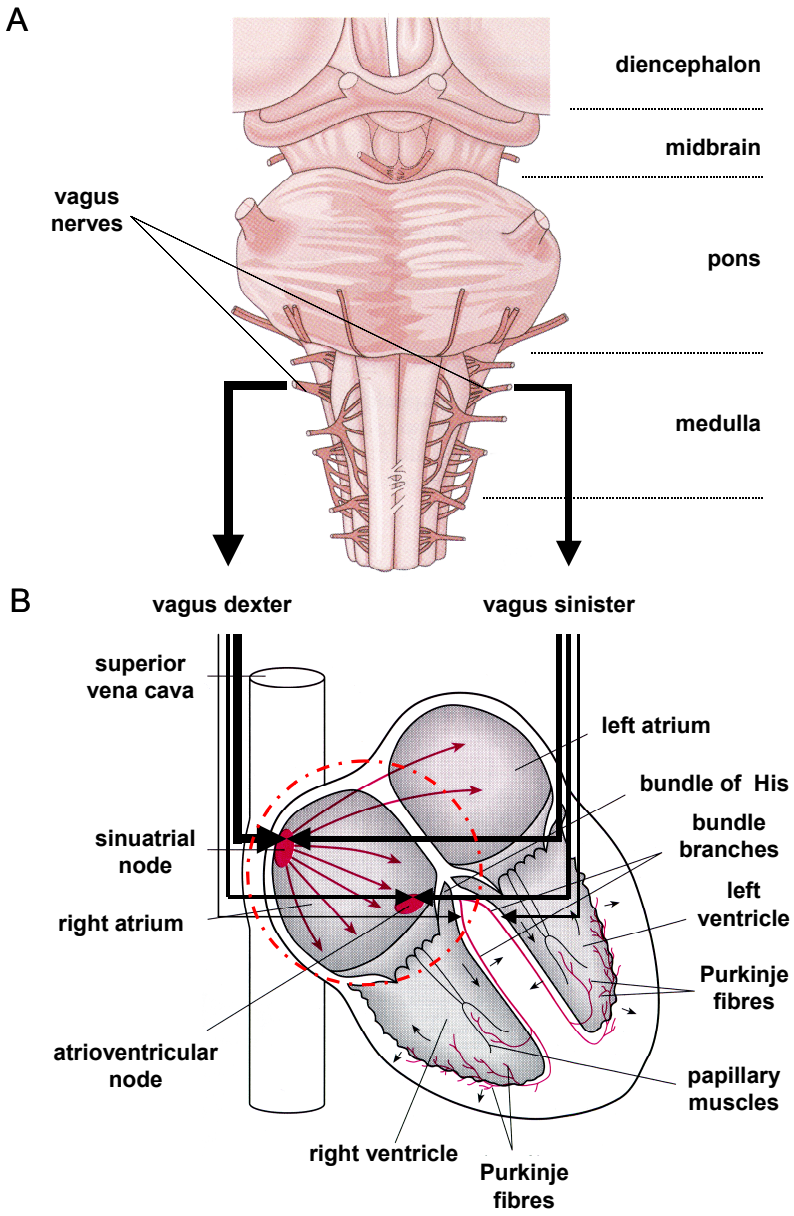

Figure 1: *Parasympathetic innervation of the heart and the cardiac conduction system* (adapted from Berne & Levy, 1988, p. 346; Saper, 2000, p. 876; Schmidt, 1992, p. 162)

A: *The brain stem and the vagus nerves (ventral view).*
Cardiac preganglionic parasympathetic fibres originate in the medulla oblongata of the brain stem. As part of the 10th cranial nerves (vagus sinister and vagus dexter) they exit the medulla bilaterally and project towards the heart.

B: *The cardiac conduction system (ventral view).*
Scheme of the cardiac pacemaker and conduction system. Black arrows indicate the vagus nerves that project to postganglionic parasympathetic neurons. The thickness of the arrows indicates the differential distribution of vagal nerve endings. The dashed circle indicates the location of most postganglionic parasympathetic neurons. The splitting of the left bundle branch into the anterior and posterior division is not shown. See text for further details.

1.1.2 Mammalian intracardiac neurons

Traditionally, it is believed that *intracardiac (ganglion) neurons* or *intrinsic cardiac (ganglion) neurons* are basically *efferent postganglionic parasympathetic neurons*. The latter are thought to be the sole cell population within cardiac ganglia that act as mere *(cholinergic) relay stations for vagal input* to the heart. Indeed, there is little doubt, that a *majority of intracardiac neurons* display *cholinergic properties*, including the capability for ACh synthesis (Leger et al., 1999; Mawe et al., 1996). Furthermore *physiological and pharmacological studies* have shown that a majority of *intracardiac neurons* do respond to *nicotinic stimulation* (or inhibition thereof), supporting the idea of a nicotinic neurotransmission (see e.g. Adams & Nutter, 1992; Bibevski et al., 2000; Cuevas & Adams, 1994; Fieber & Adams, 1991a; Hogg et al., 1999; Nutter & Adams, 1995; Poth et al., 1997). In addition, Bibevski et al. (2000) have shown that local perfusion of cardiac ganglia with specific blockers of nicotinic transmission leads to the increases in heart rate *in vivo*. This data directly links nicotinic neurotransmission to in vivo responses in heart rate discussed in the previous chapter.

Revisions of the simplistic "relay concept" for intracardiac neurons have in particular been proposed by Armour and co-workers (reviewed in Armour, 1999) and are illustrated in figure 2:

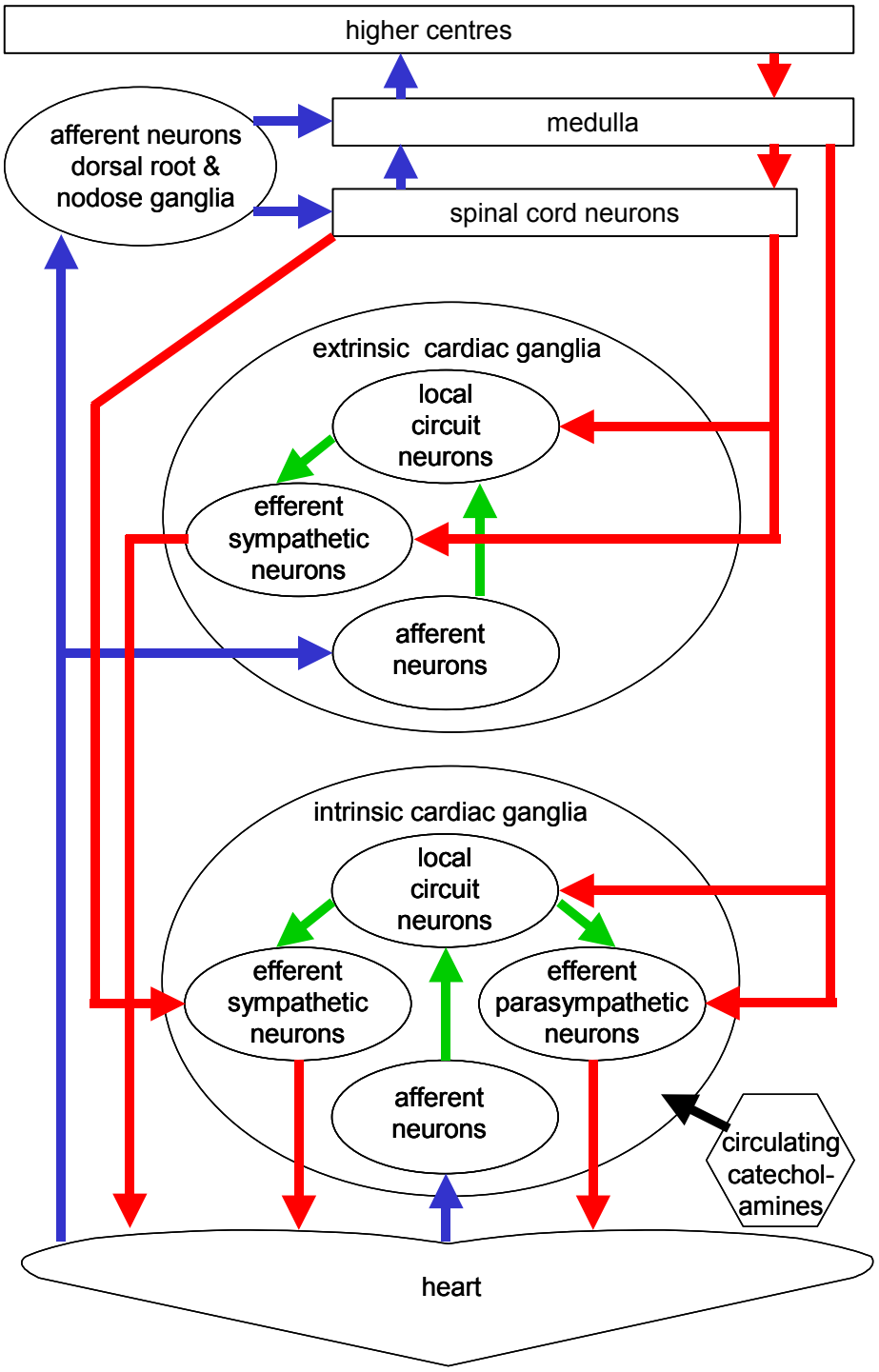

Figure 2: *Autonomic innervation of the heart. A controversial view* (adapted from Armour, 1999, p. 42)

Schematic representation of neurons and their interconnections suggested being involved in the regulation of the heart.
According to this working model of Armour, and based on anatomical and functional evidence, neurons of extrinsic cardiac ganglia not only include neurons of the paravertebral ganglia of the sympathetic chain, but also neurons of the middle and superior cervical ganglia, as well as the mediastinal ganglia.

This model is related to two major points: Firstly, intracardiac ganglions are likely to contain a *more heterogeneous cell population*: In addition to a substantial population of *efferent postganglionic parasympathetic neurons*, cardiac ganglia may also include at least small populations of *local circuit neurons*, *afferent neurons* and *efferent postganglionic sympathetic neurons*. The presence of efferent *sympathetic* neurons in intracardiac neurons is supported by *in vivo* and *in situ* experiments, which have shown that a subgroup of intracardiac neurons can elicit *cardioaugmentation* and thus exerts typical *sympathetic function* (Armour & Hopkins, 1990a; Butler et al., 1990; Huang et al., 1993; Yuan et al., 1993). *Immunohistochemical studies* have further identified *tyrosine hydroxylase* (TH), i.e. an enzyme that is required for norepinephrine synthesis, in groups of mammalian intracardiac neurons, indicating that these neurons may be of *adrenergic phenotype* in that they are able to *produce* catecholamines (Moravec & Moravec, 1989; Slavikova et al., 1993), but other studies have failed to so (Baluk & Gabella, 1990; Leger et al., 1999). Leger and co-workers, e.g. acknowledge that cardioaugmentation can occur following activation of intracardiac neurons, but they point out that intracardiac neurons that lack the enzymes to produce biogenic amines have been shown to accumulate biogenic amines: *Intracardiac neurons* may thus be able to *accumulate* and release, but not produce, *catecholamines*. *Non-neural cells* like intensely fluorescent (SIF) cells that are present in intracardiac ganglia may *release catecholamines* and thus contribute to cardioaugmentation. Furthermore, neurotransmission to and from intracardiac neurons may *not* solely be a function of ACh- (and possibly catecholamine-) release, but may be mediated by other endogenous chemical agents that can either act as *neurotransmitters* or *neuromodulators* and may be *co-released* together with ACh: *Immunohistochemical studies* have detected the presence of several *neuropeptides* such as vasoactive intestinal polypeptide (VIP), neuropeptide Y (NPY), somatostatin, substance P and dynorphin in intracardiac neurons or nerve fibres in the heart, with different expression patterns for *subpopulations of intracardiac neurons*. This suggests a *neurochemical complexity* despite the common cholinergic phenotype of most intracardiac neurons (Steele et al., 1996). This view is supported by *physiological studies* that have shown that *endogenous chemical agents* like *neuropeptides* can *modulate* nicotinic signals in intracardiac neurons, and other endogenous chemical agents such as adenosine triphosphate *(ATP)*, or *enkephalines* have been shown to *elicit* or *modulate non-cholinergic physiological mechanisms*, indicating a *functional complexity* of intracardiac neurons (Cuevas & Adams, 2000; Fieber & Adams, 1991b; Liu & Adams, 2001; Liu et al., 2000a, 2000b; Smith & Adams, 1999).

Secondly, in contrast to the "relay station" concept, various types of intracardiac neurons seem to form a *local intracardiac network*. This network appears to exert *local control* of parasympathetic, sympathetic and afferent information to and from the heart (Armour, 1999).

While immunohistochemical methods in atrial preparations have identified the somata of intracardiac neurons in the *subepicardium throughout the atria*, they are *concentrated in the interatrial septum*, close to the origins of the two caval veins and the pulmonary vein ostia. The *total number of intracardiac neurons* has been reported to be some *1500 per atria*. Individual ganglia can differ significantly in size, ranging from less than five to more than 100 neurons per ganglia. Interestingly, not all of the atrial intracardiac neurons seem to be ganglionic: While 85 - 95 % of intracardiac neurons derived from the atria of adult guinea pigs are part of ganglia (ganglionic neurons), the remaining 5 – 15 % are isolated *(individual neurons)*. The *cell size* of the great majority of neurons in these guinea pig preparations are relatively large, ranging from *15 to 40 µm* in diameter, but a substantial amount of smaller cells have also consistently been detected (Horackova et al., 1999; Leger et al., 1999; Seabrook et al., 1990). The *cell types* of atrial intracardiac neurons are mainly *uni-* or *bi-polar* (Xu & Adams, 1992a), but *multipolar* neurons have been detected, too, further supporting the idea of a heterogeneous population of intracardiac neurons (Horackova et al., 1999).

Intracardiac neuronal somata have also been detected in *ventricular preparations* in a number of mammalian species, including rats and humans. Most studies, however, seem to agree in that the density and the extent of intracardiac ganglia within the ventricles is lower than within the atria (Armour & Hopkins, 1990b; Armour et al., 1997; Moravec & Moravec, 1989; Pauza et al., 2000; Yuan et al., 1993).

The *target tissues of atrial intracardiac neurons* mostly lie *within the atria*, those of *ventricular neurons within the ventricles* (Butler et al., 1990). Major target tissues of atrial intracardiac neurons are the *atrial musculature*, and especially the *SA node*, the *AV node*, the *valves* as well as *other ganglia* (Seabrook et al., 1990; Steele et al., 1996).

1.2 General Anaesthetics

In 1948, Morton and co-workers successfully used *diethyl ether* to carry out the first general anaesthesia in public (Mutschler et al., 2001). Since these adventurous beginnings, general anaesthetic procedures have become widely employed and generally safe: In France, e.g., ~ 13.5 % of the whole population undergoes anaesthesia every year, and ~ 77 % of theses anaesthetic procedures involve general anaesthesia (Clergue et al. 1999). Furthermore, less than one death that is directly attributable to anaesthesia occurs per 200,000 procedures (Urban & Bleckwenn, 2002).

Yet there is still *need for improvement*, as the use of general anaesthetics can involve *severe side effects*. This becomes apparent in descriptions of the general anaesthesia: While no generally accepted definition of general anaesthesia seems to exist, there is consensus, that the *clinical effect(s)* of anaesthesia can involve *several components*, some of which are desired, while others are undesired (side-effects) as illustrated in figure 3: The *desired effects* include *amnesia*, *analgesia*, *unconsciousness* and *muscle relaxation*. Undesired effect can range from *shivering*, *emesis* (=vomiting), and *excitation/convulsions* to most importantly for the present thesis: *cardiovascular instability*.

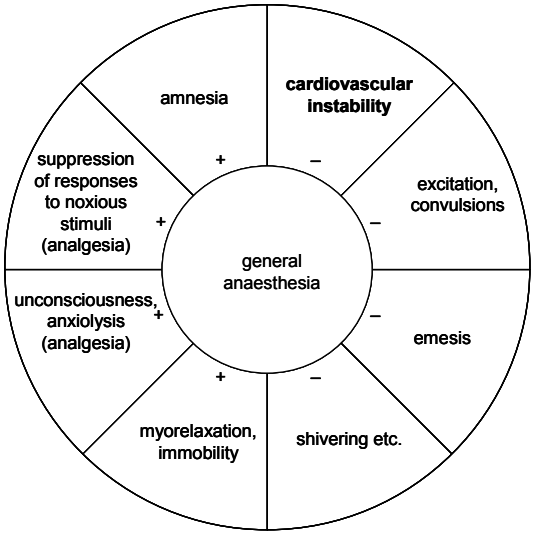

Figure 3: *Components of general anaesthesia* (based on Urban & Bleckwenn, 2002, p. 3)

Desired (+) and undesired (-) components of general anaesthesia.
Analgesia is part of two categories of the above scheme and for that reason has been put in brackets: Assuming that pain involves a conscious perception of noxious stimuli, unconsciousness may involve analgesia (= the absence of pain). Therefore, analgesia is part of unconsciousness in this scheme. In contrast, analgesia does not necessarily require unconsciousness, which is why analgesia itself comprises a separate category. Cardiovascular instability has been printed in bold to indicate its importance in the context of the present thesis.

There are some drugs such as *ether* or *chloroform* that, if solely applied, can (more or less) generate all the components of general anaesthesia and are therefore called *general anaesthetics*. In clinical application, however, the aim is not to use a single compound that generates the whole spectrum of general anaesthesia but rather use a *combination of drugs* to allow for a *fine-tuning of individual components of general anaesthesia* (Urban & Bleckwenn, 2002). Typically *3 different types of drugs* are being used: While *opioids* are used to obtain analgesia and *muscle relaxants* to achieve muscle relaxation, *general anaesthetics* are used to *achieve unconsciousness* and *amnesia* (Urban & Bleckwenn, 2002).

Our detailed knowledge concerning clinical effects and side effects of general anaesthetics is in marked contrast to our lack of understanding of the *cellular* and *molecular mechanisms* on which these mechanisms are based. Such knowledge has only begun to emerge within the last couple of years (Krasowski & Harrison, 1999; Urban & Bleckwenn, 2002; Yamakura et al., 2001) and it is the aim of the present thesis to contribute to this process: By examining the effects of i.v. anaesthetics on intracardiac neurons it may yield to a better understanding of the cardiovascular side effects of these drugs. The following chapter gives an overview of the family of general anaesthetics.

1.2.1 Molecular diversity

General anaesthetics are a chemically very heterogeneous group that includes a number of *volatile anaesthetics*, *anaesthetic gases*, *intravenous (i.v.) anaesthetics* as well as *alcohols* as illustrated in figure 4 for a selection of these drugs.

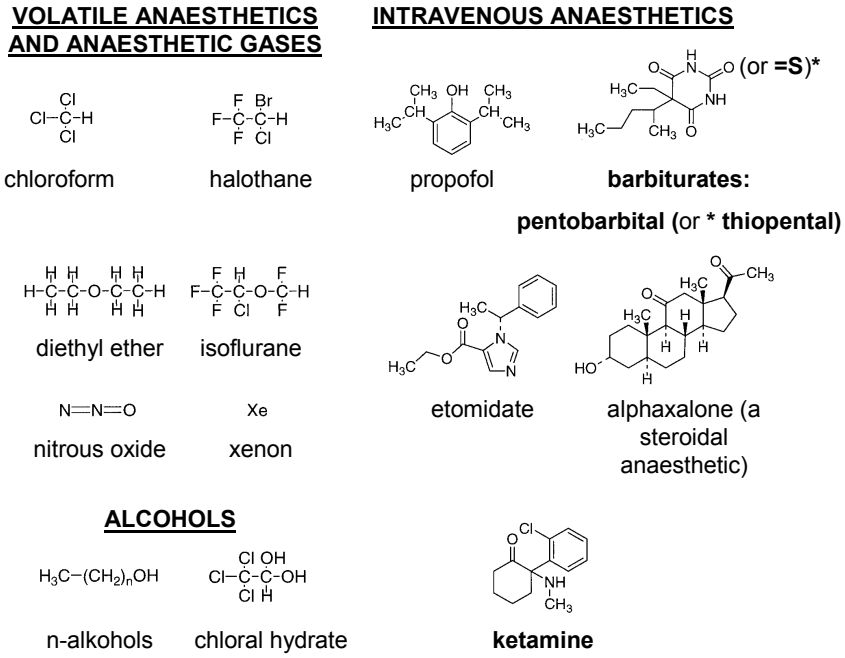

Figure 4: *Chemical structures of general anaesthetics* (from Krasowski & Harrison, 1999, p. 1279; adapted by M. Weber)

General anaesthetics can (somewhat indiscriminately) be subdivided into: volatile anaesthetics, anaesthetic gases, intravenous anaesthetics and alcohols.
The anaesthetics used in the present thesis are printed in bold.

Interestingly, some of these drugs do not exist as salts, bases and acids and were originally called *non-specific anaesthetics* (Urban & Bleckwenn, 2002). The *i.v. anaesthetics* of the present study, i.e. thiopental, pentobarbital and ketamine, however, exist as salts and bases, and have pKa values ranging from 7.5 to 8.11 (see appendix A.2), indicating that *at physiological pH values*, one substantial *fraction of the molecules* is likely to exist in the *dissociated state*, while a *second fraction* is likely to exist in the *non-dissociated state.*

Further complexity arises as several of these anaesthetics, including thiopental, pentobarbital and ketamine, exist as *stereoisomers* (or *optical isomers,* or *enantiomers*), i.e. variants of molecules of identical molecular and structural formula, but with different spatial configuration due to the presence of an asymmetric carbon atom. As a result, the

two variants exist in spatial configurations that are mirror images of each other, which cannot be rotated to completely overlay each other (see e.g. Franks & Lieb, 1994; Graf & Martin, 1998). The great majority of the commercially available isomeric anaesthetics actually are (1:1) *racemic mixtures* of the enantiomers, meaning that (both) enantiomers are present in the compound in the same quantities. Pure enantiomers can be derived from racemic mixtures, e.g. using high-performance liquid chromatography techniques (see e.g. Tomlin et al., 1999). Different enantiomers sometimes have varying anaesthetic potencies, which make them interesting for clinical use, as the sole application of the enantiomer with the higher anaesthetic potency allows for lower drug concentrations. However, due to the high costs of their purification, enantiomers are not yet widely used for anaesthetic procedures (Graf & Martin, 1998).

1.2.2 In vivo effects of thiopental, pentobarbital, and ketamine

The present thesis has focused on racemic mixtures of the *barbiturates thiopental* (also called thiopentone, thiobarbital and pentothal) and *pentobarbital* (also called pentobarbitone or nembutal), as well as the *dissociative anaesthetic ketamine*. All of them are considered to be general anaesthetics, even though none of them can be properly used for general anaesthesia in the absence of additional drugs: The *barbiturates* are *hypnotics*, but *lack analgesic properties, ketamine does have analgesic properties*, but it has to be used *together with benzodiazepines* to avoid negative psychological reactions.

Like all barbiturates, *thiopental* is a *derivate of barbituric acid* (Larsen, 2002). It is a popular *anaesthesia-inducing hypnotic drug* that leads to a *rapid loss of consciousness*, typically within fractions of a minute following the start of its i.v. administration. Figure 5 illustrates the thiopental distribution in body tissues following a typical, single i.v. bolus application at the beginning of the anaesthetic procedure.

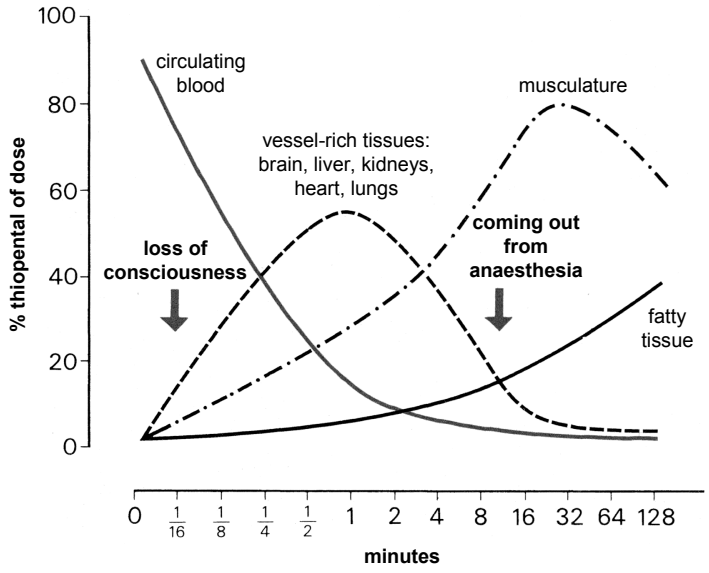

Figure 5: *Distribution and redistribution of thiopental in human body tissues* (adopted from Büch & Büch, 2001, p. 291, based on Price et al., 1960, p. 21)

Estimation of thiopental concentrations in body tissues following a single i.v. injection of thiopental.
The model describes the (re-) distribution of thiopental in the body of human adults and has been confirmed by the extraction of samples. It assumes four compartments that that are connected via a circulatory pump. The compartments correspond to different tissues with different masses, blood and lymph flow rates and concentration ratios for thiopental (tissue/blood). The central blood volume is the 1st compartment. The 2nd compartment includes the CNS, the heart, the kidneys and the liver, which have been pooled together due to similar perfusion rates and thiopental affinities. The 3rd and 4th compartment in essence are the musculature and the fatty tissue, respectively. Further assumptions include an instant thiopental mixture with the 1st compartment, an immediate distribution to the tissues, a constant tissue blood flow and an equilibrium state between any tissue and the blood that leaves this tissue. Excretion or metabolic mechanisms are not considered for the limited time period examined.

A *rapid thiopental accumulation* occurs *in the CNS* and other vessels-rich organs, such as the heart, lungs, liver and kidneys, reaching a peak value ~ 1 min following its bolus. The rapidity of this process is due to the *high lipophilicity* of thiopental, which also facilitates the penetration of the *blood-brain barrier*. The decline of the thiopental concentration in these strongly perfused tissues is also very fast: Thiopental concentrations typically reach sub-narcotic levels in the CNS (so that the patient regains consciousness) within less than ten minutes. This rapid decline is due to a *redistribution of thiopental* into tissues with lower blood circulation, in particular the *musculature,* and *not* due to its *metabolic breakdown*, as the half-life $T_{1/2\beta}$ of thiopental in the blood plasma has been determined as longer than ten hours (see Evers & Crowder, 2001). The thiopental concentration within the musculature increases somewhat more slowly, reaching peak values after about half an hour. Its subsequent decline is mostly due to another redistribution into the *fatty tissue* (Büch & Büch, 2001, according to Price et al., 1960).

Thiopental *readily binds to plasma proteins*: While ~ 85 % of thiopental in the plasma (*total thiopental*) is bound to proteins (*protein-bound thiopental*), only ~ 15 % is present as free, unbound thiopental (*free thiopental*; Burch & Stanski, 1983). This characteristic has to be taken into account for the calculation of clinically relevant concentrations of thiopental for *in vitro* experiments (see chapter 1.2.3). See appendix A.2 for further data on thiopental.

Pentobarbital also is a barbiturate with hypnotic properties, but nowadays it is no more used in humans. It is nonetheless a very interesting anaesthetic compound, as it is an *active metabolite of thiopental* in the human body that is obtained by *oxidative desulfuration* in a fraction of the thiopental molecules present (Büch & Büch, 2001; Chan et al., 1985; Charney et al., 2001). This metabolic transformation thus leads to a prolonged presence of hypnotics in the human body in particular, as pentobarbital is a *longer-acting* barbiturate (Evers & Crowder, 2001). Its half-life $T_{1/2\beta}$ in the blood plasma has been determined as ~ 30 hours (Fichtl, 2001; Wellhöner, 1988).

Pentobarbital is several folds *less lipophilic than thiopental* (Raaflaub, 1970), in line with the general tendency of oxybarbiturates to be less lipophilic than the corresponding thiobarbiturates. Its reduced lipophilicity is likely to account for an increased duration of action and latency to onset of activity, a prolonged metabolic degradation and a reduced hypnotic potency (Charney et al., 2001). The metabolites of pentobarbital themselves are not hypnotic (see e.g. Büch & Büch, 2001).

Pentobarbital also *binds to plasma proteins*, but to a smaller degree than thiopental. Franks and Lieb (1994; based on Ehrnebo & Odar-Cederlöf, 1977) report that ~ 61% of the total pentobarbital concentration in blood plasma is bound to proteins.

Ketamine differs from the barbiturates in several respects: Chemically, *ketamine* is a *derivate of phencyclidine*, which causes strong psychotomimetic activity (Larsen, 2002; White et al., 1982). The unusual *anaesthetic state caused by ketamine* already became apparent with the first use of ketamine in man:

> The *unusual analgesic and aesthetic action* of this drug with *sympathomimetic properties*, and *cerebral dissociative actions*, makes it imperative that a new terminology be developed for drugs of this type. It is suggested that the state produced by this drug be called *"dissociative" anaesthesia* (from Adams

& Werner, 1997, p. 1026; based on Domino et al., 1965; italicisation added by M. Weber).

Dissociative anaesthesia describes a *cataleptic state* that involves *amnesia*, *analgesia* and only a *superficial loss of consciousness* during which patients typically have their eyes open and often display involuntary movements of their limbs, but do not respond to commands despite their mostly intact, spontaneous respiration (see e.g. Adams & Werner, 1977; Evers & Crowder, 2001; Trevor & Miller, 2001).

Ketamine is *extremely lipophilic*, with a 5-10 times better lipid solubility than thiopental (Büch & Büch, 2001). It rapidly penetrates the CNS (and other strongly perfused tissues such as the heart (see above) and has a *rapid onset of activity*: Loss of consciousness also occurs within fractions of a minute following a typical i.v. bolus application. Ketamine also redistributes from the *strongly perfused* to less perfused tissues. A difference between ketamine and thiopental, however, is that its metabolic breakdown and to some extent urinary and biliary excretion plays a greater role during the initial decay of its concentration (Trevor & Miller, 2001): Its half-life $T_{1/2\beta}$ *in the blood plasma* is *~ 3 hours* and thus considerably shorter than that of thiopental and pentobarbital. Furthermore, only ~ 12 % of the total ketamine concentration in the blood plasma are bound to protein (Evers & Crowder, 2001; see also appendix A.2).

Table 1 illustrates further effects of thiopental and ketamine.

Drug	CBF	CMR_{O2}	ICP	MAP	HR	CO	RespR	V_E
Thiopental	– – –	– – –	– – –	–	+	–	–	– –
Ketamine	++	+/–	++	+	++	+	+/–	+/–

Table 1: *Major clinical effects of the i.v. anaesthetics thiopental and ketamine* (adopted from Evers & Crowder, 2001, p. 348)

Thiopental differs from ketamine with respect to its profile of effects and side effects.
The table shows typical effects of a single bolus application in humans.

Legend: CBF cerebral blood flow; CMR_{O2} cerebral metabolic rate for oxygen; ICP intracranial pressure; MAP mean arterial pressure; HR heart rate; CO cardiac output; RespR respiratory rate; V_E minute ventilation.

Symbols: – – – large decrease; – – moderate decrease; – slight decrease;
+++ large increase; ++ moderate increase; + slight increase;
+/– no significant change.

More data on thiopental, pentobarbital and ketamine is gathered in appendix A.2. Their effects on the cardiovascular system are discussed in the following chapter.

1.2.2.1 Cardiovascular effects

Clearly, general anaesthetics are basically in use because of their main effects on the CNS. However, following their CNS effects, the most *crucial clinical side effects* of anaesthetics are those on the *cardiovascular system* (Graf et al., 1995; Graf & Martin, 1998). In his paper on thiopental and ketamine Horwitz (1977, p. 44) already points out that: *"Potentially deleterious cardiovascular responses have been associated with virtually all drugs capable of general anaesthesia"*.

However, due to the large number of organ systems and parameters that are involved in the regulation of the cardiovascular system, it would go beyond the scope of this thesis to discuss the possible i.v. anaesthetic modulation of all of these parameters and their interplay (for introductory reviews see: Fragen &Avram (2000); Reves et al. 1999, 2000). Therefore, only *key parameters*, with a *focus on chronotropic effects*, will be discussed in the following sections.

Lieb and Mulinos using amytal have already reported a *barbiturate-induced decrease in blood pressure* in 1929. Since then, this finding has been confirmed for other barbiturates such as thiopental or pentobarbital in many studies over several decades in animals, healthy humans and in humans with chronic heart disease (see e.g. Aono et al., 2001; Manders & Vatner, 1976; Morrison et al, 1950; Naguib et al., 2003; Peiss & Manning, 1964; Price et al., 1952; Reiz et al, 1981; Scheffer et al., 1993; Seltzer et al., 1980; Sonntag et al., 1975).

Barbiturates are well known for their *negative inotropic effect*, which is attributed to a direct effect on the myocardium (Azari & Cork, 1993; Frankl & Poole-Wilson, 1981; Gelissen et al., 1996; Kissin et al., 1983; Komai & Rusy, 1984; Manders & Vatner, 1976; Park & Lynch, 1992).

A barbiturate-induced *increase in heart rate* has also been reported in a great number of studies, also in animals, healthy humans and humans with coronary heart disease (see e.g. Aono et al., 2001; Blake & Korner, 1981; Bristow et al., 1969; Christensen et al., 1982; Filner & Karliner, 1976; Manders & Vatner, 1976; Milocco et al., 1985; Morrison et al, 1950; Price et al., 1952; Reiz et al, 1981; Scheffer et al., 1993; Seltzer et al., 1980; Sonntag et al., 1975; Tarabadkar et al, 1980; Van Citters et al., 1964).

The origin of this effect, however, has been controversially discussed. Most studies seem to agree that an *indirect effect* plays a role, i.e. the *baroreceptor reflex* contributes – at least in part - to the observed positive chronotropic effect in the presence of the anaesthetic (Bristow et al., 1969; Filner & Karliner, 1976; Manders & Vatner, 1976; Reiz et al., 1981): Moderate increases in heart rate may serve as a *compensatory mechanism* to maintain cardiac output, given that blood pressure (and contractile force) is reduced following the application of barbiturates (see above).

In addition, a *direct effect*, i.e. a barbiturate effect on *cardiac pacemaker centres* and/or *neurons that are involved in the regulation of the heart rate*, is very likely to play a role. In particular, *direct barbiturate effects on sympathetic and/or parasympathetic* neurons that are involved in the regulation of the heartbeat e.g. would provide plausible alternative explanations.

Firstly, and most importantly in the context of the present study, a *suppression* of *parasympathetic cardiac neurons* could explain the observed positive chronotropic effect. Indeed, the pioneering studies of Lieb and Mulinos (1929), and Shafer et al. (1929), using amytal, have already demonstrated a barbiturate-induced suppression of the vagal innervation of the heart. Later experiments by Blake and Korner (1981), Halliwill and Billman (1992) and Murthy et al. (1982) using rabbits or dogs have demonstrated *barbiturate-induced suppression of vagal tone*, which was accompanied by *increases in heart rate*. Experiments in man by Scheffer and co-workers (1993), using sophisticated beat-to-beat analysis of cardiovascular signals in man, similarly suggest a *barbiturate-induced suppression of vagal tone* on the heart.

Secondly, as pointed out by Bristow et al. (1969), *increased (neural) sympathetic activity* or *increased catecholamine levels in the blood flow* could similarly explain the observed increases in heart rate. However, experimental evidence rather suggests a *suppression of sympathetic nervous activity* (Shimokawa et al., 1998; Skovsted et al., 1970) and a reduction of *general sympathetic outflow* from the CNS in the presence of barbiturates (Aono et al., 2001). The data of Scheffer et al. (1993) also supports a thiopental-induced inhibition of sympathetic outflow in addition to the already mentioned suppression of vagal tone. Taken together, experimental evidence rather suggests a *barbiturate-induced suppression of both parasympathetic and sympathetic nervous activity*.

Such a condition in which both, the *parasympathetic and sympathetic branch of the ANS* are similarly *down-regulated*, with very few exceptions, typically leads to an *increase in heart rate* in a wide range of mammals, including humans, due to the greater importance

of the vagal tone on heart rate under conditions of rest. These findings have been an accepted part in physiology textbooks for several years (see e.g. Berne & Levy, 1998; Thews & Vaupel, 1997), and they have recently been confirmed using state of the art electrocardiography (ECG) analysing techniques (Després et al., 2002; Just et al., 2000). Furthermore, the effect of parasympathetic tone on heart rate has even been shown to persist during conditions of heavy exercise in dogs (O'Leary et al., 1997). In sum, there is substantial *evidence that barbiturates yield a positive chronotropic effect*, which *is partly due to the vagolytic properties of these drugs*.

While cardiovascular side effects of anaesthetics are basically undesired, they may not be too dramatic in healthy subjects. Increases in heart rate, however, can represent a particularly adverse type of side effect in patients with an unstable cardiovascular system, e.g. in patients with cardiovascular disease, as it can *increase myocardial oxygen demand*. The latter depends on several factors besides heart rate, including wall tension and myocardial contractility (Reiz et al., 1981). Under certain experimental conditions, including an experimentally controlled heart rate, barbiturates have thus been shown to reduce myocardial oxygen demand (Manders et al., 1976; Reiz et al., 1981). The crux of the matter, however, is that *increased heart rate* is related to *increased myocardial work* and can lead to *increased myocardial oxygen demand* (Sonntag et al., 1975, Tarabadkar et al., 1980). A dramatic consequence of general anaesthesia that is likely to be linked to this effect has been demonstrated by Jugdutt and co-workers (1986) who found that dogs that were exposed to thiopental during acute myocardial infarction had *higher heart rates* and subsequently *greater infarct sizes* than control dogs not exposed to thiopental. A second group of dogs were not exposed to thiopental, and heart rates were artificially paced and set to a frequency comparable to that of the thiopental group during acute myocardial infarction. Here, infarcts were also larger than that of the control group – but comparable to that of the thiopental group.

Ketamine's uniqueness within the group of the general anaesthetics is also due to its *cardiostimulatory* and *sympathomimetic properties*, which – in healthy subjects - typically induce *increases in blood pressure, heart rate* and *cardiac output*. These effects have also been demonstrated over several decades in a wide range of studies in animals, healthy humans and humans with coronary heart disease (see e.g. Akine et al, 2001; Bålfors et al., 1983; Blake & Korner, 1981; Doenicke et al., 1992; Domino et al., 1965; Horwitz, 1977; Idvall et al., 1979; Inoue & Arndt, 1982; Ivankovich et al., 1974; Johnstone, 1976; Nishimura et al., 1973; Savege et al., 1976; Schwartz & Horwitz, 1975; Stanley, 1973; Traber et al.,

1968; Virtue et al., 1967). Yet, the origins of these sympathomimetic ketamine effects remain somewhat enigmatic.

Interestingly, ketamine does *not* appear to exert its positive inotropic effects via the myocardium itself, as the majority of *in vitro* studies have demonstrated a *direct negative inotropic effect* (see e.g. Diaz et al., 1976; Dowdy & Kaya, 1968; Pagel et al., 1992; Valicenti et al., 1973). Under *in vivo* conditions, however, this effect is likely to be masked by the cardiostimulatory effects of ketamine. It has been suggested that the negative inotropic effect of ketamine may only become apparent *in the absence of adrenergic transmission* (see e.g. Horwitz, 1977; Pagel et al., 1992), e.g. *in vivo* following the depletion of catecholamine stores, which may also have contributed to the decrease in cardiac performance observed in severely ill patients following ketamine application (Waxman et al., 1980).

There is very little doubt, that the *sympathomimetic* and *cardiostimulatory properties of ketamine* are *in part* centrally *mediated*. In their classical study, Ivankovich et al. (1974) were able to show that administration of ketamine through an artery catheter directly into the CNS was followed by increases in heart rate, blood pressure and cardiac output before the drug could have possibly reached the myocardium and other peripheral targets through the blood stream.

It appears to be equally clear that the sympathomimetic and cardiostimulatory effects of ketamine are partly related to catecholamines. One catecholamine effect is *systemic*, i.e. a ketamine-induced intravasal catecholamine release, which leads to a *rise in plasma catecholamine levels*. Interestingly, administration of *tranquillisers* such as diazepam or midazolam, or the *neuroleptic* droperidol has been shown to *attenuate* both, *the rise in plasma catecholamines* as well as the *cardiostimulatory* effects of ketamine (Bålfors et al., 1983; Doenicke et al., 1992; Virtue et al., 1967; Zsigmond, 1974; Zsigmond et al., 1974). A second effect seems to take place *locally* in the *periphery* and involves a *cocaine-like action* of ketamine, i.e. an *inhibition of the norepinephrine uptake* into *postganglionic, sympathetic neurons* that project towards the heart and vessels (Byrne et al., 1979; Hill et al., 1978; Miletich et al. 1973; Nedergaard, 1973; Salt et al., 1979). These results, however, have been challenged by other studies where a cocaine-like response could only be elicited at very high ketamine concentrations (see e.g. Clanachan & McGrath, 1976; Liao et al., 1979). These *sympathomimetic characteristics* are *ketamine-specific* and differ from those of other anaesthetics, including the barbiturates.

Yet, ketamine and the barbiturates do have strikingly similar effects on parasympathetic efferent neurons, suggesting that the positive chronotropic effect of ketamine may in part be due its *vagolytic properties*: Inoue and Arndt (1982) have demonstrated a *ketamine-induced suppression of vagal tone*, which was accompanied by *increases in heart rate*. In a later study, Inoue and König (1988) were able to show that the *peripheral vagal transmission inside the heart* was *suppressed* when ketamine was locally applied into the pericardium. Interestingly, ketamine altered heart rate responses not only to electrical stimulation of the vagus nerve, but also to local application of acetylcholine right into the pericardium, suggesting that cholinergic transmission is suppressed by ketamine. Furthermore, support for an inhibition of cholinergic transmission by ketamine in cardiac parasympathetic neurons comes from a recent study by Irnaten et al. (2002): They were able to show that the response of preganglionic cardiac parasympathetic neurons located in the nucleus ambiguus of the brain stem to nicotinic innervation was inhibited by ketamine, suggesting an inhibition of nicotinic transmission in particular.

In sum, despite distinct effects on central, systemic and sympathetic targets, ketamine and the barbiturates may exert similar, i.e. *inhibitory effects on* efferent parasympathetic neurons and *intracardiac neurons* in particular, thereby contributing to the observed positive chronotropic effect of these drugs.

Therefore, as neurotransmission in intracardiac ganglia (i) is mainly mediated by nicotinic innervation (see chapter 1.1) and (ii) appears to be inhibited by barbiturates and ketamine (see above), it was interesting to see, if the response of intracardiac neurons to nAChR activation was inhibited by these drugs. Further support for the plausibility of this idea comes from studies showing that nAChR are very sensitive to general anaesthetic and thus may represent one of their molecular targets, as described in chapter 1.2.4.

1.2.3 Relating molecular effects to in vivo effects

The *molecular mechanisms of anaesthetics* are typically examined in *in vitro experiments*. In order to put these molecular anaesthetic effects into a *meaningful relation to* their *clinical, i.e. in vivo effect* Krasowski and Harrison (1999, p. 1283) have specified four

> *[p]harmacological criteria* that a candidate receptor must meet to be considered as a *reasonable general anaesthetic target* […]:

1. The general anaesthetic must alter the function of the receptor at *clinically relevant concentrations*.
2. The *receptor* must be *expressed* in the *appropriate anatomical locations* to mediate the specific behavioural effects of the anaesthetic.
3. If an anaesthetic molecule shows *stereoselective effects in vivo*, these should be *mirrored by the in vitro actions at the receptor*.
4. The *hydrophobicity* of a compound within a homologous series of anaesthetics should *correlate with the in vivo anaesthetic potency and that at the target receptor* (italicisation added by M. Weber).

The presence of an effect at a clinically relevant anaesthetic concentration certainly represents the most important criteria; in particular as high concentrations of general anaesthetics can affect a huge amount of molecular targets (see e.g. Franks & Lieb, 1998) that may be unrelated to any effect or side effect that occurs during a general anaesthetic procedure. *Clinically relevant anaesthetic concentrations* for *in vitro* experiments (including the present study) at physiological pH values are typically *based on experimentally determined in vivo (total) plasma concentrations* during an anaesthetic procedure and are subsequently *corrected for protein binding* (see chapter 1.2.2). For *thiopental*, Franks and Lieb (1994) have estimated a clinically relevant, effective, free aqueous concentration (clinical EC_{50}) of *25 μM*. This estimation is based on a total thiopental plasma concentration of 40 *μg/ml* (Becker, 1978) at which 50 % of patients do not respond to a stimulus of about the painfulness of a surgical incision. The molecular weight of thiopental (FW = 241.33) and a value for protein binding of 85 % (Burch & Stanski, 1983) is furthermore taken into account. In a comparable procedure, Franks and Lieb (1994) have estimated a clinical EC_{50} of *~50μM* for pentobarbital. For *ketamine*, Krasowski and Harrison (1999) have reported a clinical EC_{50} of ~10 μM. This value roughly corresponds to the stable ketamine plasma concentration of 9.3 μM that has been observed in humans during the maintenance of ketamine anaesthesia (Idvall et al., 1979), as the protein binding value of ketamine does not play a mayor role (see chapter 1.2.2; appendix A.2).

Anaesthetic effects on a molecular target can only yield to certain physiological and clinical effects, if the target molecules are present and functional in a sufficient amount in an *anatomical location* that mediates this effect. The great majority of studies published to date have tried to comply with this criterion by referring to the presence of the target molecule, e.g. a membrane receptor, in a relevant anatomical location, while the anaesthetic effect on the receptor type is examined in an expression system. Thus, the actual physiological and pharmacological effects are merely studied in *Xenopus* oocytes or in mammalian expression systems, but not in the anatomically relevant target cells that have been reported to express this receptor. This concerns almost all of the studies that have examined clinically relevant concentrations of barbiturates and ketamine on neuronal nAChR (see e.g. Andoh et al, 1997; Coates & Flood, 2001; Coates et al., 2001; Downie et al., 2000; Flood & Krasowski, 2000; Flood & Role, 1998; Furuya et al., 1999; Kamiya et al., 2001; Sasaki et al., 2000; Tassonyi et al., 2002; Yamakura et al., 2000b). This is a drawback because recombinant nAChR channels expressed in *Xenopus* oocytes and mammalian cell lines are not necessarily functionally similar to native nAChR channels in (ganglionic) neurons (Lewis et al, 1997; Sivilotti et al., 1997). A particular setback of nAChR expressed in *Xenopus* oocytes is that *"desensitization kinetics are often more than an order of magnitude slower for the same receptor expressed in the oocyte compared to other cell systems"* (Quick & Lester, 2002, p. 461). This is crucial, as anaesthetics may partly act by altering the desensitization characteristics (see chapter 1.4.3) of the nAChR channel. Furthermore, the effects of anaesthetics on the electrophysiological properties of ligand-gated ion channels in native neurons have been shown to differ from those in expression systems, as demonstrated for $GABA_A$ channels in the absence of the (native) channel modulating GABA-receptor-associated protein (P. W. Gage, Australian National University, Canberra, Australia; personal communication). Therefore, to relate studies of anaesthetic effects on ion channels in expression systems to physiological function, it is crucial to carry out studies for the range of clinically relevant concentrations in functionally relevant native cells. This present thesis is one of the first studies that support this approach by examining clinically relevant anaesthetic concentrations on native neuronal receptors in an anatomically relevant tissue.

The criteria of *stereoselectivity* allows to make a distinction between molecular targets that are merely sensitive to general anaesthetics and those that are sensitive *and* actually contribute to the general anaesthetic effect: As the S(–) isomers of thiopental and pentobarbital are about two times as potent as the R(+) isomers in their ability to

abolish the righting reflex (Christensen & Lee, 1973; Haley & Gidley, 1970; 1976), any plausible molecular target should thus display the same stereoselectivity pattern in *in vitro* experiments or be ruled out as a molecular target *for the main effect* of these general anaesthetics. However, as *in vivo* stereoselectivity data is not available for the cardiovascular side effects of these barbiturates, the use of the stereoselectivity criteria in *in vitro* studies is of limited use. For *ketamine*, the S(+) isomer is roughly three times more potent as the R(–) isomer in abolishing the righting reflex (Marietta et al., 1977; White et al., 1980, 1985). Three studies have included attempts to compare the cardiovascular effects of ketamine enantiomers and the racemate in humans, but their results are controversial: Pfenninger et al (1994) and White et al. (1980) showed that patients receiving the S(+) isomer displayed smaller rises in heart rate than those receiving the racemate. Yet, in a later study of the same group, White et al. (1985) were not able to replicate this finding. The present thesis has thus focused on the racemic mixtures of anaesthetics.

The hydrophobicity criterion is based on the so-called *Meyer-Overton correlation*, saying that the *anaesthetic potency* of (non-specific) anaesthetics is *positively correlated* to their *lipid solubility* (Urban & Bleckwenn, 2002). The classical examples that support this rule are the n-alcohols. Yet, the problem is that *exceptions* to the Meyer-Overton hypothesis, i.e. drugs with different anaesthetic potencies than to be expected from their lipid solubility do exist. Examples for this rule are *nonanaesthetics* or *nonimmobilizers*, i.e. highly lipid soluble drugs without an anaesthetic potency (see e.g. Koblin et al., 1994; Krasowski & Harrison, 1999). The existence of such drugs limit the use of the *correlational criteria*, but they are nonetheless helpful as their main molecular targets can be ruled out as mediators of the anaesthetic effect (Franks & Lieb, 1998).

1.2.4 Molecular effects of thiopental, pentobarbital, and ketamine

The *Meyer-Overton correlation* has also lead to the believe that the *lipid portions* of *neuronal membranes* are the major *molecular target sites* of general anaesthetics. This believe had to be abandoned for several reasons: (i) Several *exceptions* to the Meyer-Overton hypothesis were discovered (see chapter 1.2.3 on *nonanaesthetics*). *Stereoselectivity* also threatens this hypothesis as enantiomers can differ substantially in their *in vivo* potency despite their common lipid solubility, i.e. identical abilities to disrupt the lipid bilayer of membranes (Krasowski & Harrison, 1999). (ii) Clinically relevant concentrations of several anaesthetics have been shown to inhibit the soluble enzyme *firefly luciferase* in the absence

of any membrane lipids, suggesting that proteins may alternatively represent important general anaesthetic targets (Franks & Lieb, 1984).

Nowadays, a large body of evidence supports the view that *membrane proteins*, and a number of *ligand-gated ion channels (LGIC)* in particular, are the *prime molecular targets of general anaesthetics*. This does *not* necessarily *contradict* the *Meyer-Overton hypothesis*, as not only membrane lipids, but also ion channels do have *lipophilic sections*, such as their *membrane-spanning segments*, as illustrated in figure 14 and 15 in chapter 1.4.3. Not all LGIC are similarly susceptible to general anaesthetics: *Clinically relevant concentrations* of general anaesthetics have been shown to target *glutamate receptor channels* and a *superfamily of fast-acting LGIC* including nicotinic ACh-, $GABA_A$-, glycine-, and 5-HT_3- receptor channels (reviewed in: Franks & Lieb, 1994, 1998; Krasowski & Harrison, 1999; Yamakura et al., 2001). The phylogenetic tree of this superfamily of channels is illustrated in figure 6.

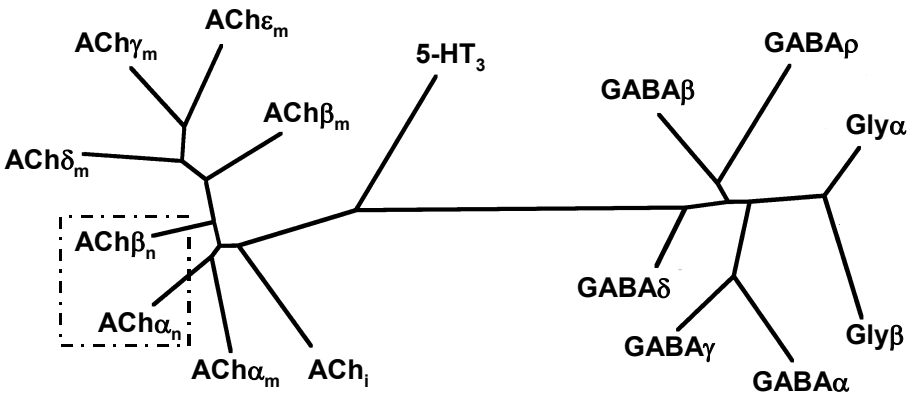

Figure 6: *The anaesthetic-sensitive superfamily of fast-acting, ligand-gated ion channels* (adapted from Franks & Lieb, 1998, p. 5)

Phylogenetic tree of the evolutionary history of the channel subunits.
The distance between the subunits indicate the similarity of their DNA base sequence, with shorter distances for greater DNA homologies. The dashed rectangle indicates the relative subunits for the present thesis.

Symbols:
- Receptor type: ACh nicotinic acetylcholine receptor; 5-HT_3 serotonin receptor; GABA $GABA_A$ receptor; Gly glycine receptor.
- Subunit type: α, β, γ, δ, ε, ρ
- Subscript letters: $_m$ muscle; $_n$ neuronal; $_i$ invertebrate.

Interestingly, clinically relevant concentrations of *general anaesthetics* have been shown to *potentiate* the *inhibitory* $GABA_A$ and *glycine receptor-mediated (whole-cell) currents*, but *inhibit* the *excitatory glutamate,* $5\text{-}HT_3$ and *nACh receptor-mediated (whole-cell) currents* (see Franks & Lieb, 1994, 1998; Krasowski & Harrison, 1999; Yamakura et al., 2001).

Even though all of these receptors types have been shown to be sensitive to clinically relevant concentrations of general anaesthetics, *not all of them* appear to be *important for the generation of the general anaesthetic state*. The *prime molecular target for the generation of general anaesthesia* seems to be the $GABA_A$ receptor channel for at least two reasons: Firstly, *in vitro* experiments with clinically relevant concentrations of several volatile and intravenous anaesthetics have displayed a similar stereoselectivity *pattern* (see chapter 1.2.3) on the $GABA_A$ receptor channel than *in vivo* (Dickinson et al., 2000; Hall et al., 1994; Tomlin et al., 1998; 1999). Furthermore, the $GABA_A$ *receptor channel* has also been shown to be *sensitive to clinically relevant concentrations of* basically *all volatile and intravenous anaesthetics with the exception of ketamine* (Yamakura et al., 2001). This is the second point: Ketamine's failure to potentiate $GABA_A$ receptor responses is crucial as it may be related to the *unique dissociative type of anaesthesia* caused by *ketamine* (see chapter 1.2.2; Flood & Krasowski, 2000). The main effect of *ketamine* appears to be the *inhibition of NMDA receptor channels* (Lodge et al., 1982; Anis et al., 1983), which mirrors its stereoselectivity pattern for the loss of the righting reflex (see chapter 1.2.3; Zeilhofer, 1992).

Ketamine's stereoselectivity pattern on nAChR is controversial: An inhibition in line with its *in vivo* stereoselectivity has been detected by Lodge et al. (1982), but not by Sasaki et al. (2000). Yet, ketamine's effects on the nAChR channel may nonetheless play a role in generating some aspects of its anaesthesia, as pointed out by Flood and Krasowski (2000; p. 1424): *"The inhibition of nAChRs by general anaesthetics may mediate analgesia, as well as inattentiveness and delirium"*.

The general anaesthetic effect caused by the *barbiturates* is also *unlikely* to be primarily due to an *action on the nAChR*. Downie and co-workers (2000) have clearly demonstrated that clinically relevant concentrations of thiopental inhibit neuronal nAChR channels of the CNS, but with a stereoselectivity pattern that is not compatible with that observed *in vivo* (see chapter 1.2.3). On page 782 they conclude: *"[A]lthough thiopental inhibition of nAChR does not actually produce anaesthesia, the fact that these receptors can be very sensitive to anaesthetizing concentrations of this intravenous agent suggests that they may be involved in the generation of anaesthetic side effects"*.

This may include the *generation of cardiovascular effects* and their (nicotinic-mediated) *neuronal regulation* in particular, given that basically all of the *neuronal nAChR channel subtypes* tested to date, including the highly Ca^{2+} permeable α_7 homomer, are *sensitive to clinically relevant concentrations* of the barbiturates and ketamine, with somewhat varying subunit specificities (Andoh et al, 1997; Coates & Flood, 2001; Coates et al., 2001; Downie et al., 2000; Flood & Krasowski, 2000; Flood & Role, 1998; Furuya et al., 1999; Kamiya et al., 2001; Sasaki et al., 2000; Tassonyi et al., 2002; Yamakura et al., 2000b; see chapter 1.4.3 for details on nAChR subunits).

Even though the inhibition of neuronal nAChR channels by clinically relevant concentrations of these drugs has now firmly been established, the detailed *mechanism of the inhibition* have *not yet been fully* resolved. Speaking generally and in terms of *kinetics*, this inhibition can be due to *decreases in agonist affinity, open gating rate*, or *increases in desensitization* (Dilger, 2002). However, detailed kinetic studies on i.v. anaesthetic actions on the neuronal nAChR are very scarce at present and have mainly been carried out by a single research group (see below).

Most of the data on neuronal nAChR for the barbiturates and ketamine *supports a non-competitive inhibiting mechanism*. Yet, a competitive inhibition was observed with thiopental for human neuronal α_7 homomers expressed in *Xenopus* oocytes and with ketamine for high concentrations of nicotine for the sympathetic ganglionic nAChR-type of PC12 cells (Andoh et al., 1997; Coates et al., 2000; Coates & Flood, 2001; Furuya et al., 1999; Yamakura et al., 2000b). *Ketamine may also exert a use-dependent inhibition*, i.e. increasing current inhibition with repetitive ACH applications, as was demonstrated for $\alpha4\beta2$ and $\alpha4\beta4$ heteromers in some (Coates & Flood, 2001; Flood & Krasowski, 2000), but not all studies (Yamakura et al., 2000b). A use-dependent block of neuronal nAChR channels by barbiturates has not been reported to date.

Whole-cell recordings with the barbiturate *thiopental* have demonstrated a *voltage-independent inhibition* of nAChR activation-induced currents, i.e. the percentage of the current inhibition in the presence of thiopental was independent of the holding potential from–30 mV to –70 mV. Yet, only the $\alpha7$ homomer and the sympathetic ganglionic-type nAChR have been examined to date (Andoh et al., 1997; Coates et al., 2001). The *ketamine inhibition* of these receptor types and $\alpha4\beta4$ heteromers was similarly voltage-independent (Coates & Flood, 2001; Flood & Krasowski, 2000; Furuya et al., 1999), but a *voltage-dependent effect* was demonstrated for $\alpha3\beta4$ and $\alpha4\beta2$ heteromers (Coates & Flood, 2001; Yamakura et al., 2000b).

Single channel recordings of neuronal nAChR currents in the presence of barbiturates and ketamine are also lacking. Studies on the *muscle-type nAChR* have shown that clinically relevant concentrations of the barbiturates and ketamine *shorten the mean open time of the channel*, while the *amplitudes of the single currents remain unaffected* (Gage et al., 1985; Jacobson et al., 1991; Wachtel et al., 1988; Wachtel & Wegrzynowicz, 1992).

Also for the *muscle-type nAChR*, it has been shown that barbiturates and ketamine are able to interact with both, *open* and *closed states* of the channel, but *strongly prefer an interaction with the open state* (de Armendi et al, 1993; Dilger et al., 1997; Downie et al., 2000; Scheller et al., 1996). For the *neuronal nAChR*, the *data is less clear:* A preferential interaction with the open channel state is *not* supported by the data of Downie et al. (2000) for the neuronal, CNS-type $\alpha_4\beta_2$ nAChR. However, this study contradicts detailed *kinetic analyses* of nAChR-induced currents in sympathetic ganglionic neurons by Andoh and co-workers. Their data suggests an *accelerated current decay* in the presence of the anaesthetics, which is likely to be due to an *open channel block* and/or an *enhancement of receptor desensitization* (Andoh et al. 1997, Furuya et al., 1999, Sasaki et al., 2000).

Relatively *little is known about actual barbiturate and ketamine binding sites* on the nAChR. One study has detected barbiturate-sensitive, but not barbiturate-binding sites on the neuronal nAChR: Yamakura et al. (2000a) have shown that *single point mutations near the middle of the 2nd transmembrane segment* (M2) of the $\alpha_4\beta_2$ (at α_4-Val^{254} and β_2-Val^{253}) and $\alpha_4\beta_4$ (at α_4-Val^{254} and β_4-Phe^{255}) nAChR significantly *alters the channel sensitivity to pentobarbital, but not for ketamine*, when valine (Val) residues were replaced with phenylalanine (Phe) residues or vice versa. For the closed, i.e. the *resting or desensitized states of the muscle-type nAChR, possible binding sites have* been identified. As illustrated in figure 7, Arias et al. (2001) suggest that *pentobarbital is located within the channel pore*, in close proximity to the narrow crevice of the channel that is presumed to be composed of a highly conserved leucine ring (Unwin, 2000). Ketamine appears to bind to a different site within the channel pore, which is located more towards the extracellular end of the pore. Yet, an alternative ketamine-binding site at the intracellular side of the narrow crevice cannot be excluded, either (Arias et al., 2002).

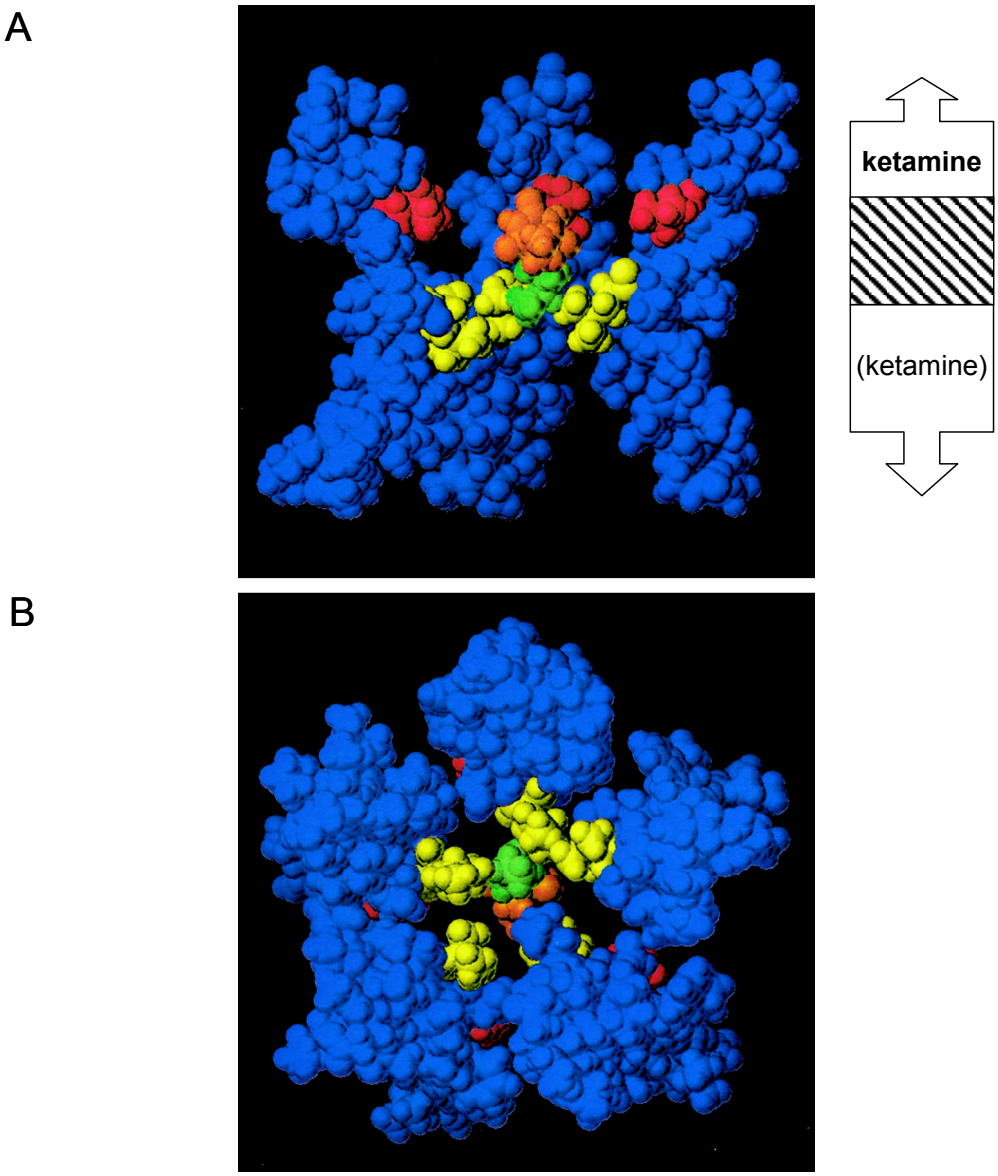

Figure 7: *Model of the complexion of pentobarbital with the pore-lining M2 segments of the (muscle-type) nAChR in the closed (resting) state* (adapted from Arias et al., 2001, p. 504)

Blue: Pore-lining 2nd transmembrane segments (M2).
Red: Residues at position 13 of M2.
Yellow: Residues at position 9 of M2.
Orange: Pyrimidine ring of pentobarbital.
Green: 1-methylbutyl group of the 5' chain of pentobarbital.

A: *Lateral view of the channel pore complexes together with pentobarbital.*
The pentobarbital molecule is located between the residues 9 and 13 of the M2 segment, at the narrow crevice of the channel. The scheme on the right hand side illustrates that ketamine is likely to have a different location inside the channel pore, presumably between position 13 and 20 or alternatively beyond position 9 more towards the cytoplasm (see Arias et al., 2002). Only three of the five M2 segments are shown.
Top: extracellular end (c-terminal) of M2, bottom: cytoplasmic end (n-terminal) of M2.

B: *Cross-sectional view of the channel pore complexes together with pentobarbital.*
Viewed from the cytoplasmic end.

As Ca^{2+} homeostasis is crucial for the regulation of various neuronal functions (see chapter 1.3), it is of interest to find out if anaesthetics alter intracellular Ca^{2+} signalling. This is a central part of the present thesis and a research question mostly neglected by the mainly electrophysiological approach of other groups. The relevance of this research question became apparent with studies demonstrating the high Ca^{2+} permeability of nAChR in rat intracardiac neurons and the finding that nAChR activation is followed by CICR from ryanodine-sensitive stores (see chapters 1.3.3 and 1.4.3). The importance of this (highly Ca^{2+} permeable) nAChR for the neurotransmission in intracardiac ganglia (see chapter 1.1) and its likely sensitivity to i.v. anaesthetics as suggested by studies from expression systems (see above) have further indicated that Ca^{2+} signals following nAChR activation may be significantly altered by general anaesthetics. *Voltage-dependent Ca^{2+} channels* represent another player of the neuronal Ca^{2+} signalling system and could also contribute to some of the Ca^{2+} signals studied in the present thesis (see chapter 1.3.3), but they are unlikely to play a direct role in the mediation of the anaesthetic effect or side effect, given that these channels, with few exceptions, *are relatively insensitive to clinically relevant concentrations of general anaesthetics* (reviewed in Franks & Lieb, 1994). Furthermore, little is known about the effects of i.v. anaesthetics on *intracellular Ca^{2+} release channels* in neurons. The data from other cell types is *controversial* and effects appear to vary with tissue type. For example, in rat papillary muscles, experimental evidence suggests that thiopental inhibits ryanodine-induced Ca^{2+} release from the sarcoplasmic reticulum (SR; Komai and Rusy, 1994), whereas in rat smooth aortic muscle, thiopental has been shown to induce Ca^{2+} release from the SR (Mousa et al., 2000). Studies from our lab on skeletal muscle preparations have demonstrated that (high) concentrations of general anaesthetics can enhance Ca^{2+} release from the SR (Kunst et al., 1999, 2000).

The present study investigates the effect of i.v. anaesthetics on parasympathetic intracardiac neurons. Given that modulation of nAChR in autonomic neurons may contribute to cardiovascular side effects of i.v. anaesthetics, it was of interest to determine if these drugs affect nAChR-activated membrane currents and cytoplasmic Ca^{2+} levels in rat intracardiac neurons.

1.3 Neuronal CA^{2+} -homeostasis

Intracellular *Ca^{2+} signalling* is mostly based on *(brief) pulses of Ca^{2+}*, i.e. transient increases of the intracellular, cytosolic free Ca^{2+} ion concentration $[Ca^{2+}]_i$. This seemingly simple Ca^{2+} signalling principle is known to regulate a *diversity of (Ca^{2+} -dependent) cellular processes* in mammalian cells, including excitability, exocytosis, contraction, metabolism, transcription, fertilization and proliferation. *Ca^{2+} -dependent cellular targets* or *effectors* include *Ca^{2+} -binding proteins* (e.g. calmodulin or troponin C), *Ca^{2+} -sensitive enzymes* (e.g. Ca^{2+}/calmodulin-dependent protein kinase, protein kinase C or adenylate cyclase), *transcription factors* (e.g. CREB-binding proteins) and *Ca^{2+} -dependent ion channels* (e.g. Ca^{2+} -activated potassium channels; reviewed in Berridge, 1998; Berridge et al. 2000, 2003). Yet, Ca^{2+} signals, in particular *excessive increases* of $[Ca^{2+}]_i$, have also been implied in *cell death*, including apoptosis and necrosis. The major *self-destructive mechanisms* that are triggered include *activation of catabolic enzymes*, *generation of free radicals*, and *impairment of cellular structures* and *functions of organelles*, in particular the *mitochondria* (see e.g. Berridge et al., 1998; Ferrari et al., 2002).

The key players of the complex Ca^{2+} signalling system are the *cell membrane* and the *membranes of organelles*, in particular the *endoplasmic reticulum (ER)*, as the equivalent to the sarcoplasmic reticulum (SR) of muscle cells, and the *mitochondria*. These organelles play an active role in the maintenance of the Ca^{2+} homeostasis of cells by acting as *Ca^{2+} storage facilities that* either take-up or release Ca^{2+} (see e.g. Berridge et al., 2003). The *nucleus* is affected by cytosolic Ca^{2+} signals, but *does not* seem to *play a major role in the generation of cytosolic Ca^{2+} signals* (reviewed in Bootman et al., 2000). Figure 8 gives an overview of the major Ca^{2+} signalling components.

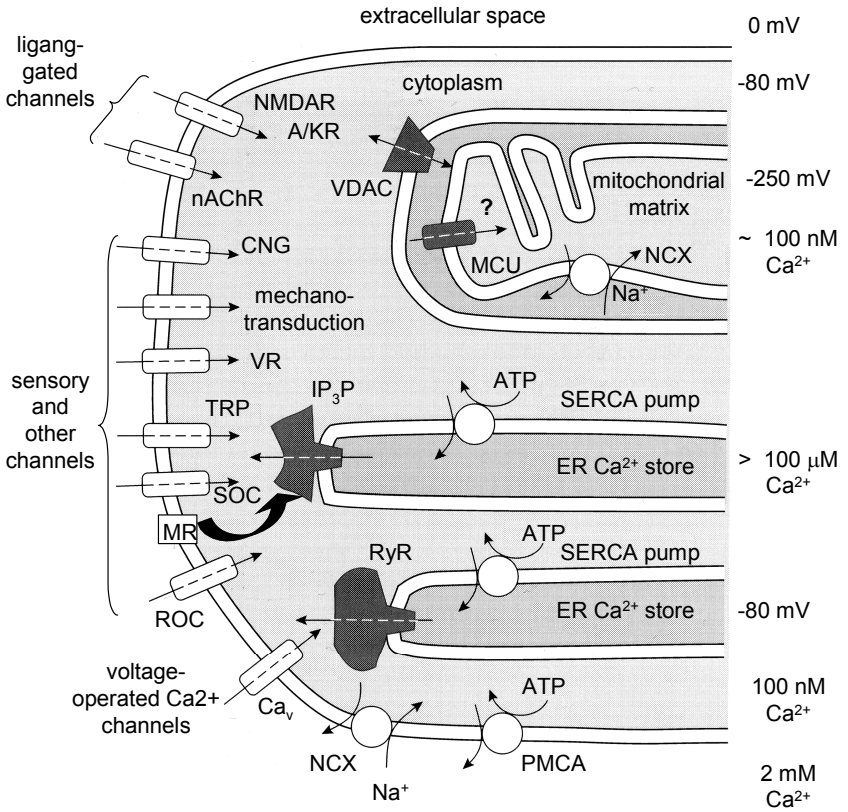

Figure 8: *Major components of the Ca^{2+} signalling system* (based on Hille, 2001; p. 271, adapted by M. Weber)

Important receptors and transporters for the Ca^{2+} signalling of various cell types illustrated in one cell.
The figure illustrates Ca^{2+} signalling components with a focus on Ca^{2+} permeable channels and transporters. The question mark besides the mitochondrial uniporter indicates that the corresponding molecule has not yet been identified and that RyR could alternatively carry out Ca^{2+} uptake in mitochondria. The thick, black arrow indicates metabotropic pathways such as IP_3 –mediated induction of Ca^{2+} release from the ER. All membrane potentials are measured against the extracellular fluid. Second-messenger-operated channels that are present in the cell membrane of specific cell types include the CNG, SOC, TRP and VR (see Hille, 2001; Bakowski & Parekh, 2002; Putney, 2003).

Legend: A/K AMPA/kainate receptor; ATP adenosine triphosphate; Ca_v voltage-dependent Ca^{2+} channel; CNG cyclic nucleotide gated channel; ER endoplasmic reticulum; IP_3R inositol-1,4,5-trisphosphate receptor; MCU mitochondrial Ca^{2+} uniporter; MR metabotropic receptor; nAChR nicotinic acetylcholine receptor; NCX Na^+/Ca^{2+} exchanger; NMDAR N-methyl-D-aspartate receptor; PMCA plasma membrane Ca^{2+} -ATPase; ROC receptor-operated channel; RyR ryanodine receptor; SERCA pump sarco(endo)plasmic reticulum Ca^{2+} -ATPase pump; SOC store-operated channel; TRP transient receptor potential channel; VDAC voltage-dependent anion channel; VR vanilloid receptor.

1.3.1 Concentration gradients for Ca^{2+} ions

Ca^{2+} signals take advantage of electrochemical gradients for Ca^{2+} ions across the cell membrane, and the membranes of the ER and the mitochondria: The *extracellular free Ca^{2+} ion concentration* is in the *low millimolar range* (~ 1-2 mM). The *free Ca^{2+} ion concentration in the cytosol* ($[Ca^{2+}]_i$) of a *resting* mammalian cell is *extremely low*, typically about *100 nM*, with a *range from about 30 to 200 nM* (see e.g. Armstrong et al., 2002; Hille, 2001). The concentration gradient for free Ca^{2+} ions between the exterior of the cell and the cytosol is thus ~ 10000:1. The resulting theoretical equilibrium potential for Ca^{2+} ions can be estimated using the Nernst equation:

$$E_{ion} = (R * T)/(z_{ion} * F) * \ln([ion]_o/[ion]_i) \quad (1)$$

where R is the gas constant, T the absolute temperature, z the charge of the ion, F Faraday's constant, $[ion]_a$ the free ion concentration outside of the cell and $[ion]_i$ the free ion concentration inside the cytosol. For calcium ions (z = +2), a temperature of 37 °C (= 310.15 °K), and the values of the constants R (= 8.3145 V * C * mol^{-1} * K^{-1}) and F (= 96485 C * mol^{-1}), equation (1) can be written as:

$$E_{Ca} = 0.0133634\ V * \ln([Ca]_o/[Ca]_i) \quad (2)$$

Assuming an extracellular free Ca^{2+} concentration of 1 mM to 2.5 mM (the latter was used in the present thesis), and a $[Ca^{2+}]_i$ of ~ 100 nM, then the *equilibrium potential* for Ca^{2+} ions is in the range of about +123 to +135 mV (see e.g. Hille, 2001; for formulas and constants).

A high concentration gradient for free Ca^{2+} ions also exists between the *ER* and the cytosol. The free Ca^{2+} ion concentration in the ER has been difficult to assess and varies somewhat depending on the measurement technique, but most studies have detected values in the range of *several hundred μM* (Alvarez & Montero, 2002; Meldolesi & Pozzan, 1998). While it is clear that Ca^{2+} ions in resting cells are driven from the SR/ER into the cytosol, the exact quantification of the driving force is speculative, as little is known about the electrochemical potentials across the SR/ER membrane (Fink & Veigel, 1996).

The free Ca^{2+} ion concentration in the *mitochondrial matrix* of resting cells is in the range of that in the cytosol $[Ca^{2+}]_i$ (~ 100 nM), but there is a considerable driving force

for Ca^{2+} ions into the mitochondrial matrix due to the negative membrane potential across the inner mitochondrial membrane (IMM; up to –180 mV against the cytosol; Brini, 2003), as illustrated in figure 8.

1.3.2 The dynamics of Ca^{2+} signalling

Berridge et al.(2000, 2003) describe the *onset of the cytosolic Ca^{2+} -signal* as an *"on-reaction"*, its *termination* as an *"off-reaction"* as illustrated in figure 9:

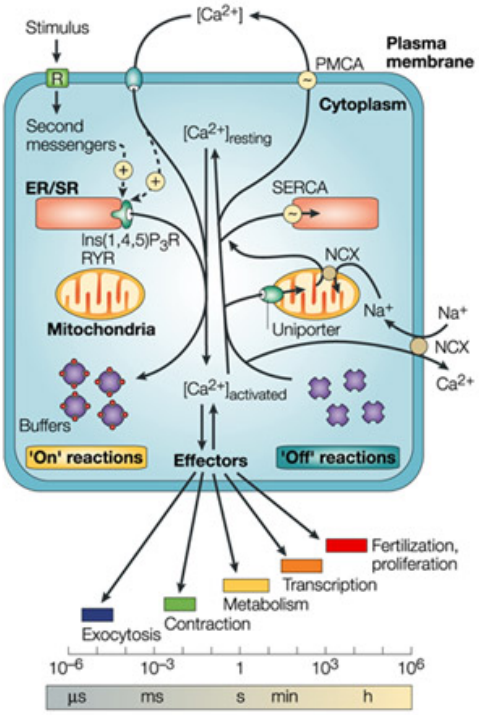

Figure 9: *The "on-" and "off-reactions" of the Ca^{2+} signalling system and the initiated responses* (from Berridge et al., 2003; p. 518)

Figure summarizing the steps from the initiation of the Ca^{2+} signal and the activation of the physiological response to the termination of the Ca^{2+} signal.
During "on reactions" a stimuli acts on receptors and initiates either a Ca^{2+} influx into the cytosol through Ca^{2+} permeable channels of the cell membrane or a Ca^{2+} release from the ER/SR through RyR or IP_3R channels. Most of the Ca^{2+} ions readily bind to Ca^{2+} buffers, but a small fraction binds to effectors (see beginning of chapter 1.3 for examples) to initiate cellular processes. This can require Ca^{2+} signalling to last from the microsecond up to the hours range. During "off reactions", Ca^{2+} separates from buffers and effectors and is removed from the cytosol and transported into the ER/SR, and the extracellular fluid through exchangers and ATP -driven pumps for Ca^{2+}. Mitochondria provide temporary Ca^{2+} storage by an initial, rapid Ca^{2+} uptake and a subsequent, slow release into the cytosol.

Legend: ER/SR endoplasmic/sarcoplasmic reticulum; $Ins(1,4,5)P_3R$ inositol-1,4,5-triphosphate receptor; NCX Na^+/Ca^{2+} exchanger; PMCA plasma-membrane Ca^{2+} -ATPase; R receptor; RyR ryanodine receptor; SERCA sarco(endo)plasmic reticulum Ca^{2+} -ATPase.

Interestingly, Ca^{2+} signalling can occur within very *different time frames*, ranging from several microseconds for exocytosis to several hours, e.g. for cell proliferation (see e.g. Berridge et al., 2003). When Ca^{2+} signalling is required over long periods of time long lasting rises of $[Ca^{2+}]_i$ can be avoided using $[Ca^{2+}]_i$ oscillations, i.e. repetitive, but brief rises in $[Ca^{2+}]_i$ (see e.g. Berridge et al., 1998).

The *spatial aspects* of Ca^{2+} signalling are similarly diverse, ranging from *local, subcellular* to *"global" Ca^{2+} signals* that affect the entire cell (reviewed in Berridge, 1997; Berridge et al., 2000). The present study has examined global, *spike-like events*, i.e. Ca^{2+} transients that almost instantly affect the entire cytosol where the fura-2 fluorescence signals that correspond to the Ca^{2+} signal, typically last *less than a minute* (see chapter 3).

The *onset* of the Ca^{2+} signal is basically due to an influx of Ca^{2+} ions across the cell membrane through *Ca^{2+} -permeable ion channels*, or to a Ca^{2+} release from intracellular stores, mainly the ER or SR, through the *Ca^{2+} permeable inositol-1,4,5-trisphosphate receptor* ($Ins(1,4,5)P_3R$; IP_3R) and *ryanodine receptor (RyR) channels*. Interestingly, *mitochondria are rather unlikely to contribute to the onset of the Ca^{2+} signal*, as Ca^{2+} ions are basically driven from the cytosol into the mitochondrial matrix due to the electrochemical gradient for Ca^{2+} ions across the IMM (see chapter 1.3.1).

The *activation of the intracellular Ca^{2+} release channels* is mediated through *second messengers*. Two newly discovered *intracellular Ca^{2+} release pathways* are the nicotinic acid adenine dinucleotide phosphate (*NAADP*) and the *sphingolipid*-derived messenger pathways. These pathways are *independent of* the traditional intracellular Ca^{2+} release mechanisms through *RyR* and *IP_3R channels* (Berridge et al., 2003).

IP_3R channels are tetrameric channels of identical or different subunits. Three different subunits types have been identified (Taylor & Laude, 2002). Ca^{2+} release from intracellular stores through IP_3R channels is accomplished through a *G-protein-mediated, phospholipase C (PLC) -dependent metabotropic pathway* that leads to the generation of the *freely diffusible second messenger IP_3* (see e.g. Aidley et al., 1998). IP_3 subsequently diffuses through the cytoplasm and binds to IP_3 receptors located in the membrane of the SR or ER where it evokes a Ca^{2+} release through the IP_3R channel given that a moderate $[Ca^{2+}]_i$ of ~ 100-300 nM is present (see e.g. Ehrlich et al., 1994). A PLC –dependent, and thus most likely IP_3 -mediated, Ca^{2+} release from intracellular stores has been demonstrated in rat intracardiac neurons following activation of metabotropic, purinergic receptors (P2YR; Liu et al., 2000b), as well as *muscarinic AChR (mAChR*; Beker et al., 2003). The

major steps of the suggested mAChR-induced Ca^{2+} mobilizing pathway are illustrated in figure 10 in chapter 1.3.3.

The other major group of intracellular Ca^{2+} release channels are the *ryanodine receptor channels (RyR)*, which are discussed in more detail in chapter 1.4.1. RyR channels are important for the Ca^{2+} signalling system, as the *Ca^{2+} acts as agonist on RyR channels* to induce *calcium-induced calcium-release (CICR)*, where Ca^{2+} release from the ER/SR through RyR channels is activated by increases in $[Ca^{2+}]_i$. CICR thus acts as an *amplifier of Ca^{2+} signals*. Our study (Beker et al, 2003) has also demonstrated the presence of *CICR following nAChR activation in rat intracardiac neurons*, as illustrated in figure 10.

Ca^{2+} permeable channels of the plasma membrane are the other major contributor to the onset of Ca^{2+} signals. Some Ca^{2+} permeable channels such as the *second-messenger-operated channels* (SMOC) *of the plasma membrane* are mainly present in specific cell types such as sensory neurons (see e.g. Hille, 2001; Bakowski & Parek, 2002; Putney, 2003). Figure 8 also illustrates the major SMOC.

Ca^{2+} -permeable channels that are present in most excitable cells are *receptor-operated channels (ROC)* and *voltage-operated Ca^{2+} channels (Ca_v)*. Voltage-operated Ca^{2+} -channels are discussed in more detail in chapter 1.4.2. Very Ca^{2+} -permeable ROC of the plasma membrane include the *N-methyl-D-aspartate receptor (NMDAR) channels* (Mayer & Westbrook, 1987), the *purinergic P2X receptor channels* and the *nAChR channels* (Rogers & Dani, 1995). Interestingly, these channel families are distinct with respect to their presumed evolutionary history, amino acid sequences and architecture (see e.g. Aidley, 1998; Hille, 2001).

Using patch-clamp whole cell recordings in combination with fura-2 measurements, Rogers and Dani (1995) have determined the *fractional Ca^{2+} current*, i.e. the percentage of the inward current that is carried by Ca^{2+} ions, through *NMDAR channels*. Using hippocampal neurons, a holding potential of –50 mV and a Mg^{2+} -free extracellular recording solution, it was determined as 12.4 %. Glutamate receptors are very common in the CNS, but are hardly present in the peripheral nervous system (PNS; e.g. Hille, 2001; Kemp & McKernan, 2002). While no study to date has demonstrated glutamate receptor-induced currents in rat intracardiac neurons, their presence in these cells cannot be totally excluded, given that polymerase chain reaction (PCR) and immunohistochemistry techniques suggests the presence of NMDAR and non-NMDAR subtypes also in cardiac ganglia (Gill et al., 1998).

The study of Gill and Dani (1995; see above) has determined the fractional Ca^{2+} current through *P2X receptors (P2XR)* channels in sympathetic neurons as 6.5 % under the experimental conditions outlined above. Fieber and Adams (1991b) have demonstrated the presence of functional Ca^{2+} permeable P2XR channels in rat intracardiac neurons. The *neuronal nAChR channel*, which is also very permeable to Ca^{2+} -ions, is discussed in more detail in chapter 1.4.3.

The *offset* of the $[Ca^{2+}]_i$ signals is due to a system of *ATP-driven Ca^{2+} pumps*, *exchangers,* and (possibly) *uniporters* that together with certain *proteins* remove free Ca^{2+} ions from the cytosol (see e.g. Berridge et al., 2000, 2003):

ATP-driven Ca^{2+} pumps include the *plasma-membrane Ca^{2+} -ATPases (PMCA)* and their relatives, the *sarco(endo)plasmic reticulum Ca^{2+} -ATPase (SERCA)* of the SR/ER membrane. These pumps are thought to transport Ca^{2+} ions out of the cytosol by allowing two Ca^{2+} ions to bind to cytosolic binding sites of the unphosphorylated pump. Subsequent binding and hydrolysis of ATP yields a conformational change of the pump that enables the access and the release of Ca^{2+} ions to the extracellular fluid in the case of the PMCA, or the lumen of the SR/ER in the case of the SERCA pumps, respectively (see e.g. Armstrong et al, 2002; Wuytack et al., 2002).

Mitochondria can also accumulate substantial amounts of Ca^{2+} ions in their interior compartment. The mitochondrial Ca^{2+} uptake system mostly is a low Ca^{2+} affinity mechanism, i.e. its activation requires large (local or global) rises of $[Ca^{2+}]_i$ (typically > 1 μM). Ca^{2+} ions are thought to pass the outer mitochondrial membrane (OMM) fairly freely through the large pores of the *voltage-dependent anion channel* (VDAC; porin), and subsequently enter the mitochondrial matrix according to their electrochemical gradient through *Ca^{2+} uniporters* located in the inner mitochondrial membrane (IMM; see chapter 1.3.1; Brini, 2003; Hajnóczky et al., 2002). Newer data suggests that RyR, which have been shown to be present in the IMM (Beutner et al., 2001), may alternatively be responsible for the mitochondrial Ca^{2+} uptake in excitable cells (Hajnóczky et al., 2002). The relatively rapid uptake of Ca^{2+} ions from the cytosol into the mitochondrial matrix is followed by a *slow release back into the cytosol*, which is mainly achieved by a *Na^+/Ca^{2+} exchanger (NCX)* supported by a *H^+/Ca^{2+} exchanger*. The *"permeability transition pores"*, which are permeable to Ca^{2+} ions and small molecules may also be involved in the mitochondrial Ca^{2+} -uptake and -release under certain (pathological) conditions (Babcock & Hille, 1998; Brini, 2003). *Na^+/Ca^{2+} exchangers* are also present in the plasma membrane of many cell types, as illustrated in figure 8 and 9.

Binding of Ca^{2+} ions to membrane surfaces and *proteins* inside the cell is another very important factor that contributes to the low resting $[Ca^{2+}]_i$. The great majority of Ca^{2+} ions inside the cell are actually bound to membrane surfaces and proteins. The *total Ca^{2+} concentration inside the cytosol* e.g. is in the range of 1-2 mM (see e.g. Armstrong et al., 2002). Mammalian cells possess a selection of Ca^{2+} binding proteins with different kinetic properties, including relatively fast Ca^{2+} binding proteins such as calbindin D-28 and calretinin, or slower ones such as parvalbumin (see e.g. Berridge et al., 2003). Endogenous buffer capacities have been shown to vary between different types of neurons (Palecek et al., 1999), probably due to variations in the intracellular concentration of their Ca^{2+} binding proteins. I am not aware of any study that has assessed the effects of the intracellular Ca^{2+} binding capacity of rat intracardiac neurons.

The following chapter describes the cholinergic Ca^{2+} signalling system in rat intracardiac neurons.

1.3.3 Cholinergic Ca^{2+} signalling in rat intracardiac neurons

Given that acetylcholine is the major neurotransmitter in rat intracardiac neurons (see chapter 1.1) and likely to evoke Ca^{2+} signals through activation of mAChR (see chapter 1.3.2) and the highly Ca^{2+} -permeable nAChR channel (see chapter 1.4.3), it can be reasoned that activation of cholinergic receptors may represent a particular important mechanism for the activation of Ca^{2+} signals in these cells. We have therefore examined the cholinergic Ca^{2+} signalling mechanisms in rat intracardiac neurons in more detail (Beker et al., 2003): It was shown that activation of both, mAChR and nAChR leads to a single, global intracellular rise in $[Ca^{2+}]_i$ following each agonist application:

Selective mAChR activation was achieved by applying ACh in the presence of mecamylamine to block nAChR channels. The resulting Ca^{2+} transient persisted in Ca^{2+} -free extracellular recording solution, but was abolished in the presence of U-713122, a PLC inhibitor. These data suggest that mAChR activation leads to an increase in $[Ca^{2+}]_i$ that is due to a PLC –dependent, and most likely IP_3 -mediated Ca^{2+} release from intracellular stores, as illustrated in the middle of figure 10.

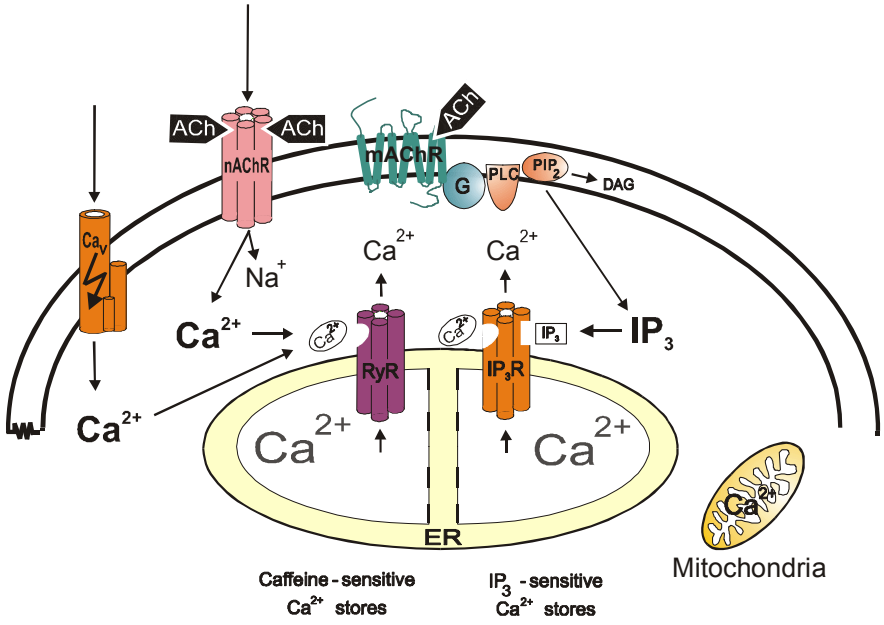

Figure 10: *Model of the Ca^{2+} mobilizing pathways following cholinergic receptor activation in rat intracardiac neurons* (from Beker et al., 2003, p. 1962; adapted by M. Weber)

The model summarizes the major steps likely to be involved in the generation of Ca^{2+} signals following cholinergic receptor activation.
Selective activation of nAChR induces Ca^{2+} influx through nAChR channels and a subsequent calcium-induced calcium release (CICR) from ryanodine-sensitive intracellular stores (Beker et al., 2003). In addition, nAChR –induced inward currents are likely to depolarize the cell membrane and activate voltage-operated channels including Ca^{2+} channels and initiate Ca^{2+} influx through these channels, which may similarly trigger CICR. Selective activation of mAChR induces Ca^{2+} release from intracellular stores through a PLC –dependent second-messenger pathway that is likely to generate IP_3 (Beker et al., 2003). The voltage-gated Ca^{2+} channel is illustrated with two auxiliary subunits (see chapter 1.4.2 for details of the receptor structure). Ca^{2+} pumps and transporters are not shown.
Legend: ACh acetylcholine; Ca_v voltage-operated Ca^{2+} channel; DAG diacylglycerol; ER endoplasmic reticulum; G G-protein; IP_3(R) inositol-1,4,5-trisphosphate (receptor); mAChR muscarinic acetylcholine receptor; nAChR nicotinic acetylcholine receptor; PIP_2 phosphatidylinositol-4,5-biphosphate; PLC phospholipase C; RyR ryanodine receptor.

In contrast, nAChR activation was achieved by applying ACh in the presence of atropine, a mAChR antagonist. $[Ca^{2+}]_i$ transients following nAChR activation depended on the presence of Ca^{2+} in the extracellular recording solution and Ca^{2+} -influx following nAChR activation induced CICR. The observed CICR was ryanodine-sensitive; suggesting that Ca^{2+} release from the ER through RyR channels amplifies the nAChR –induced Ca^{2+} transient as illustrated in figure 10.

Rathouz and Berg (1994) have demonstrated *activation of voltage-gated Ca^{2+} channels following nAChR activation* for chick ciliary ganglion neurons. It can be reasoned that the *nAChR -induced depolarization* of rat intracardiac neurons is similarly *likely to activate voltage-operated Ca^{2+} channels*, when cells are not clamped close to their resting membrane potential using the voltage-clamp technique (see chapter 1.5.3). The recruitment of voltage-operated Ca^{2+} channels is also likely to be intensified by a *concurrent activation of*

voltage-activated sodium channels. Influx of Ca^{2+} through voltage-operated Ca^{2+} channels is thus likely to contribute to the nAChR -induced $[Ca^{2+}]_i$ transient in unclamped cells.

The three receptor channel types, namely the nAChR, RyR and the voltage-gated Ca^{2+} channel, that are likely to be involved in the nicotinic Ca^{2+} signalling system are discussed in the following chapters in more detail.

1.4 Ion channels

The present chapter describes ion channels that are likely to play a crucial role in the Ca^{2+} signalling following nAChR activation, with a focus on nAChR. Voltage-gated Ca^{2+} channels and RyR channels are discussed more briefly.

1.4.1 Ryanodine receptor channels

Ryanodine receptor (RyR) channels are well known for their role in *excitation-contraction coupling in muscle cells*, but they have also been shown to *mediate Ca^{2+} release from the endoplasmic reticulum (ER) of non-muscle cells*, including *neurons* (see e.g. McPherson & Campbell, 1993b).

RyR are *homotetramers* of extremely large (~ 560 kDa) subunits that are sometimes associated with smaller immunophilins molecules (~ 12kDa; Sharma et al., 1998, 2000). Each of the main subunits contains a *very large N-terminal domain* (~ 4000 amino acids), where the ligand binding sites and regulatory sites are mostly located. The C-terminal domain (~ 1000 amino acids) corresponds to the pore containing *transmembrane assembly* with its *four transmembrane segments* (M1 to M4; Rossi & Sorrentino, 2002). The main part of the RyR is located on the cytoplasmic site of the SR/ER membrane, as illustrated in figure 11A.

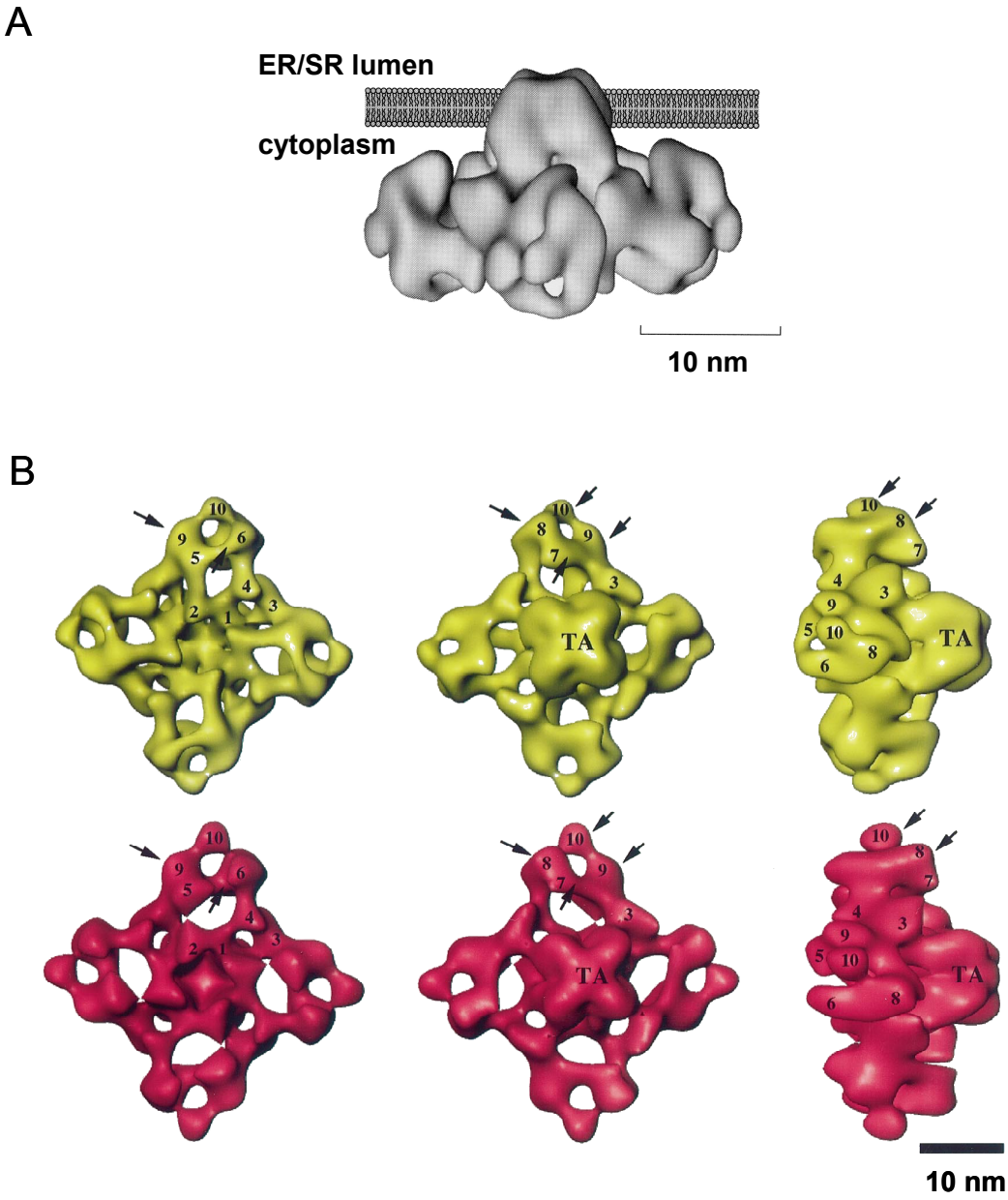

Figure 11: *Surface reconstructions of RyR channels* (based on Hille, 2001, p. 273; Sharma et al., 1998, p. 18432; adapted by M. Weber)

A: *Illustration of a RyR1 reconstruction together with the SR/ER membrane.*
The picture shows a side view of a 3-D reconstruction of a completely assembled tetrameric RyR1 channel in its location in the SR/ER membrane. The major part of the receptor extends into the cytosol. The channel reconstruction is based on cryo-electron microscopy.

B: *Comparison of the surface structure of reconstructed models of the RyR1 and RyR2.*
These surface structure images are also based on cryo-electron microscopy. The upper row shows a reconstruction of a RyR1 tetramer from different perspectives, the lower row that of a RyR2 tetramer. The pictures on the left side show the surfaces of the receptors that face the cytoplasm, the middle pictures those that face the SR/ER, and the pictures on the right show a side view. The arrows point towards differences between the RyR1 and RyR2, and the numbers on the upper subunit refer to 10 putative structural domains. TA denotes the transmembrane assembly.

The family of mammalian RyR includes *three subtypes* with a high average amino acid homology of about 70 % (Fill & Copello, 2002; Rossi & Sorrentino, 2002, Sharma et al., 1998, 2000). The *RyR1* and the RyR have been called *skeletal-type* and *cardiac-type*, respectively, for their predominance in these muscle tissues, and the *RyR3 brain-type* due to its presence in the brain. Yet, *each receptor type* is *expressed in a wide range of tissues. All three RyR types* are present in neurons of the *brain* (Fill & Copello, 2002; McPherson & Campbell, 1993a; Sharma et al., 2000), and the "cardiac type" is the most *predominant isoform in the brain* (Berridge, 1998, McPherson & Campbell, 1993a).

RyR channels are *fairly permeable to Ca^{2+} ions*, with selectivity for divalent ions over monovalent ions of approximately 5:1. They have *extremely large single channel currents* in the range of 30 to 130 pS (see Hille, 2001). These properties *ensure that large* (local) *rises of $[Ca^{2+}]_i$ can occur* following activation of (single) RyR. Furthermore, Ca^{2+} ions act as agonists on RyR: RyR *activate upon physiological rises of $[Ca^{2+}]_i$* from resting $[Ca^{2+}]_i$, but are inactive at low nanomolar and (unphysiologically) high, i.e. millimolar $[Ca^{2+}]_i$ (see e.g. Berridge et al., 2003; Ehrlich et al., 1994). These channel properties contribute to *calcium-induced-calcium-release (CICR)*, i.e. the phenomenon that (local) *rises in $[Ca^{2+}]_i$ can activate Ca^{2+} release from nearby RyR* that "sense" these rises in $[Ca^{2+}]_i$.

The *RyR1* is functionally different from the other RyR isoforms in that it uses the *dihydropyridine receptor (DHPR*; see chapter 1.4.2) as a *voltage sensor* for the depolarization of the cell membrane e.g. during excitation-contraction coupling in skeletal muscle: Following membrane depolarization, the DHPR initiates *Ca^{2+} -release through RyR1* channels of the SR via a *direct physical link* with RyR1, most likely via a protein-protein interaction. A major influx of Ca^{2+} ions across the cell membrane does not occur. Not all RyR1 channels are coupled to DHPR. These "uncoupled RyR1 channels" can be recruited through *CICR* where Ca^{2+} release from neighbouring, "coupled RyR1 channels", initiates a Ca^{2+} release from "uncoupled RyR1 channels". In contrast, activation of RyR2 or RyR3 is *independent of any physical link between the DHPR and RyR2* and is only achieved by CICR: A Ca^{2+} flux across the cell membrane through Ca^{2+} permeable channels, in particular voltage-gated Ca^{2+} channels (Ca_v), activates RyR channels to allow for a Ca^{2+} release from the SR/ER (Fill & Copello, 2002).

RyR are also activated by a number of other agonists, including *adenine nucleotides, caffeine,* and *ryanodine*. Ryanodine, however, is a difficult agonist to work with, given that low concentrations of ryanodine lock the RyR in a low conducting state, while channel inhibition occurs at high concentrations. The most commonly used *pharmacological*

activator of RyR is *caffeine*, which *easily penetrates the cell membrane*. It is thought to act by *enhancing the Ca^{2+} sensitivity of the RyR*, thereby enabling Ca^{2+} release from the SR/ER at resting $[Ca^{2+}]_i$ (Ehrlich et al., 1994; Fill & Copello, 2002; Herrmann-Frank et al., 1999; McPherson & Campbell, 1993b). Yet, RyR activation can be modulated by a number of intrinsic and extrinsic chemical agents (reviewed in Berridge et al., 2003), possibly including various anaesthetics. An interesting example of an intrinsic modulator of SR/ER Ca^{2+}-release S100A1, an intracellular Ca^{2+} binding protein of the EF-hand type: We (Most et al., 2003b) have shown that caffeine-induced Ca^{2+} release from intracellular stores in skeletal muscle is enhanced by S100A1, an intracellular Ca^{2+} binding protein of the EF-hand type. Interestingly, S100A1 has also been shown to enhance Ca^{2+} release from the SR in cardiac muscle through an interaction with the RyR2 (Most et al., 2003a). Due to the predominance of the RyR2 in neurons (see above), it can be speculated that S100A1 could also play a role in the mediation of Ca^{2+} release from neuronal ER. With respect to extrinsic modulators, other studies from our lab have shown that (high) concentrations of general anaesthetics can also modulate Ca^{2+} release from the SR in skeletal muscle (see chapter 1.4.2). Caffeine has also been used in the present study as a pharmacological means to activate RyR channels and to examine anaesthetic effects on RyR channels.

This approach is related to experiments by Smith and Adams (1999) and Beker et al. (2003) in which caffeine and ryanodine were used to demonstrate that *functional RyR channels are present in rat intracardiac neurons*, as activation of RyR by caffeine induced $[Ca^{2+}]_i$ transients that could be inhibited by high concentrations of ryanodine. Yet, no study to date has examined the distribution of RyR subtypes in rat intracardiac neurons.

1.4.2 Voltage-gated Ca^{2+} channels

Voltage-gated Ca^{2+} channels (Ca_v) are part of a *superfamily of voltage-gated channels* that includes the voltage-gated potassium and sodium channel families. Ca_v are *present in virtually all excitable cell types* and under physiological conditions mainly allow for a Ca^{2+} influx following membrane depolarization. They are *blocked by* a number of divalent cations including *Cd^{2+}, Co^{2+}, Mn^{2+}, Ni^{2+}* and *Mg^{2+}*, but are *permeable* for some other, *physiologically relatively unimportant divalent ions*, including *Ba^{2+}* or *Sr^{2+}*. Ca_v are *marginally permeable to monovalent ions*, but with extremely low permeability ratios in relation to that for Ca^{2+} ions (P_X/P_{Ca} ~ 1:1000; summarized in Hille, 2001).

The key component of all functional Ca_v is the *α1 subunit* (~ 190 kDa), which *includes* the *channel pore*, the *voltage sensor*, the *gating mechanism* and the most important *regulatory sites*. Most Ca_v additionally include one or several *auxiliary subunits* labelled α2, β, γ and δ (Catterall, 2000; Ertel et al., 2000; Hille, 2001). Figure 12 illustrates a *trans-membrane-folding model* of the α1 subunit of a Ca_v with an intracellular, auxiliary β subunit. The $Ca_v1.2$ shown here is expressed in cardiac muscle and a very similar form of this channel type is expressed in neurons (Catterall et al., 2000; Ertel et al., 2000).

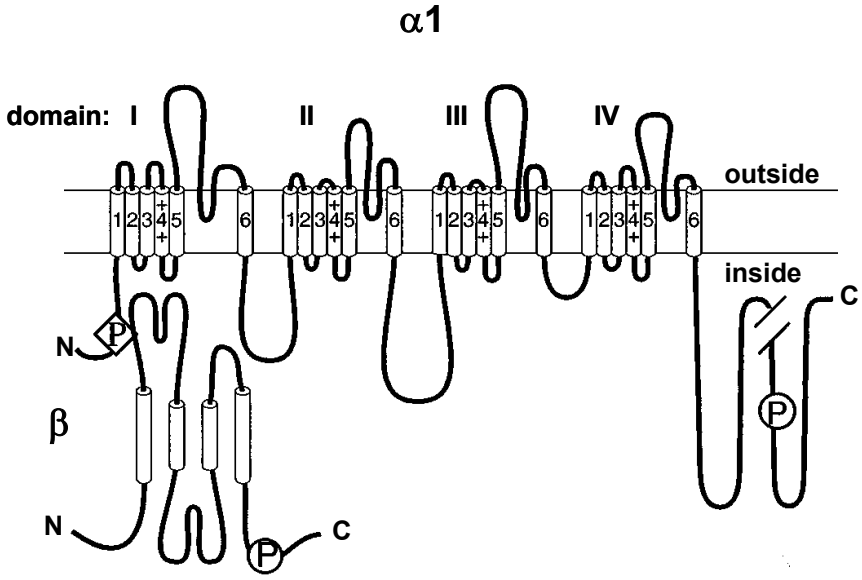

Figure 12: *Transmembrane-folding scheme of a voltage-gated Ca^{2+} channel* (based on Catterall, 2000, p. 527, adapted by M. Weber)

Model illustrating the α1 and β subunit of a cardiac-type $Ca_v1.2$ channel.
The α1 subunit of Ca_v consists of four domains with six transmembrane segments each. The aggregation of the 4 domains forms the channel pore. The 4th transmembrane segments of the domains in essence represent the voltage sensor. The β subunit contributes to the modulation of the channel behaviour. Both subunits contain sites that are phosphorylated by protein kinases. Presumed α-helices are drawn as cylinders.

Legend: α1, β subunits of the channel; C c-terminal; N n-terminal; P phosphorylation sites; I to IV are channel domains; 1 to 6 are transmembrane segments; + voltage sensors of the 4th transmembrane segments.

The α1 subunits of Ca_v consist of an alignment of *four domains that* form the channel pore. Each domain consists of *six transmembrane segments* (S1 to S6). The S4 segments of the domains are thought to correspond to the *voltage-sensor*, which undergoes a conformational change and initiates channel opening following membrane depolarization (Catterall, 2000).

The family of voltage-gated Ca^{2+} channels is very *heterogeneous* with respect to their *evolutionary history*, *electrophysiological* and *pharmacological properties*, as illustrated in figure 13:

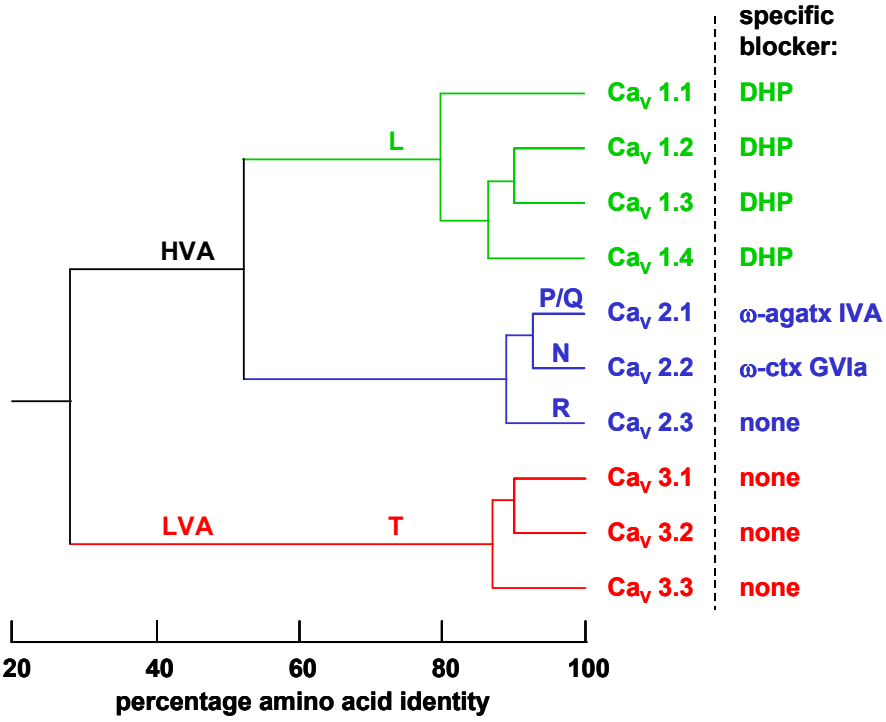

Figure 13: *The voltage-gated calcium channel family* (based on Ertel et al., 2000, p. 533; Catterall, 2000, p. 524; Hille, 2001, p. 117; adapted by M. Weber)

Comparison of the amino acid sequences reveals three subfamilies of voltage-gated calcium channels. Analysis of the amino acid sequences of α1 subunits has led to the identification of 10 family members ($Ca_v1.1$ to $Ca_v3.3$) of the voltage-gated calcium channel family, which can be grouped into three subfamilies labelled Ca_v1 to Ca_v3. Individual family members have distinct electrophysiological and pharmacological properties (see text).

Legend: Ca_v voltage-activated calcium channel; DHP dihydropyridines, HVA high-voltage activated (Ca_v); LVA low-voltage activated (Ca_v); L, N, P/Q, T and R refer to Ca_v subtypes according to a phenomenological nomenclature; Ca_v 1.1 to 3.3 refer to Ca_v subtypes according to a clone nomenclature; ω-agatx IVA ω-agatoxin IVA; ω-ctx GVIA ω-conotoxin GVIA.

Early electrophysiological experiments have revealed the existence of two major groups of Ca_v that were called *high-voltage activated (HVA)* and *low-voltage activated (LVA) calcium channels*. LVA Ca_v have a relatively *low activation threshold*, i.e. they only require a relatively minor depolarization for channel opening. Activation of LVA Ca_v is followed by a brief (single-channel) current that is terminated by a fast, and voltage-dependent inactivation mechanism. LVA Ca_v are also called *T-type* Ca^{2+} *channels* to describe the *t*iny conductance and *t*ransient single-channel current. They were originally discovered in cardiac muscle (Nilius et al., 1985), and later in neurons (Nowycky et al., 1985). In

contrast, the activation of HVA Ca_v requires a large depolarization of the cell membrane. These channels often lack a fast inactivation mechanism and can still be recorded when cells are held at depolarized membrane potentials. HVA Ca_v were originally called *L-type Ca^{2+} channels* to describe their *l*arge conductance and *l*ong-lasting single-channel currents. They are *sensitive to dihydropyridines* such as nifedipine or BayK8644 and are therefore called *dihydropyridine receptor (DHPR) channels* (Hille, 2001; Moreno Davila, 1999; Nilius et al., 1985). Dihydropyridine receptors are typically present in muscle cells, with a tissue specific subtype distribution, but at least two of the four subtypes are also present in neurons (see Catterall, 2000; Nowycky et al., 1985).

Further studies in *neurons* have revealed the presence of *HVA Ca^{2+} channels* that are *insensitive to dihydropyridines,* and with single-channel current characteristics in between those of the L- and T-type. These Ca_v types were originally called *N-type* Ca^{2+} channels to denote their presence in *n*eurons (Nowycky et al., 1985), but were later subdivided into a new N-type category and the P/Q-, and "R" –type categories due to distinct pharmacological properties: *N-type Ca_v* are *irreversibly blocked by low concentrations of ω-conotoxin GVIA*, and *P/Q –types* are sensitive to *ω-agatoxin IVA*. The "R"-type accounts for the *r*esidual current that is neither sensitive to ω-conotoxin GVIA nor ω-agatoxin IVA (see figure 13 for an overview). Aside from these pharmacological differences, however, these channel types are functionally very similar (Hille, 2001; Moreno Davila, 1999).

The *electrophysiological* and *pharmacological properties of Ca_v currents in rat intracardiac neurons* were examined in detail by Xu and Adams (1992b): Inhibition of the voltage-dependent whole-cell Ca^{2+} currents by Cd^{2+} had a half-maximal inhibition of 3.6 μM, and total current inhibition occurred at 100 μM. About 70 % of the voltage-dependent Ca^{2+} current was inhibited by a 300 nanomolar, i.e. maximally effective, concentration of ω-conotoxin GVIA, suggesting the *predominance of N-type Ca^{2+} channels in rat intracardiac neurons*. 50 % of the residual current could be inhibited by very high concentrations the dihydropyridine nifedipine, suggesting the *additional presence of L-type Ca^{2+} channels*. The demonstration of a ω-conotoxin GVIA and dihydropyridine –*in*sensitive current further suggests the presence of at least a third *type of Ca_v* in these cells. The I-V curve of the currents manifested the *dominance of HVA Ca^{2+} channels*, given that a large depolarization to about – 20 mV was required to initiate channel opening and that currents were maximal at about + 20 mV.

1.4.3 nAChR channels

nAChR channels are *cation-permeable ion channels* that mediate fast synaptic transmission. Activation of the nAChR under physiological conditions allows for an influx of cations that is accompanied by a transient membrane depolarization (see e.g. Aidley, 1998; Hille, 2001).

nAChR channels, with both their muscle and neuronal receptor type, are part of a *superfamily of fast-acting ligand-gated ion channels* described in chapter 1.2.4. The phylogenetic tree of this superfamily is also illustrated in figure 6 of chapter 1.2.4.

Mostly based on studies of the *muscle-type nAChR* channel from the electric ray *Torpedo* (see e.g. Aidley, 1998), these channels are thought to have a large *pentameric structure* of ~ 290 kDa (Miyazawa et al., 1999) in which the *five subunits enclose the common ion pore* (see figure 15). Based on biochemical studies, mutation experiments, and hydropathy plots, it is suggested that each subunit has a very large extracellular n-terminal domain, *four membrane-crossing segments* (M1 to M4), with a large cytoplasmic loop between M3 and M4 and a short extracellular c-terminal domain (Ortells & Lunt, 1995; Unwin, 2000). Figure 14 shows a hydropathy plot of a nAChR α-subunit.

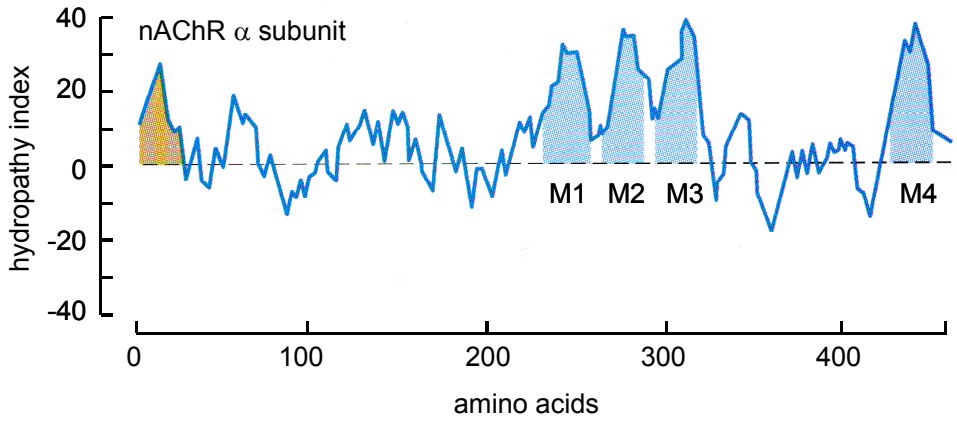

Figure 14: *Hydropathy indices of an α -subunit of the (muscle-type) nAChR* (adopted from Nicholls et al., 2001, p. 50, based on Schofield et al., 1987, p. 223)

Hydropathy indices are used to identify likely membrane-crossing segments of membrane receptors. Calculating a „moving sum" from hydropathy values of subsequent amino acids of the amino acid sequence derives the hydropathy index. Positive values correspond to lipophilic regions, negative values to hydrophilic regions. Brown regions indicate the signal sequence, blue regions the presumed transmembrane regions M1 to M4.

Hydropathy plots have contributed to models of the likely receptor structure as illustrated in figure 15.

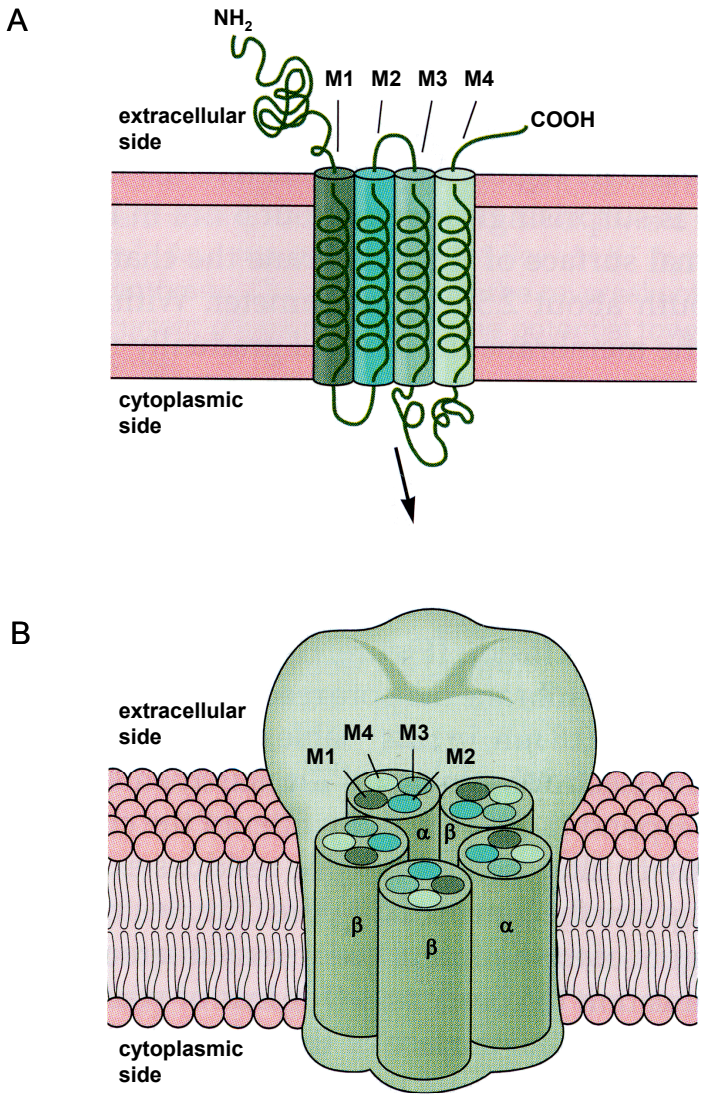

Figure 15: *Presumed membrane topology of the nAChR* (from Kandel & Siegelbaum, 2000, p. 200)

A: *Model of the membrane topology of an individual subunit.*
The model is based on hydropathy plots, biochemical studies, and mutation experiments.

B: *Model of the membrane topology of a nAChR with its five subunits.*
The model assumes an assembly of the five subunits around a central, common hydrophilic pore. The five M2 regions are the presumed pore lining segments (see text).

The membrane-spanning M2 regions mainly represent the pore forming segments of the ion channel (Leonard et al., 1988), but small fraction of the M1 segment also seem to contribute to the pore lining (Wilson & Karlin, 1998, 2001). The exact location of the channel gate is still fairly unclear: Cryo-electron microscopic data of Unwin (1995) suggests a location of the gate at a narrow kink that is formed by split α-helices of the pore lining M2-segents that extend into the channel pore at about the middle of the bilayer. In contrast, newer biochemical data indicates a location of the gate

more towards the cytoplasmic side of the channel (Wilson & Karlin, 1998). Cryo-electron microscopy has made it possible resolve more functionally relevant details of the channel structure, as illustrated in figure 16: (i) The cytoplasmic channel wall contains *transverse tunnels* that may act as (pre) -selectivity filter for ions in the vicinity of the channel pore. (ii) The extracellular channel wall contains *tunnels* that represent *access pathways for the ACh molecules to their binding sites*, as they connect the ACh binding sites with the adjacent water-filled space enclosed by the extracellular segments of the channel. The α *subunit* is thought to include the entire *ACh binding site*, but residues of neighbouring *"non-*α *subunits"*, namely the γ and δ subunits, are likely to contribute to the guiding of ACh into its binding sites (Miyazawa et al., 1999; Unwin, 2000).

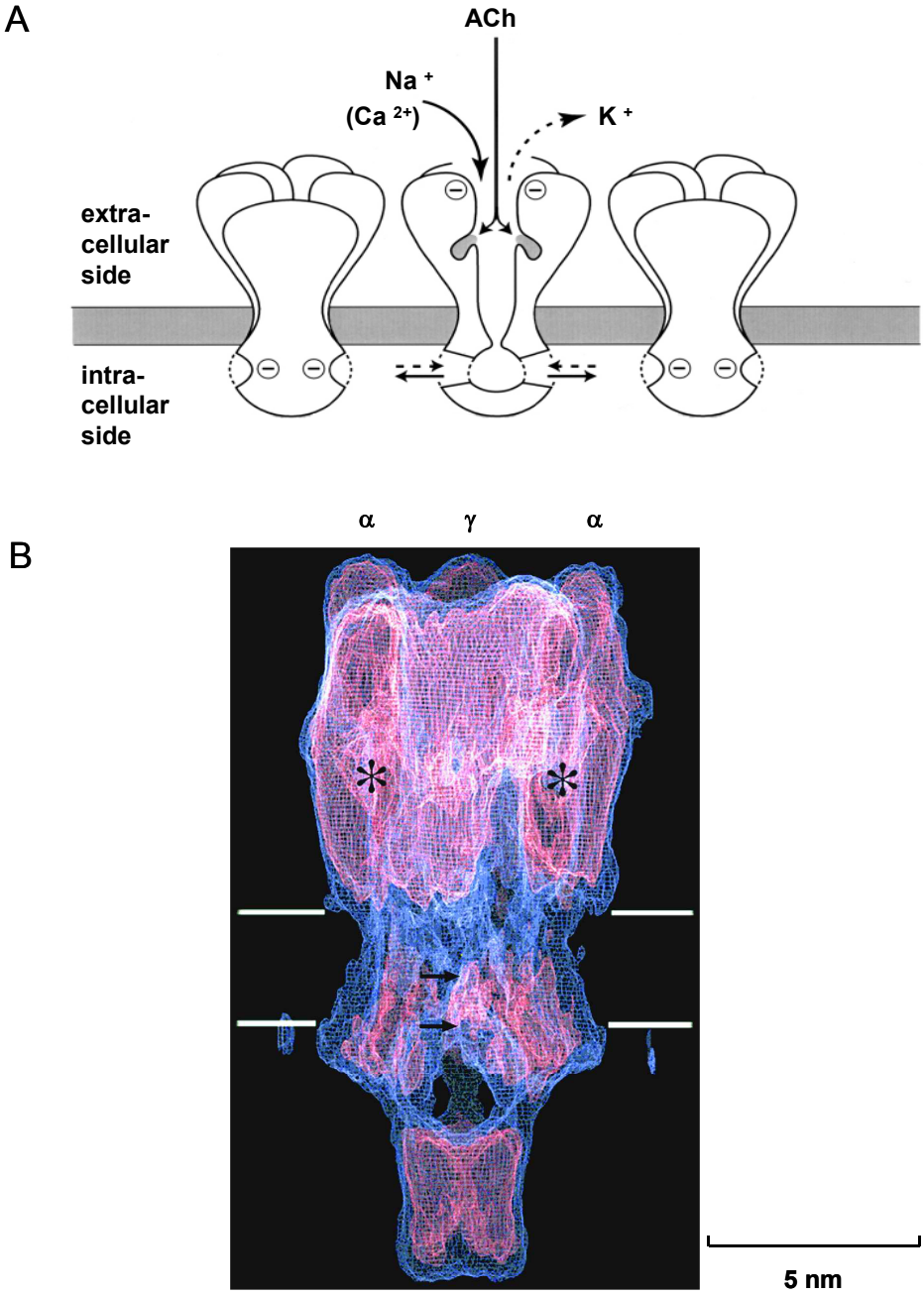

Figure 16: *Current model of the (muscle-type) nAChR* (based on Miyazawa et al., 1999, p. 180; Unwin, 2000, p. 1820; Hille, 2001, plate 4; adapted by M. Weber)

A: *Schematic illustration of the newly discovered tunnels of the nAChR.*
High resolution cryo-electron microscopy has revealed the presence of (i) access routes for ACh molecules to their binding sites in the extracellular wall of the α subunits and (ii) transverse tunnels in the cytoplasmic wall that may act as (pre-) selectivity filter for ions to the channel pore. Rapsyn molecules are likely to be linked to the cytoplasmic channel end are not shown. Ca^{2+} is printed in brackets due to the low Ca^{2+} permeability of the muscle-type, but the high Ca^{2+} permeability of the neuronal-type nAChR.

B: *Reconstruction model of the (muscle-type) nAChR channel based on cryo-electron microscopy.*
The entire receptor is ~ 160 Å long. The γ subunit is likely to lie directly in between the two α subunits, the δ subunit anticlockwise of the left α subunit, and the β subunit clockwise of the right α subunit. Asterisks indicate the putative binding sites for ACh in the extracellular channel wall. The upper arrow indicates the putative gate of the closed pore, and the lower arrow the constricting part of the open pore.

The fully assembled *fetal* (or extrajunctional) *muscle-type nAChR channel* is a *heteropentamer* that closely resembles the nAChR of the electric ray Torpedo: It includes two α subunits and three non-α subunits, namely one β, γ and δ subunit each ($\alpha_2\beta\gamma\delta$). The *adult* (or junctional) *muscle-type nAChR channel* has a somewhat different structure ($\alpha_2\beta\varepsilon\delta$) that contains one ε subunit instead of the γ subunit (Dilger, 2002; Hille, 2001; Waxham, 1999). The highly conserved muscle type α and β subunits have been denoted α1 and β1, respectively, to avoid confusion with newly discovered nAChR subunits in neurons (McGehee, 1999, Role & Berg, 1996). *Muscle-type nAChR channels* are *sensitive to α- bungarotoxin*, and have a relatively *low Ca^{2+} permeability* (Le Novère et al., 2002), as illustrated in figure 17:

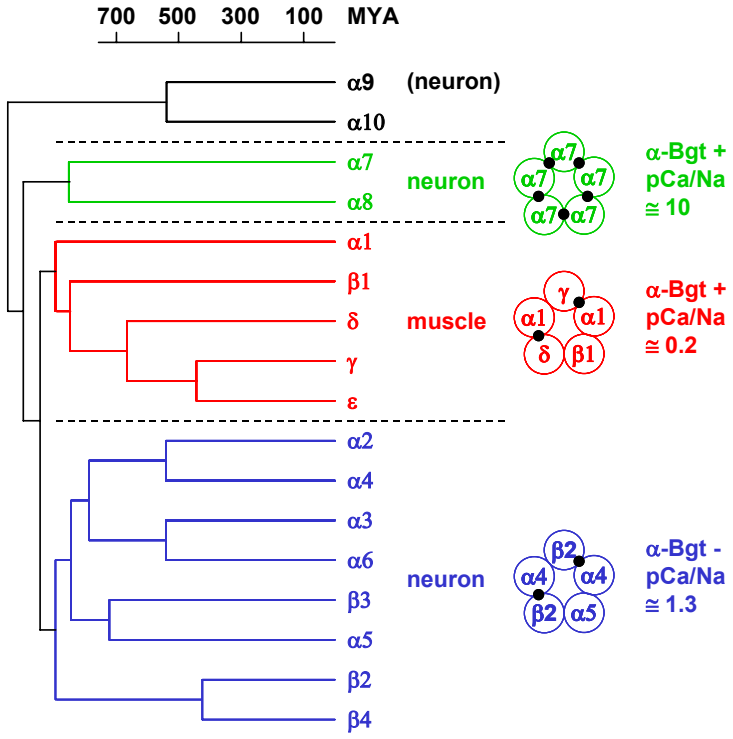

Figure 17: *The phylogeny of nAChR subunits* (based on Le Novère et al., 2002, p. 448)

Phylogenetic differences of nAChR subunits are related to different properties of the assembled channels. The length of each horizontal tree branch corresponds to the approximated time between the divergence of individual subunits and their "subunit ancestors". Phylogenetic differences are related to particular channel properties e.g. the α-bungarotoxin sensitivity or the Ca^{2+} permeability of the channels. The drawings on the right hand side indicate subunit compositions of assembled channels with the presumed ACh binding sites drawn as black dots.

Legend: α1 to α10, β1 to β4, γ, δ and ε are nAChR subunits; α-Bgt α-bungarotoxin; + sensitive; – insensitive; MYA million years; pCa/pNa relative Ca^{2+}/Na^{+} permeability of the channel; • presumed ACh binding sites.

Neuronal nAChR channels are also *pentameric pore-forming membrane proteins*, but they are more diverse than the muscle type, given that they are assembled from a pool of nine α (α2-α10) and three β (or "non-α") subunits (β2-β4; Elgoyhen et al., 2001; Le Novère et al., 2002; McGehee, 1999). The neuronal-type α subunits are homologous to the muscle-type α1 subunit and (with the possible exception of the α_5 subunit) include the key residues that form the ACh binding site. The nomenclature for the *neuronal-type β subunits* is unfortunate, given that they are rather *distinct from the muscle-type β1 subunit* (Le Novère et al., 2002; McGehee, 1999). Furthermore, neuronal-type nAChR can form *functional homopentamers*: *"α9 and α10 form homopentamers by themselves and heteropentamers together. Similarly, α7 and α8 make up homopentamers on themselves and heteropentamers together. α2-α6 and β2-β4 are included in a range of complex heteropentamers […]"* (Le Novère et al., 2002, p. 448), in particular heteromers that are assembled from combinations of α and β subunits (McGehee, 1999). Interestingly, *currents through homomeric nAChR can be blocked by* nanomolar concentrations of *α-bungarotoxin*, while currents through nAChR channels of the various α/β combinations cannot (Elgoyhen et al., 2001; McGehee, 1999).

Interestingly, the *Ca^{2+} permeability of neuronal nAChR* is *several folds higher than* that of the *muscle type* (Costa et al., 1994; Vernino et al., 1992; 1994). It is thus not surprising, that the *"fractional Ca^{2+} current"* (see chapter 1.3.2) through neuronal nAChR channels is very high, ranging from 4.7 % in rat sympathetic neurons to 11.7 % in expression systems for the α7 nAChR channel, when cells are clamped at potentials from –50 to –70 mV (Fucile et al., 2003; Rogers & Dani, 1995; Rogers et al., 1997). Several studies have confirmed the particularly high Ca^{2+} permeability of the α7-homomeric channel (see e.g. Castro & Albuquerque, 1995; Seguela et al., 1993). This channel property may be physiologically significant, in particular as the α7-homomeric channel, unlike the NMDA receptor channel, allows for its substantial Ca^{2+} influx from resting membrane potentials without prior and strong depolarization (Couturier et al., 1990; Role & Berg, 1996). Substantial Ca^{2+} fluxes through neuronal nAChR channels have not only been demonstrated with electrophysiological techniques, but also using intracellular Ca^{2+} fluorescent indicators (see e.g. Fucile et al., 2003; Rathouz & Berg, 1994; Rogers & Dani, 1995; Rogers et al., 1997; Vernino, 1994). The latter is important as they demonstrate that activation of neuronal nAChR can lead to intracellular Ca^{2+} signals. Taken together, these results indicate that *neuronal nAChR* are likely to represent an

important player in the generation of intracellular Ca^{2+} signals (Rathouz et al., 1997). The Ca^{2+} permeability of some neuronal nAChR channels is indicated in figure 17.

The *pharmacological profiles* to various agonists as well as antagonists (Chavez-Noriega et al., 1997; Le Novère et al., 2002; McGehee, 1999; Michelmore et al., 2002) as well as the *desensitization characteristics* of neuronal nAChR channels have been shown to *vary between nAChR channels of different subunit compositions* (Le Novère et al., 2002; Quick et al., 2002).

Such differences are interesting, as *nAChR channels* expressed *in the CNS differ from* those *expressed in the peripheral nervous system*: Prominent subunit gene products in the *CNS* are the β2 and in particular the *α4, but hardly the α3 subunit*. In contrast, the *α3, but not the α4 subunit* is very *prominent in the PNS* (McGehee, 1999; Role & Berg, 1996).

In *rat intracardiac neurons*, the *α3-subunit* and either the *β2* or *β4-subunits* mainly contribute to the nAChRs, but there is evidence suggesting that *α7 homomeric channels may also be present*, given that gene products for α7 subunits are present in about half the cells studied, and nAChR-induced whole-cell currents were partly blocked by the homomeric nAChR channel blocker α-bungarotoxin (see above; Bibevski et al., 2000; Cuevas & Berg, 1998; Hogg et al., 1999; Poth et al., 1997).

Adams and co-workers have determined the permeability of the nAChR channel for various ions (X) in relation to that for sodium ions (P_X/P_{Na}) in rat intracardiac neurons: (i) The channel is *hardly permeable to anions*, with a relative permeability for chloride ions $P_{Cl}/P_{Na} \leq 0.05$ (Fieber & Adams, 1991a). (ii) The channel is only *weakly selective among the alkali metals*: The relative permeability (P_X/P_{Na}) for Cs^+ and K^+ were determined as 1.27 and 1.23, respectively. (iii) The *selectivity among* the *divalent cations* is similarly *weak*, with relative permeabilities (P_X/P_{Na}) for Mg^{2+}, and Ca^{2+} of 1.1 and 0.65, respectively (Nutter & Adams, 1995). Fieber and Adams (1991a) have determined an even higher P_{Ca}/P_{Na} of 0.93. *The Ca^{2+} permeability of the nAChR channel in rat intracardiac neurons* is thus approximately four to six folds higher than that of the cholinergic skeletal muscle endplate channel (Adams et al., 1980).

The fundamental *electrophysiological properties* of nAChR –induced whole-cell currents in rat intracardiac neurons have been examined by Fieber and Adams (1991a): Application of ACh using a focal pressure application system (see chapter 2.5) on voltage-clamped neurons held at negative holding potentials and exposed to PSS was followed by the onset of an inward-current within milliseconds. The activated current lasted for several seconds. The current-voltage (I-V) relation curve of nAChR -induced

currents displayed a *strong inward rectification* with a reversal potential of about – 3 mV, when the patch-pipette contained a Cs^+ -based solution to block K^+ currents. The inward rectification of the channel did not depend on the presence of Cs^+ ions, but was also observed when Cs^+ was replaced by K^+ as the main cation in the pipette solution.

In sum, in rat intracardiac neurons, *activation of the nAChR under physiological conditions,* allows for an *influx of mainly Na^{2+} and Ca^{2+} ions* that is accompanied by a transient *membrane depolarization* and a *substantial increase in cytoplasmic Ca^{2+} levels which may be further amplified by CICR from ryanodine sensitive stores* (Beker et al., 2003) and possibly also voltage-gated Ca^{2+} channels.

The view presented so far was too simplistic in that it has neglected the presence of *subconducting*, as well as *desensitized channel states* (see e.g. Aidley, 1998; Hille, 2001). While subconducting states are basically demonstrated in single channel recordings, desensitization can easily be observed in whole-cell recordings. In the case of the nAChR, desensitization corresponds to (partial) *inactivation of the channel following prolonged or repeated exposure to agonists* such as ACh (Ochoa et al., 1989). The (onset of) desensitization can on occur on several time scales (Feltz & Trautmann, 1982; Sakmann et al., 1980) and it can be modulated by endogenous and exogenous chemical agents (possibly including anaesthetics, see chapter 1.2.4), as well as covalent modifications of the channel structure (Ochoa et al., 1989). The *time course of the recovery process from desensitization* can similarly occur on several time scales, ranging from *seconds* to *minutes* following removal of ACh (Hille, 2001). As desensitization affects the size of the physiological response, e.g. the current or $[Ca^{2+}]_i$ response following nAChR activation, it is crucial to *avoid, minimize* or *control the extent of any desensitization* in the experiment. It should e.g. be ensured that: (i) Agonists are only briefly applied. (ii) Higher than necessary agonist concentrations are avoided. (iii) Agonist application is followed by a thorough washout of the perfusion chamber. (iv) The time intervals in between subsequent agonist applications are sufficiently long, or at least (v) kept constant for both, the experimental and control condition. These points have also been taken into account during the experiments of the present thesis (see chapter 2.5).

1.5 Measurement techniques

The present thesis has focused on *cell physiological techniques*, i.e. *ratiometric Ca^{2+} fluorescence* measurements and *patch-clamp* recordings in rat intracardiac neurons. Photospectrometry recordings supplemented these studies as an independent means of artefact control for the Ca^{2+} fluorescence measurements.

1.5.1 Spectrophotometry

Spectrophotometry can be used to *measure the absorption spectra* of solutions. In the present thesis, this technique was used to assess, whether cadmium heavy metal ions or (lipophilic) i.v. anaesthetics that are present in the solutions (see chapter 3.1) interfere with the absorption characteristics of the Ca^{2+} indicator fura-2. This was done as a means of *artefact assessment*, as various chemical agents, including heavy metal ions and lipophilic compounds, have previously been shown to interfere with the absorption properties of fura-2 and other fluorescent probes (Grynkiewicz et al., 1985; Marchi et al., 2000; Roe et al., 1990; Usai et al., 1999).

The basic idea of spectrophotometry is to illuminate a sample with *monochromatic light* and measure the amount of the *transmitted light*, i.e. the light that passes through the sample. By relating the amount of the transmitted light in the presence of the sample to that transmitted during a blank reading in the absence of the sample, it is possible to calculate the amount of light that was absorbed by the sample. Monochromatic light is typically generated by letting the light of one (or several) light sources pass through several optical elements onto an *optical grating*, which generates a *diffraction pattern* of light that involves a range of different wavelengths. The wavelength of the generated light depends on its angle in relation to the grating (see e.g. Vogel, 1997). By positioning a so called *exit slit* at a certain angle in relation to the grating, it is thus possible to shield all but a single wavelength from passing through the exit slit and the sample located behind the slit. By changing the orientation of the grading, varying wavelengths can alternatively be passed through a fixed exist slit and an entire *absorption spectrum* of a sample can be determined. After the exit slit, the light passes series of mirrors, the sample itself and it is finally detected by a *photodiode detector* (see e.g.: http://www.beckmancoulter.com; or: Operating instructions, DU Series 600 Spectrophotometer, Beckman Instruments, Inc., Fullerton, CA, USA). A scheme of the photospectrometer that was used in the present thesis is presented in figure 21 in chapter 2.2.

1.5.2 Fura-2 fluorescence recordings

Fluorescence is an attribute of certain chemical compounds called *fluorophores*. It is a very brief form of *luminescence*, which Lankowicz (1983, p. 1) describes as *"the emission of photons from electronically excited states"*. The *fluorescence lifetime*, during which a fluorescence compound is in an excited state, typically lasts about 10^{-8} seconds. This excited state is caused by *absorption* of light, i.e. an input of energy for the subsequent fluorescence *emission* as well as other forms of "energy disposal". "Energy disposal" other than fluorescence emission is the reason for the so called *stokes shift* (see e.g. Vogel, 1997), i.e. the phenomenon that fluorescence excitation occurs at lower wavelengths (i.e. higher energy) than fluorescence emission (see figure 18 for fura-2). Using specific wavelength filters or dichroic mirrors, stokes shift can be used to ensure that only the emitted light, but not the excitation light, reaches the detection unit of a fluorescence microscope.

The development of fluorescence microscopic techniques together with highly Ca^{2+} sensitive fluorescent dyes have enabled the study of intracellular Ca^{2+} signals in intact, living cells at a high spatial and temporal resolution. Roger Y. Tsien and co-workers have undertaken the key steps towards modern intracellular Ca2+ indicators, by developing *highly Ca^{2+} -sensitive (fluorescent) buffers* with a high *selectivity against magnesium ions and protons* (Tsien, 1980). Furthermore, *membrane permeable Ca^{2+} dyes* that can be *loaded into cells without disrupting the cell membrane* were developed: These dyes were based on the previously developed polar Ca^{2+} dyes to which *esterifying groups* were *added* to *mask* their *polar groups*. Once inside the cell, de-esterification by endogenous esterases takes place, thereby trapping the polar dye molecules inside the cell (Tsien, 1981). Finally, *dual-wavelength ratiometric dyes* were developed (Grynkiewicz et al., 1985). Before that, only *single-wavelength intensity modulating dyes* that – upon binding to Ca^{2+} - merely change the *intensity* of their excitation and emission spectra were available. This is different with the *two types of dual-wavelength dyes* developed by Tsien and co-workers, namely the *dual-emission* and *dual-excitation* dyes (Grynkiewicz et al., 1985): Upon binding to Ca^{2+}, dual emission dyes such as indo-1 display marked shifts of their emission spectra, while dual excitation dyes such as fura-2 shift their excitation spectra, (summarized in Kao, 1994). Figure 18 illustrates how different Ca^{2+} concentrations affect the excitation and emission spectra of fura-2: The intensity of the emitted light (at 510 nm) from fura-2 containing solutions increases with increasing free Ca^{2+} concentrations when excited with 340 nm (F_{340}), but decreases when excited with 380 nm (F_{380}). This effect is used advantageously during ratiometric fura-2 recordings, as the *excitation* of the sample is *switched rapidly between 340*

nm and *380 nm*. Each F_{340} recording is then put into relation to its subsequent F_{380} recording by calculating the ratio F_{340}/F_{380} ($R(F_{340}/F_{380})$) and an established calibration procedure (see chapter 2.3; Grynkiewicz et al., 1985) relates each $R(F_{340}/F_{380})$ value to a corresponding free Ca^{2+} concentration. The great advantage of the ratiometric technique over the single-wavelength approach to approximate $[Ca^{2+}]_i$ is the *relative independence* of *$R(F_{340}/F_{380})$ from mere fluorescence intensities and changes thereof*. This procedure is based on the idea that *changes in fluorescence intensities that are unrelated to changes in* $[Ca^{2+}]_i$ are likely to affect F_{340} and F_{380} in a similar manner, but the creation of the ratio $R(F_{340}/F_{380})$ eliminates this (unwanted) effect. In cells loaded with fluorescent Ca^{2+} indicators, changes of emitted fluorescence intensities that are unrelated to changes in $[Ca^{2+}]_i$ include *loss of dye* by bleaching or leakage, varying *cell thickness* and changing *illumination intensities* (see e.g. Grynkiewicz et al., 1985; Kao, 1994). Yet, the ratiometric principle is only applicable under the assumption that the *$[Ca^{2+}]_i$* remains basically *unchanged within one recording cycle* including one illumination at 340 nm and one at 380 nm. This assumption only holds true if switches between recordings at 340 nm and 380 nm illumination can be executed very rapidly, typically in the low millisecond range. Figure 18 shows the *excitation* and *emission spectra* of Ca^{2+} -free and -saturated solutions.

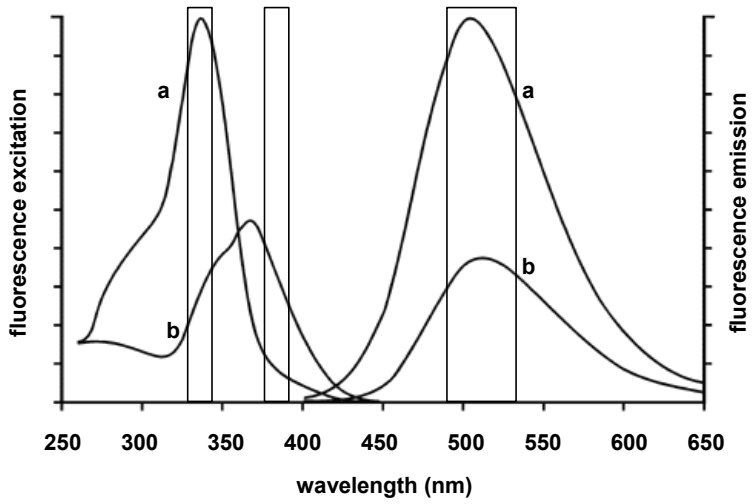

Figure 18: *Excitation and emission spectra of Ca^{2+} -free and Ca^{2+} -saturated fura-2 calibration solutions* (adopted from Molecular Probes, Inc., http://www.probes.com)

Wavelength shift for fura-2 excitation spectra but not for its emission spectra.
For excitation spectra recordings (the curves on the left), light was collected at 510 nm. For emission spectra recordings (the curves on the right), excitation was at 340 nm only. Vertical bars indicate the full width at half maximum (FWHM) of the excitation or emission light obtained by typical excitation or emission filters in fura-2 experiments (for filter spectra see e.g. Omega Optical, Inc., http://www.omegafilters.com).

Legend: (a) Ca^{2+} -saturated fura-2 calibration solutions; (b) Ca^{2+} -free fura-2 calibration solutions (see chapter 2.5; Grynkiewicz, 1985).

From figure 18, it becomes apparent that the *peaks of the emission spectra* of Ca^{2+} bound and Ca^{2+} free fura-2 fall within a very narrow range of each other. Furthermore, the 510 nm emission filters used in fura-2 experiments typically have a greater FWHM than the excitation filters, as more photons can be collected when broader filters are used. The 510 nm bandpass filter can even be totally omitted under some circumstances to collect photons emitted from an even wider range of the emission spectra, given that a dichroic mirror properly separates between the excitation and emission spectra.

1.5.3 Patch-clamp recordings

The patch-clamp technique became famous as an electrophysiological method that allows direct measurements of *single channel currents*. Yet, the famous publication of Neher, Sakmann and co-workers (Hamill et al., 1981) has not just provided detailed information on single-channel recording, but has already specified a *whole-cell recording configuration*. The process of establishing this traditional whole cell recording configuration is illustrated in figure 19A: After a tight seal between the patch pipette and the cell membrane has been established, (electrical) access to the cytosol is obtained by breaking through the membrane patch with a brief pulse of suction.

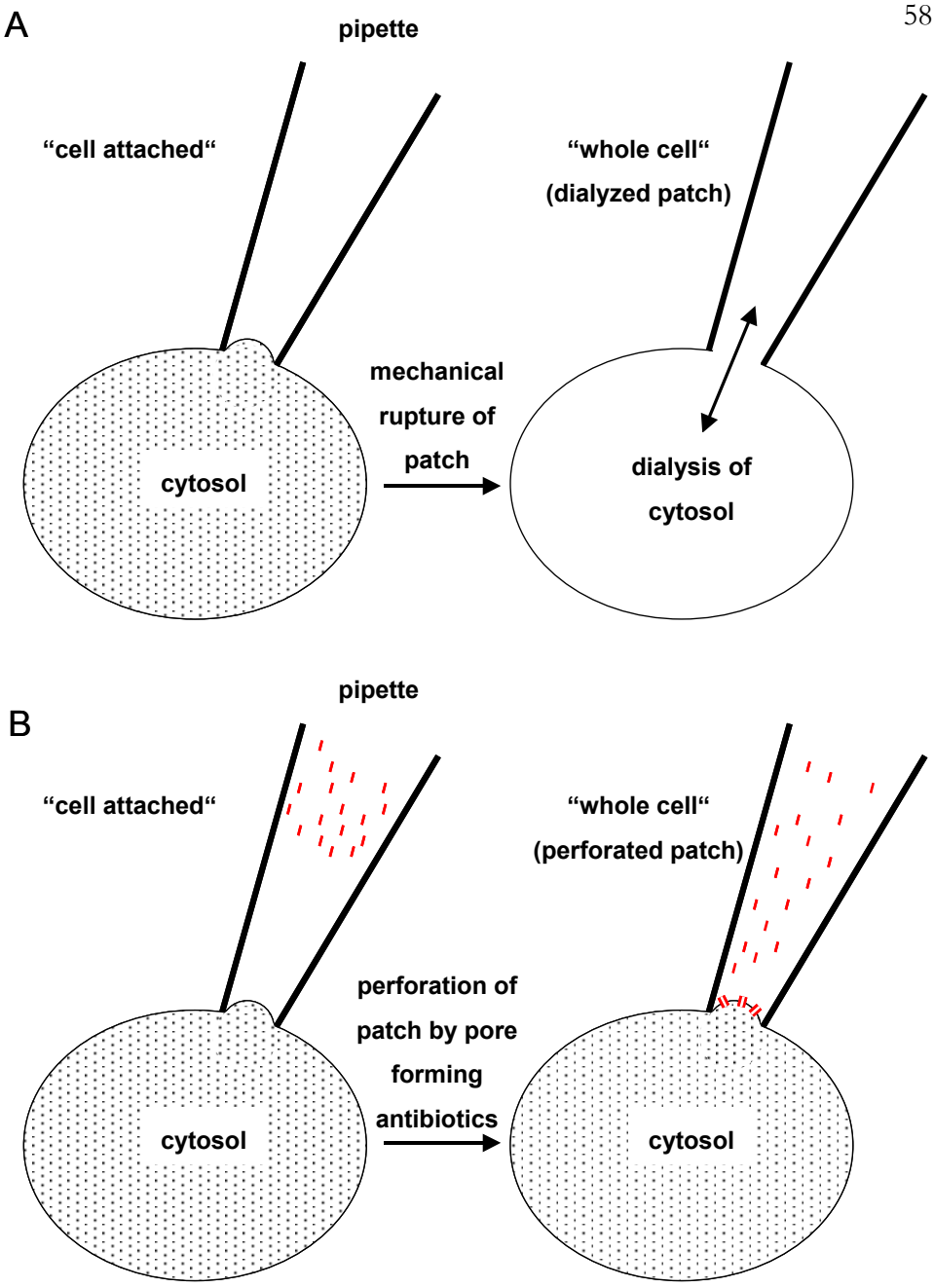

Figure 19: *Scheme of the procedures that lead to the whole-cell recording configurations of the patch-clamp technique* (based on Hamill et al., 1981, p. 93; Horn & Marty, 1988; Rae et al., 1991).

The cell-attached configuration, i.e. a tight seal between the pipette and the cell membrane is required before any of the whole-cell recording configurations can be established.

A: *The traditional ("dialysed-patch") whole-cell recording configuration*
Mechanical rupture of the patch provides electrical access to the cell interior and the cytosol is dialyzed with the pipette solution.

B: *The "perforated-patch" whole-cell recording configuration*
The tip of the patch pipette is filled with antibiotic-free solution to allow the establishment of a proper cell-attached configuration, as the antibiotic otherwise interferes with the seal formation. Due to diffusion, the antibiotics (illustrated as red spots) that were back-filled into the pipette, eventually reach the tip of the pipette where they form pores into the membrane patch enclosed by the pipette. As the pores are selective for small cations, electrical access to the cell interior is established while the macromolecular composition of the cytosol remains mostly undisturbed.

Whole cell patch-clamping offers several advantages in comparison with the traditional technique of inserting two microelectrodes into the cell: (i) *Leak currents*, which are a consequence of inserting a microelectrode into the cell, *can be neglected*. (ii) The seal between the pipette and the cell membrane can be in the range of several GΩ (the so-called giga-seal) thereby enabling recordings at a much *lower level of noise*. (iii) The standard form of whole-cell patch-clamping *(*the so-called *dialysed-patch recording)* involves the *dialysis of the cytosol* with the solution of the patch pipette. As the volume of the solution inside the patch-electrode is several orders of magnitude larger than that of the cell volume, the composition of the electrode solution basically dictates the composition of the intracellular milieu after completion of the dialysis, thereby providing a well-known intracellular solution (Marty & Neher, 1995; Numberger & Draguhn, 1996). However, dialysis of the cell interior also involves a washout of diffusible cytosolic components, including second-messengers such as cyclic adenosine monophosphate (cAMP) or IP_3, and any cellular process that depends on diffusible intracellular compounds will eventually be disturbed. This may explain the rundown of some physiological responses following the establishment of the dialysed patch configuration (Numberger & Draguhn, 1996). Depending on the experimental question at hand, this can either be an advantage or a disadvantage.

To avoid dialysis of the cytosol, the *"perforated patch"* whole-cell recording configuration has been developed by Horn and Marty (1988) and further improved by Rae et al. (1991). In perforated patch-recordings, electrical access to the interior of the cell is established with the help of *pore-forming antibiotics* such as nystatin (Horn & Marty, 1988) or amphotericin B (Rae et al., 1991). When solely applied from one side of the cell membrane, these antibiotics form pores that are selective for small cations such as Na^+ or K^+ ions (Numberger & Draguhn, 1996). Furthermore, the pores do not allow passage of divalent ions or uncharged molecules with a molecular weight above ~ 200 Da, which means that macromolecules cannot cross the cell membrane. Taken together, these properties leave the composition of the cytosol relatively undisturbed (Horn & Marty, 1988). Rae et al. (1991) have proposed a simple procedure obtain the perforated-patch configuration: The patch pipette is "tip-filled" with an antibiotic free solution and back-filled with the antibiotic-containing solution. The initial lack of antibiotics in the tip of the pipette allows establishing a tight seal of a proper cell attached configuration. Due to diffusion, the antibiotics eventually reach the tip of the

pipette and the cell membrane and form pores into the membrane patch as illustrated in figure 19B.

The *patch*-(voltage-)*clamp* technique is an *advanced form of the voltage-clamp* technique. Voltage-clamping in general make it possible to hold (= *"clamp"*) *the membrane potential* of cells at a desired value and simultaneously record currents across the cell membrane. The resulting control over the membrane potential has greatly facilitated the study of ion channels in cells, as it provides a possibility to specifically eliminate – or activate – the contribution of voltage-gated ion channels to the membrane currents in excitable cells. This greatly reduces the complexity of the physiological events studied. Hille (2001, p.34-35) describes the traditional two-electrode voltage clamp as follows:

> Voltage-clamps […] consist of an *intracellular electrode* and *follower circuit* to measure the membrane potential, a *feedback amplifier* to amplify any difference (error signal) between the recorded voltage and the desired value of the membrane potential, and a *second intracellular electrode for injecting current* from the output of the feedback amplifier (italicisation added by M. Weber).

The two-electrode voltage-clamp technique is still in use in experiments with very large cells, e.g. certain muscle cells or *Xenopus* oocytes, but the patch-voltage-clamp technique now appears to be the standard electrophysiological technique for smaller cells (< ~ 50 μm in diameter). This success was made possible with the *development of a fast amplifier* to virtually simultaneously record voltage and inject *current using a single electrode*. This extension of the *voltage-clamp principle* to the "single-electrode situation" of the patch-clamp recording is achieved with the *current-to-voltage (I-V) converter* of a patch-clamp amplifier. The I-V converter is part of the *preamplifier* or *"headstage"* to which the pipette holder of the patch-pipette is connected (see e.g. Hamill et al., 1981; Numberger & Draguhn, 1996; Sigworth, 1995). It is illustrated in figure 20 as part of an extended circuit equivalent diagram of a whole cell recording.

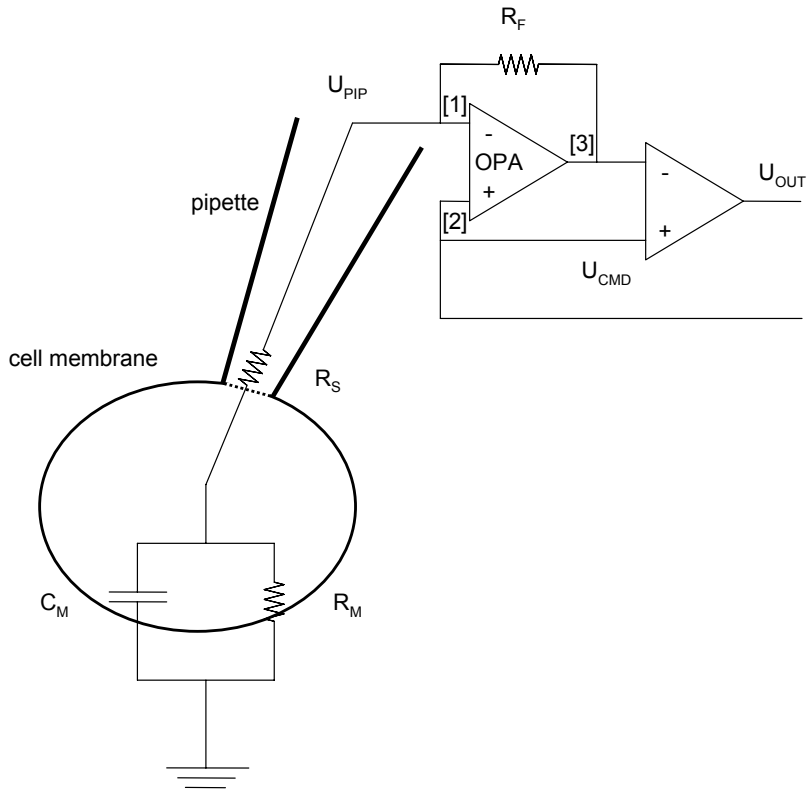

Figure 20: *Circuit diagram of a whole-cell patch-clamp recording* (based on Numberger & Draguhn, 1996; p. 69 & 88)

Circuit diagrams of a whole-cell recording and a simplified version of a patch-clamp amplifier.
The circuit diagram in the upper right corner of the illustration shows the key components of a patch-clamp amplifier (see text for details). The main components of the current-to-voltage converter are an operational amplifier (OPA, illustrated as a triangle, with its two inputs, denoted as [1] and [2], and its single output, denoted as [3]), and a feedback resistor (R_F). The second differential amplifier (also illustrated as a triangle) is already part of the main amplifier. U_{PIP} denotes the pipette potential, U_{CMD} the command potential, and U_{OUT} the output potential. The signal ground of the patch-clamp amplifier is not shown. The key components of the whole-cell equivalent circuit are the series resistor (R_S), the membrane resistor (R_M) and the membrane capacitor (C_M).

The two central characteristics of the I-V converter are: (i) The input resistance (R_{OPA}) of the operational amplifier (OPA) typically is ~ 10^{12} Ω, which is several orders of magnitude higher than that of the feedback resistor (R_f; $R_{OPA} >> R_f$). This means that basically all of the current to and from the patch pipette flows through the feedback resistor while hardly any of it flows through the OPA. (ii) At the output of the OPA (labelled [3]), a strongly amplified potential ($U_{[3]}$) that is proportional to the potential difference between the two inputs of the OPA ([1], [2]; $U_{[3]} \sim (U_{[2]} - U_{[1]})$) is generated. This means that any difference between the pipette (U_{PIP}) and command potential (U_{CMD}) causes a potential ($U_{[3]}$) at the output of the OPA. This has two consequences: (i) Current flows through R_F and into the pipette to rapidly *compensate* the previous

current flow at the pipette. (ii) The output potential of the OPA ($U_{[3]}$) is relayed to the main amplifier where the command potential (U_{CMD}) is subtracted and the remainder is recorded and transformed into current (according to a calibration factor). As these processes occur *extremely rapidly*, it is possible to *record and compensate* any current flow to and from the cell, while the cell is held at the desired holding potential (see e.g. Numberger & Draguhn, 1996).

2 MATERIALS AND METHODS

2.1 Preparation and Cell Culture

Parasympathetic neurons from rat intracardiac ganglia were dissociated and placed in tissue culture. The dissociation procedure of these neurons has been described previously (Xu & Adams, 1992a) and was in accordance with guidelines of Animal Experimentation Ethics Committees of the University of Queensland and the University of Heidelberg. In detail, Wistar rats (3-8 days old) were killed by decapitation, the chest cavity was opened and heart, lungs, oesophagus, thymus and all connecting vessels were taken out en bloc and transferred into dissection solution. Subsequently, lungs, oesophagus, trachea and bronchi, thymus, ventricles, aorta and the left atria were removed. The vena cava was cut open and the residual atrial tissue was stretched out and fixed with fine metal pins onto a sylgard coated petri dish, covered with dissection solution containing collagenase type II (0.8 mg ml^{-1}) and incubated for 52-62 min at 37°C. After the enzymatic treatment, clusters of ganglia were dissected, transferred to a sterile culture dish containing culture media, cut into 3 to 4 peaces and triturated approximately 20 times using a Pasteur pipette with a narrow, fire-polished opening. The isolated neurons were plated on laminin-coated glass cover slips and incubated at 37°C for 36 - 84 h under a 95% air, 5% CO_2 atmosphere before they were used for experiments. Figure 23 shows examples of the dissociated, cultured intracardiac neurons during patch-clamp experiments.

2.2 Spectrophotometry

The i.v. anaesthetics thiopental and ketamine were screened for interferences with the absorption characteristics of fura-2 using photospectrometry. Recording solutions were based on standard (Ca^{2+}-) EGTA solutions containing 0 nM $[Ca^{2+}]_s$ (EGTA solution) or > 0.1 mM $[Ca^{2+}]_s$ (Ca^{2+} -EGTA solution; see: chapter 2.5 and Grynkiewicz et al., 1985). Absorption spectra of solutions containing either 0 (control) or the clinically relevant concentration of the anaesthetics (25 μM for thiopental, and 10 μM for ketamine), and 0 or 10 μM fura-2 pentapotassium salt were recorded with a UV/vis spectrophotometer (Beckman DU 640, Beckman Instruments, Inc., Fullerton, CA, USA) with a wavelength range from 190 to 1100 nm, a spectral excitation bandwidth of ≤ 1.8 nm and a

photodiode for the detection of the transmitted light. Photons were collected from the full wavelength range of the spectrometer, since pre-experiments showed that the signal to noise ratio was not sufficient when a 510 nm bandpass filter was inserted between the solutions and the detection diode. Similarly, a 10 μM fura-2 pentapotassium salt concentration was chosen to provide a sufficient signal to noise ratio of the dye-related signal and to be within the concentration range of fura-2 to be expected inside cells under the experimental conditions. A scheme of the photospectrometer is presented in figure 21 (see chapter 1.5.1 for details on the operating principle).

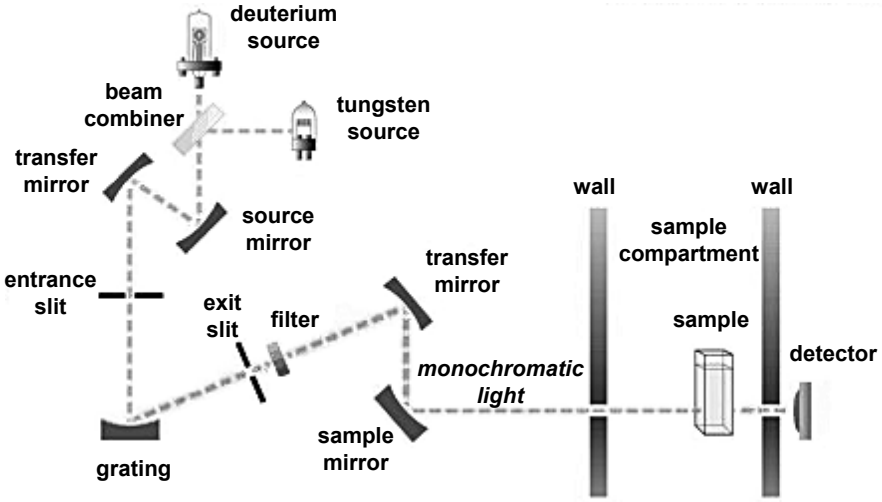

Figure 21: Operating principle of a Beckman DU 600 spectrophotometer

(adopted from http://www.beckmancoulter.com)

Schematic of a Beckman DU series 600 photospectrometer.
The presence of a deuterium and a tungsten source allows the illumination of the sample in the UV as well as in the visible range of the light, respectively. A beam combiner is necessary to ensure that the path of the light from both light sources is identical before further optical elements are passed. The key component of the spectrophotometer is the optical grating as it represents the basis for the generation of monochromatic light (see chapter 1.5.1 for details). Monochromatic light illuminates the sample and a photodiode detector collects the transmitted light.

2.3 Fura-2 fluorescence recordings

Intracellular $[Ca^{2+}]_i$ transients in response to application of ACh or caffeine, were determined in fura-2 loaded rat intracardiac neurons using single cell ratiometric photometry. Neurons were incubated for ~ 1 h at room temperature in fura-2 loading solution. Subsequently, they were washed in (physiological salt solution) PSS and a recovery period of ~ 30 min before experiments was used. Mainly isolated neurons were selected for the experiments to minimize synaptic contacts and the activation of nearby

cells. Fura-2 loaded cells were illuminated with light from a 75 W xenon arc lamp, which was split by an optical chopper (OC-4000 Optical Chopper, Photon Technology International (PTI), South Brunswick, NJ, USA) and passed alternately through 340 and 380 nm bandpass filters. A 510 nm bandpass emission filter was used and a variable aperture set around the cell image. The emitted light was collected by a Hamamatsu R 928 photomultiplier tube, the output of which was digitised using a PTI interface and sampled at 5 Hz using Felix 1.1 software (PTI) run on a 133 MHz computer. Figure 22 illustrates the major parts of the photometry system:

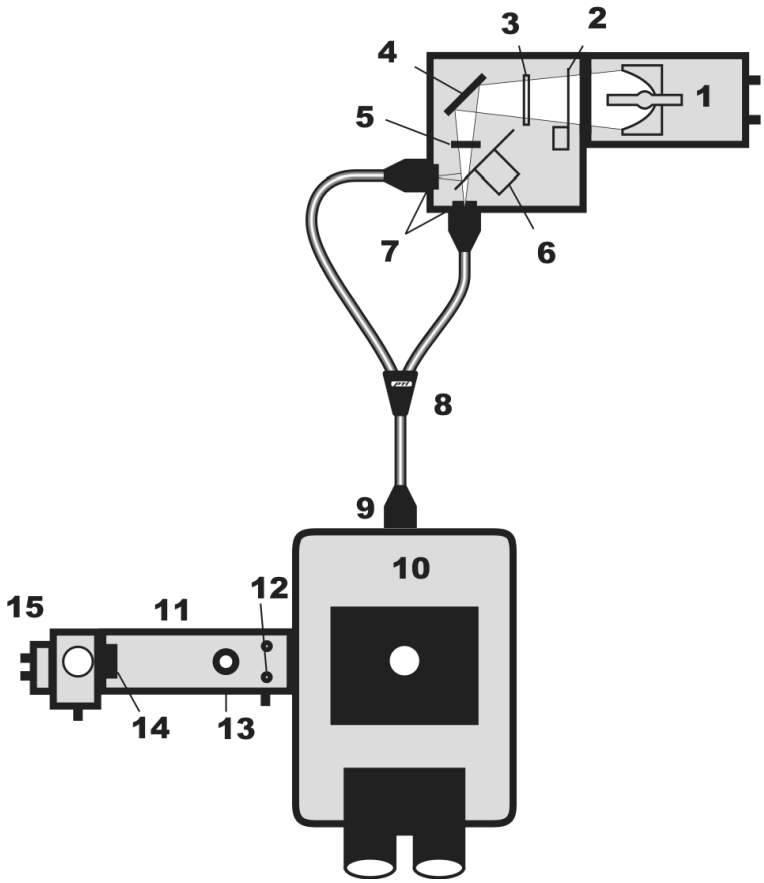

Figure 22: *The PTI photometry system*

(from http://www.pti-nj.com)

Schematic of the ratiometric PTI photometry system.
Light from the xenon arc lamp is split by an optical chopper and passed alternately through 340 and 380 nm excitation filters and via fibre optical cables to the microscope. Using the viewing eyepiece, the variable aperture is set around the cell image to selectively detect the light emitted from the cell of interest, subsequently passed through a 510 nm emission filter and collected by a photomultiplier tube. The photomultiplier output is digitised and sampled for storage on a personal computer.

Legend: 1 arc lamp housing; 2 shutter; 3 iris; 4 IR trap; 5 broadband filter; 6 optical chopper; 7 340 and 380 nm filters; 8 bifurcated fibre optical cable; 9 fibre optic adapter; 10 microscope; 11 photometer; 12 adjustable iris; 13 viewing eyepiece; 14 510 nm emission filter; 15 photomultiplier.

Some experiments were carried out on a ratiometric imaging system based on an Olympus IX 70 microscope with UV optics, a Polychrome II monochromator (Till Photonics, Gräfeling, Germany) alternating between 340 nm and 380 nm illumination, a Hamamatsu C3077 CCD camera with a C2400-80 intensifier head to collect the fluorescence images, a Meteor II frame grabber board (Matrox, Dorval, Quebec, Canada), and Simple PCI 5.0 (Compix Inc., Imaging Systems, Cranberry Township, PA, USA) software run on a 1600 MHz computer.

Changes in intracellular $[Ca^{2+}]$ ($\Delta[Ca^{2+}]_i$) were obtained measuring the ratio of the intensity of the emitted 510 nm fluorescence $R(F_{340}/F_{380})$ when the cell was illuminated with 340 nm light (F_{340}) to that when illuminated with 380 nm light (F_{380}) and converting this ratio to approximate Ca^{2+} concentrations using the equation:

$$[Ca^{2+}]_i = K_d \times \frac{R - R_{min}}{R_{max} - R} \times \frac{S_{f2}}{S_{b2}} \qquad (3)$$

where R_{min} and R_{max} are the F_{340}/F_{380} ratios of the Ca^{2+}-free and Ca^{2+}-saturated fura-2 sample, respectively, S_{f2} is F_{380} of the Ca^{2+}-free fura-2 sample and S_{b2} is F_{380} of the Ca^{2+} bound sample. An eleven-step calibration procedure during which $[Ca^{2+}]$ was increased from approximately 0 to saturation of the dye at > 1 mM $[Ca^{2+}]$ was used to determine the numerical values for the constants in this equation using fura-2 pentapotassium salt and standard (Ca^{2+}-) EGTA solutions (Grynkiewicz et al., 1985). Under the experimental conditions of the PTI set-up and the imaging set-up, the dissociation constant K_d was determined as 179 and 196 nM, respectively.

A concentration-response curve with thiopental as antagonist for nAChR activation was obtained by measuring the peak increase in $[Ca^{2+}]_i$ ($\Delta[Ca^{2+}]_i$) at each antagonist concentration and the experimental data points were fitted using the equation

$$\Delta[Ca^{2+}]_i/\Delta[Ca^{2+}]_{i(max)} = 1/[1+([A]/EC_{50})^{n}] \qquad (4)$$

where $\Delta[Ca^{2+}]_i/\Delta[Ca^{2+}]_{i(max)}$ represents the relative peak increase in $\Delta[Ca^{2+}]_i$, [A] is the antagonist concentration, EC_{50} is the concentration giving half-maximal inhibition and *n* is the Hill coefficient.

2.4 Patch-clamp recordings

Membrane currents were measured with the whole-cell recording method of the patch-clamp technique, using either the conventional, dialyzed (Hamill et al., 1981) or the perforated patch (Horn & Marty, 1988; Rae et al., 1991) recording configuration. The perforated patch configuration takes advantage of pore forming antibiotics, in the present study amphotericin B, to obtain electrical access to the cell interior without dialyzing cytoplasmic components, which are important in maintaining various functional responses in cells. The pipette was first tip-filled with an antibiotic-free solution to prevent disruption of seal formation and then backfilled with the amphotericin B containing solution (see chapter 1.5.3). Pipettes were pulled from borosilicate glass (Harvard Apparatus, Reading, UK) using a Sutter Instruments P-87 pipette puller, were fire polished and had resistances of ~ 2.5 MΩ.

Filled patch pipettes were mounted on a pipette holder connected with the head stage of a patch-clamp amplifier (EPC-7, List-Medical, Darmstadt, Germany or RK300, Bio-Logic, Claix, France). Voltage protocols were applied using Clampex software (Version 8.0, Axon Instruments Inc., Union City, CA, USA). Signals were filtered at 200 Hz, digitised at 1 kHz (Digidata 1200 interface, Axon Instruments Inc.) and stored on the hard disc of a Pentium PC for further analysis. Figure 23 shows dissociated intracardiac neurons during one of the patch-clamp experiments.

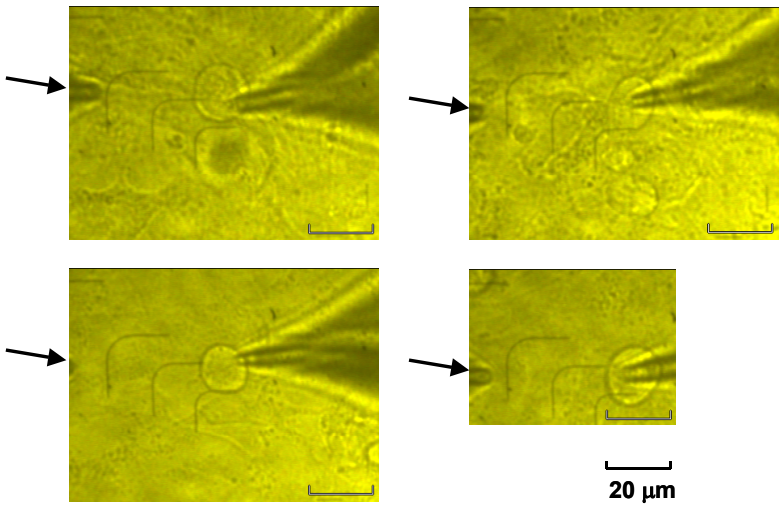

Figure 23: Agonist application and patch-clamping of cultured rat intracardiac neurons

Focal application of agonists on single rat intracardiac neurons during patch-clamp experiments.
The arrow indicates the tip of the pipette of the focal pressure application system with which the agonists were applied to the cells. The pipette on the right hand side is the patch pipette. The picture shows typical neonatal rat intracardiac neurons with their spherical cell bodies and their lack of pronounced dendritic trees and axons. The pictures were acquired using the Hamamatsu imaging system described in chapter 2.3.

2.5 Solutions and Drugs

Solutions for absorption measurements and for the calibration procedure of the fura-2 signal were standard (Ca^{2+}-) EGTA solutions containing 10 mM EGTA, 100 mM KCl, 10 mM K-MOPS, and either 10 mM $CaCl_2$ (Ca^{2+} -EGTA solution) or no added Ca^{2+} (EGTA solution), respectively (Grynkiewicz et al., 1985). The free Ca^{2+} ion concentration of the solution $[Ca^{2+}]_s$ was > 0.1 mM in the Ca^{2+} -EGTA solution and approximately 0 in the EGTA solution. The dissection solution contained (mM): 140 NaCl, 3 KCl, 2.5 $CaCl_2$, 0.6 $MgCl_2$, 7.7 glucose and 10 histidine (pH adjusted to 7.2 with NaOH). The culture media was high glucose Dulbecco's Modified Eagle Media, with 10 % (v/v) fetal calf serum, 100 U ml^{-1} penicillin and 0.1 mg ml^{-1} streptomycin. The fura-2-loading solution was based on physiological saline solution (PSS) containing (mM): 140 NaCl, 3 KCl, 2.5 $CaCl_2$, 1.2 $MgCl_2$, 7.7 glucose and 10 HEPES (pH adjusted to 7.2 with NaOH) to which pluronic-127 and fura-2 AM ester from stock solutions (1 mM fura-2/AM in DMSO) was added to obtain a final concentration of 0.02 % pluronic-127 and 5 μM fura-2 AM. During experiments, rat intracardiac neurons were continuously superfused with ~ 2 ml PSS/min. The relatively large Ca^{2+} concentration of 2.5 mM was chosen for the PSS due to a previous study in rat intracardiac neurons that has shown that nAChR induced currents reach a peak value at this Ca^{2+} concentration, with reduced currents for lower as well as higher Ca^{2+} concentrations (Fieber & Adams, 1991a). This indicates that the presence of 2.5 mM Ca^{2+} in the PSS creates are favourable condition for the observation of sufficiently large nAChR induced currents and possibly $[Ca^{2+}]_i$ transients, too. Racemic mixtures of thiopental, pentobarbital or ketamine were added to the extracellular solution, stirred thoroughly and bath applied prior to agonist application. Perfusion volume during wash-in of the anaesthetics (≥ 5 min) was approximately ten-fold the chamber volume (1 ml) to ensure that the desired anaesthetic concentrations were obtained before agonist application, while perfusion volume during washout (≥ 10 min) was approximately twenty-fold chamber volume to ensure almost complete removal of the anaesthetics. Estimated clinically relevant anaesthetic concentrations were taken from the literature (Franks & Lieb, 1994; Krasowski & Harrison, 1999; Yamakura et al., 2001) and are free aqueous concentrations corrected for protein binding. Thiopental concentrations are nominal values not adjusted for the 9 % sodium carbonate content of the powder. Agonists were applied to the cell soma of intracardiac neurons by pressure ejection (3-8 p.s.i.;

Picospritzer II, General Valve Corp., Fairfield, NJ, USA) from a micropipette (3 - 5 μm diameter) positioned about 40 - 80 μm from the cell soma as shown in figure 23. Nicotinic ACh receptor activation was obtained by focal application of maximally effective ACh concentrations (300 - 500 μM), with maximally effective concentrations of the muscarinic receptor antagonist atropine (≥ 100 nM) present both in the bath solution and extracellular pipette solution. In unclamped cells and perforated patch-clamp experiments, 500 μM ACh or 10 mM caffeine were applied for 1.2 s and a delay of at least 5 min between agonist applications was maintained. In dialyzed patch-clamp experiments, 300 μM ACh was applied for 0.1 s and a delay of ≥ 70 s between ACh applications was maintained to minimise receptor desensitization while recording duration for I-V curves remained acceptable. Agonists were applied several times before the superfusion of the anaesthetic and experiments were continued only if stable responses to agonist application were obtained. The pipette solution for perforated patch experiments contained (mM): 75 K_2SO_4, 55 KCl, 5 Mg SO_4 and 10 HEPES, titrated with N-methyl-D-glucamine to pH 7.2. A stock solution of 60 mg ml^{-1} amphotericin B in DMSO was prepared daily and diluted in pipette solution, providing a final concentration of 240 μg ml^{-1} amphotericin B in 0.4 % DMSO, which was kept on ice and protected from light. The pipette solution for dialyzed patch experiments contained (mM): 140 CsCl, 2 MgATP, 2 CsBAPTA, 10 HEPES titrated with CsOH to 7.2. All experiments were carried out at room temperature (22°C).

All chemical reagents used were of analytical grade. The following drugs were used: Acetylcholine chloride, amphotericin B, atropine sulphate, DMSO, ketamine hydrochloride, pentobarbital sodium salt, tetrodotoxin, thiopental sodium salt (Sigma Chemical Co., St. Louis, MO), caffeine (Fluka Chemie, Buchs, Switzerland), collagenase (type II; Worthington, Biochemical Corp., Lakewood, NJ, USA), CsBAPTA, fura-2/AM, fura-2 pentapotassium salt, and pluronic-127 (Molecular Probes, Eugene, OR), ω-conotoxin GVIA (Alomone Labs, Ltd., Jerusalem, Israel).

2.6 Data Analysis

Peak (F_{340}/F_{380}) and resting (F_{340}/F_{380}) values of ratiometric fluorescence transients were determined by averaging F_{340}/F_{380} values obtained from a 1.5 s period during the peak response and a 5 s period prior to the agonist application, respectively. Peak and resting F_{340}/F_{380} ratios were then transformed to peak and resting $[Ca^{2+}]_i$, using

equation (3), and peak increases in $[Ca^{2+}]_i$ ($\Delta [Ca^{2+}]_i$) were calculated by subtracting resting $[Ca^{2+}]_i$ from peak $[Ca^{2+}]_i$. ACh-evoked peak current amplitudes and $\Delta [Ca^{2+}]_i$ in the presence of the anaesthetic (or antagonist) were averaged and compared to the mean control response obtained in the absence of the anaesthetic in each individual cell. With one exception, mean control responses were determined by averaging responses obtained before and after superfusion with the anaesthetic (or antagonist) to take into account cell rundown or incomplete recovery during washout that may occur during the experiment. In a control experiment involving the use of the N-type Ca^{2+} channel blocker ω-conotoxin GVIA as antagonist mean control responses were uniquely based on responses obtained before the wash-in of the toxin, as its effects are virtually irreversible (Boland et al., 1994; Feng et al., 2001). Data are expressed as the mean ± S.E.M. and were analysed statistically using Student's (paired, two-tail) *t*-test with the level of significance being taken as $P < 0.05$ (*), 0.01 (**) or 0.001 (***). Levels of significance were conservatively adjusted using the Bonferroni method when multiple comparisons between experimental conditions in the same experiments were carried out.

3 RESULTS

3.1 Preliminary experiments

3.1.1 Assessment of fura-2 quenching by i.v. anaesthetics

3.1.1.1 Spectrophotometry

Several chemical agents ranging from heavy metal cations (Grynkiewicz et al., 1985; Marchi et al., 2000; Usai et al., 1999), to caffeine (Muschol et al., 1999) are known to interfere with fura-2 measurements. In particular, a red shift of the excitation spectra and quenching of the fura-2 signal was reported with increasing hydrophobicity of solutions (Roe et al., 1990). Since many anaesthetics, including ketamine and a number of barbiturates, are very lipophilic (reviewed in Franks & Lieb, 1994; Krasowski & Harrison, 1999), ketamine and thiopental as a representative of the barbiturates and a close chemical relative of its metabolite pentobarbital (Büch & Büch, 2001; Chan et al, 1985; Charney et al, 2001; Evers & Crowder, 2001) were screened for interferences with the absorption characteristics of fura-2 using photospectrometry.

Firstly, the effect of thiopental on the absorbance of the (Ca^{2+}) –EGTA solutions in the absence of fura-2 was examined. As shown in figure 24A, 25 μM *thiopental increased the absorbance of the solutions only in a minor degree in the wavelength range used for the fura-2 ratiometric measurements* (see also legend of figure 24), but progressively increased for wavelengths smaller than 330 nm.

Secondly, the effect of thiopental on the absorbance of (Ca^{2+}) –EGTA solutions in the presence of 10 μM fura-2 was examined. As shown in figure 24B, the *absorbance changes in the presence of 25 μM thiopental* can *still* be *observed in the presence of 10 μM fura-2*.

Finally, the effect on 25 μM thiopental on the absorption characteristics of fura-2 itself was examined. To eliminate the non-specific effect of thiopental on (Ca^{2+}) - EGTA solutions in general (in the absence of the dye), the absorbance of the dye-free solutions was subtracted from that of dye-containing solutions. As shown in figure 24C, the resulting absorbance curves were virtually identical for solutions in the absence and presence of thiopental, over the complete wavelength spectra of relevance for fura-2 excitation, showing that *25 μM thiopental did not interfere with the absorption characteristics of fura-2*.

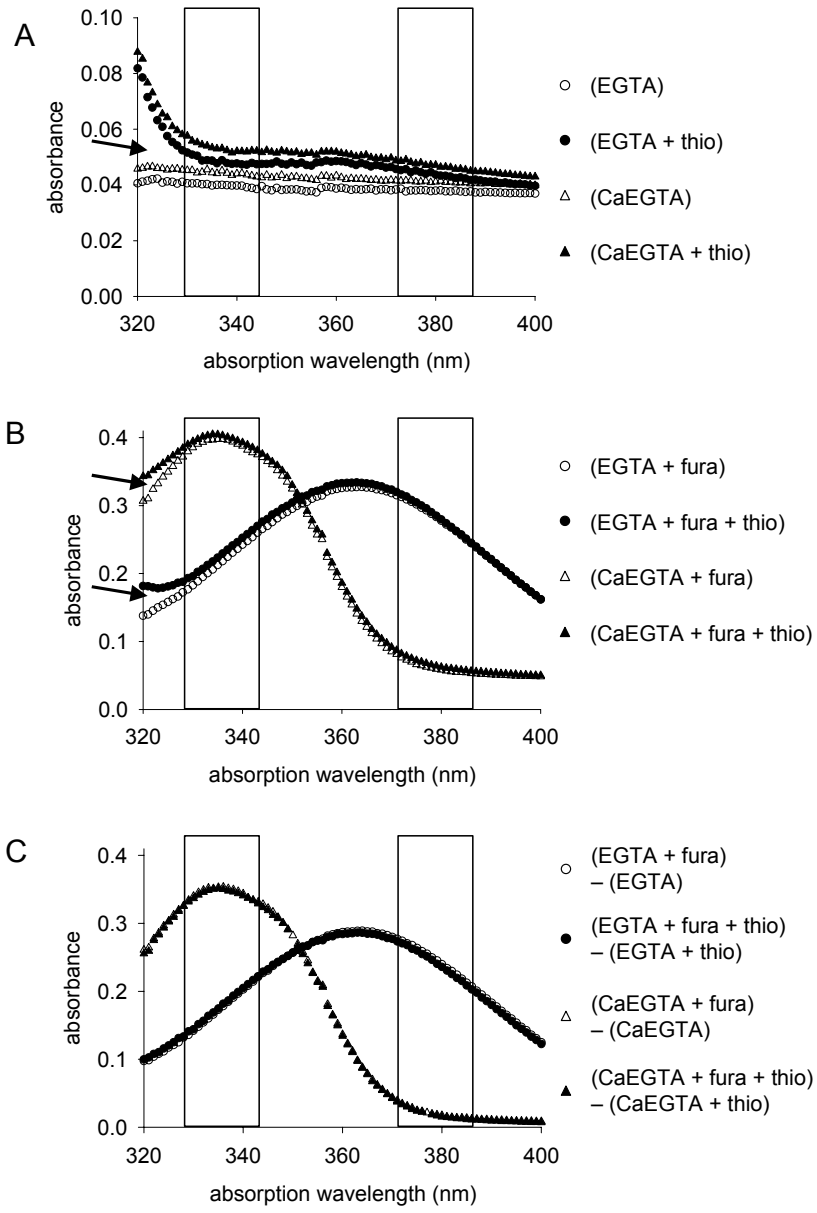

Figure 24: Effects of thiopental (thio) on the absorption spectra of Ca^{2+} -free or Ca^{2+} -containing solutions in the absence or presence of fura-2 pentapotassium salt

Vertical bars indicate the full width at half maximum (FWHM) of the excitation light obtained by the use of typical excitation filters or monochromators in fura-2 experiments (for filter spectra see e.g. Omega Optical, Inc., http://www.omegafilters.com).

A: Absorption spectra of EGTA and Ca^{2+} -EGTA solutions in the absence of fura-2 and the presence of 0 (control) or 25 μM thiopental.

Thiopental marginally increased absorbance in both Ca^{2+} -free and Ca^{2+} -containing solutions and was more pronounced at excitation wavelengths < 330 nm as indicated by the arrow.

B: Absorption spectra of EGTA and Ca^{2+} -EGTA solutions containing 10 μM fura-2, and 0 (control) or 25 μM thiopental.

The thiopental-induced increase in absorbance at < 330 nm (as observed in A) was still apparent in the presence of fura-2 as indicated by arrows.

C: Absorbtion spectra obtained by subtracting the absorption curves of solutions containing no fura-2 (see A) from the corresponding curves of solutions containing 10 μM fura-2 pentapotassium salt (see B).

The subtraction eliminates unspecific absorbance effects of thiopental on solutions in general from possible effects on fura-2 itself.

Similar spectrophotometric measurements were carried out using 10 μM ketamine. Firstly, as can be seen in figure 25A, *10 μM ketamine marginally increased the absorbance of the dye-free (Ca^{2+}) -EGTA solutions over the complete wavelength range of relevance for fura-2 excitation.*

Secondly, as shown in figure 25B, the *absorbance increase induced by 10 μM ketamine* was *hardly detectable in the presence of 10 μM fura-2* in the (Ca^{2+}) –EGTA solutions.

Finally, to eliminate the non-specific effect of ketamine on (Ca^{2+}) -EGTA solutions in general (in the absence of the dye), the absorbance of the dye-free solutions was subtracted from that of dye-containing solutions. As shown in figure 25C, the resulting absorbance curves were virtually identical for solutions in the absence and presence of ketamine, showing that *ketamine did not interfere with the absorption characteristics of fura-2*.

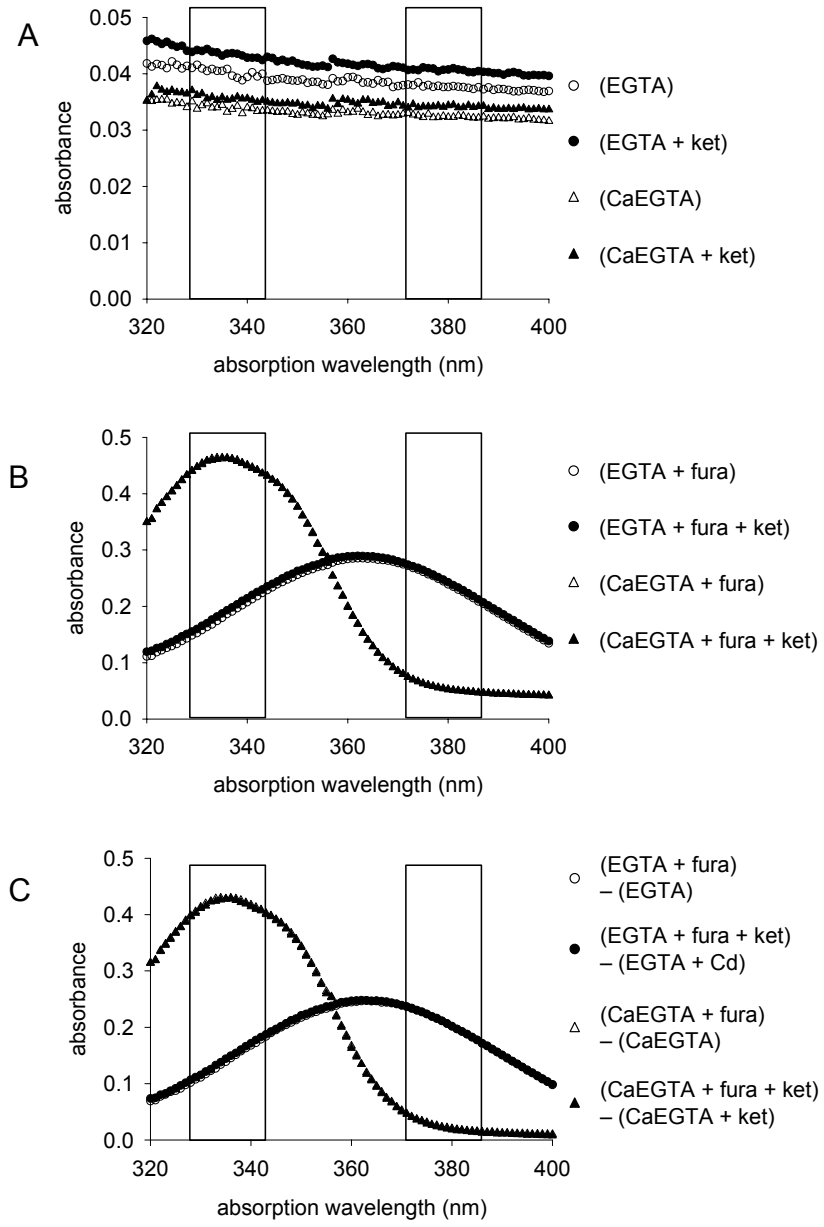

Figure 25: Effects of ketamine (ket) on the absorption spectra of Ca^{2+} -free or Ca^{2+} -containing solutions in the absence or presence of fura-2 pentapotassium salt

Vertical bars indicate the full width at half maximum (FWHM) of the excitation light obtained by the use of typical excitation filters or monochromators in fura-2 experiments (for filter spectra see e.g. Omega Optical, Inc., http://www.omegafilters.com).

A: Absorption spectra of EGTA and Ca^{2+} -EGTA solutions in the absence of fura-2 and the presence of 0 (control) or 10 μM ketamine.

Ketamine marginally increased the absorbance in both Ca^{2+} -free and Ca^{2+} -containing solutions over the complete wavelength range of relevance for fura-2 excitation.

B: Absorption spectra of EGTA and Ca^{2+} -EGTA solutions containing 10 μM fura-2, and 0 (control) or 10 μM ketamine.

The increased absorbance in the presence of ketamine (as observed in A) was hardly detectable in the presence of fura-2.

C: Absorbtion spectra obtained by subtracting the absorption curves of solutions containing no fura-2 (see A) from the corresponding curves of solutions containing 10 μM fura-2 pentapotassium salt (see B).

The subtraction eliminates unspecific absorbance effects of ketamine on solutions in general from possible effects on fura-2 itself.

Further tests to exclude an interference of the anaesthetics with emission characteristics of the dye were carried out on an actual ratiometric fura-2 set-up.

3.1.1.2 Calibration of the fura-2 signal on a ratiometric photometry set-up

To exclude any thiopental or pentobarbital-induced quenching of the ratiometric fura-2 signal, standard calibration procedures (see chapter 2.3; Grynkiewicz et al., 1985) were carried out on the ratiometric imaging set-up (see chapter 2.3) both in the absence (control: K_d = 196 ± 7 nM, R_{min} = 0.738 ± 0.003, R_{max} = 1.411 ± 0.026, S_{f2}/S_{b2} = 1.487 ± 0.024; n = 8) and presence of 25 μM thiopental (K_d = 190 ± 4 nM, R_{min} = 0.735 ± 0.002, R_{max} = 1.410 ± 0.017, S_{f2}/S_{b2} = 1.487 ± 0.017; n = 8), and in the absence (control: K_d = 189 ± 5 nM, R_{min} = 0.720 ± 0.004, R_{max} = 1.470 ± 0.027, S_{f2}/S_{b2} = 1.595 ± 0.030; n = 9) and presence of 50 μM pentobarbital (K_d = 194 ± 6 nM, R_{min} = 0.715 ± 0.005, R_{max} = 1.449 ± 0.033, S_{f2}/S_{b2} = 1.609 ± 0.039; n = 10), respectively. None of these values was significantly different from those obtained under the control condition ($P > 0.3$ for all values) indicating that *neither 25 μM thiopental nor 50 μM pentobarbital does interfere with the spectral characteristics of fura-2*.

Similar control experiments were carried out for the dissociative anaesthetic ketamine. The following values were obtained in the absence (control: K_d = 210 ± 12 nM, R_{min} = 0.720 ± 0.004, R_{max} = 1.470 ± 0.027, S_{f2}/S_{b2} = 1.595 ± 0.030; n = 9) and presence of 10 μM ketamine (K_d = 189 ± 5 nM, R_{min} = 0.730 ± 0.007, R_{max} = 1.410 ± 0.011, S_{f2}/S_{b2} = 1.532 ± 0.025; n = 11). Neither the K_d, and R_{min} nor S_{f2}/S_{b2}, differed significantly from control conditions ($P > 0.05$ for all cases). Only R_{max} was significantly ($P < 0.05$), but *marginally smaller in the presence of ketamine* (96% of control) indicating that accordingly *corrected R_{max} values, i.e. reduced by 4 %, may have to be applied when fluorescence ratios are transformed into approximate $[Ca^{2+}]_i$* (see chapter 2.3) when ketamine is present.

3.1.1.3 Resting $[Ca^{2+}]_i$ in fura-2 loaded intracardiac neurons

In fura-2 loaded, unclamped intracardiac neurons, the mean resting $[Ca^{2+}]_i$ was 46 ± 4 nM in the absence and 44 ± 4 nM[1] (n = 30) in the presence of the i.v anaesthetics. The *lack of effect of the i.v anaesthetics on resting Ca^{2+} levels* indicates that in unstimulated neurons, resting $[Ca^{2+}]_i$ and thus concentration gradients for Ca^{2+} ions were unchanged by the i.v. anaesthetics.

3.1.2 Voltage-gated Ca^{2+} -channels contribute to nAChR-induced $[Ca^{2+}]_i$ transients in intracardiac neurons

Activation of the non-selective cationic nAChR channel in rat intracardiac neurons mediates not only Na^+ influx, but also a considerable Ca^{2+} influx (Adams & Nutter, 1992; Fieber & Adams, 1991a), which results in an increase in $[Ca^{2+}]_i$ that can be detected with fura-2 (Beker et al., 2003). This cationic influx leads to a depolarization that could be strong enough to activate voltage-gated channels, including voltage-gated Ca^{2+} channels (Ca_v) that in turn may contribute to the increases in $[Ca^{2+}]_i$ initiated by nAChR-activation. As these effects have not previously been assessed in rat intracardiac neurons, nAChR-induced Ca^{2+} transients were elicited in the presence or absence of the Ca^{2+} -channel blocking agents Cd^{2+} or ω-conotoxin GVIA.

In one series of experiments, nAChR-induced $[Ca^{2+}]_i$ transients were evoked by 500 µM ACh in the presence of 1 µM Atropine and the absence (control) or presence of 100 µM $CdCl_2$ bath applied. The $CdCl_2$ concentration is typically used to non-selectively block Ca_v and it has been shown to induce a total inhibition of the corresponding current in rat intracardiac neurons (Xu & Adams, 1992b). As illustrated in figure 26, *$CdCl_2$ appeared to reversibly inhibit nAChR-induced $\Delta[Ca^{2+}]_i$* in all cells examined (n = 4). In addition, *resting $[Ca^{2+}]_i$ appeared to continuously increase starting with the application of $CdCl_2$ and was even greater during washout in all cells examined* (n = 4).

---

[1] Average resting $[Ca^{2+}]_i$ was 45 ± 4 nM when approximations of $[Ca^{2+}]_i$ using formula (3) were based on the corrected (i.e. reduced by 4 %) R_{max} value for the ketamine condition (see chapter 3.1.1.2).

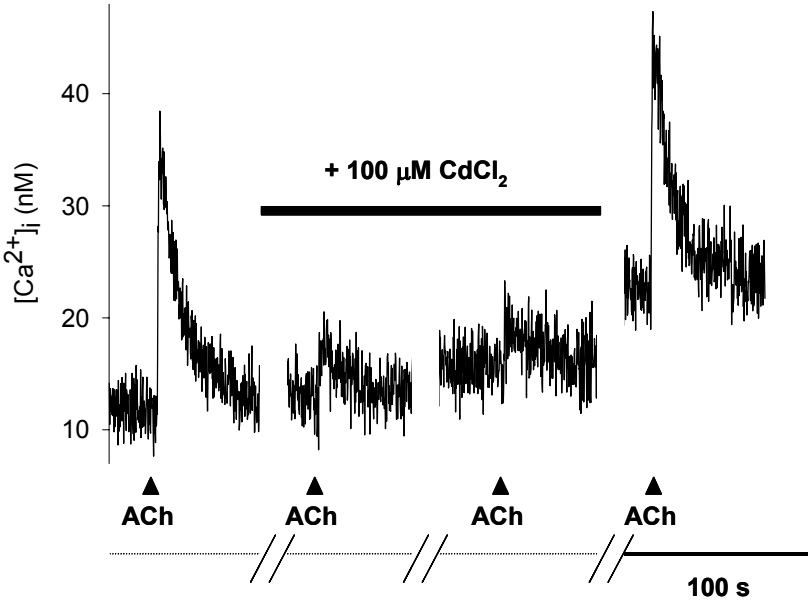

Figure 26: $CdCl_2$ appears to diminish nAChR-induced $[Ca^{2+}]_i$ transients

Approximate $[Ca^{2+}]_i$ transients in response to focal application of 500 µM ACh obtained in the absence (control) and presence of 100 µM $CdCl_2$ in the bath solution.
The bath solution also contained 1 µM atropine to inhibit mAChR.

Due to these apparent increases in resting $[Ca^{2+}]_i$ we have suspected an interaction of Cd^{2+} with fura-2 and therefore carried out further control experiments using $CdCl_2$ to assess the validity of the above experiment.

We have recently shown that the application of ACh in the presence of mecamylamine to block nAChR channels activates muscarinic AChR (mAChR) and a subsequent, transient increase in $[Ca^{2+}]_i$ due to Ca^{2+} release from internal stores via a phospholipase C (PLC) dependent second-messenger pathway. Given that increases in $[Ca^{2+}]_i$ were not dependent on the presence of Ca^{2+} in the extracellular solution (Beker et al., 2003) and assuming that Cd^{2+} at the concentrations used merely blocks Ca_v, it was expected that increases in $[Ca^{2+}]_i$ are unaffected by the presence of $CdCl_2$.

However, activation of *mAChR-induced increases in $[Ca^{2+}]_i$* by 500 µM ACh in the presence of 3 µM mecamylamine *appeared to be similarly inhibited in the presence of 100 µM $CdCl_2$* (n = 2) as can be seen in figure 27. In addition, *resting $[Ca^{2+}]_i$ again appeared to continuously increase* starting with the application of $CdCl_2$ and was even greater during washout in all cells examined (n = 2).

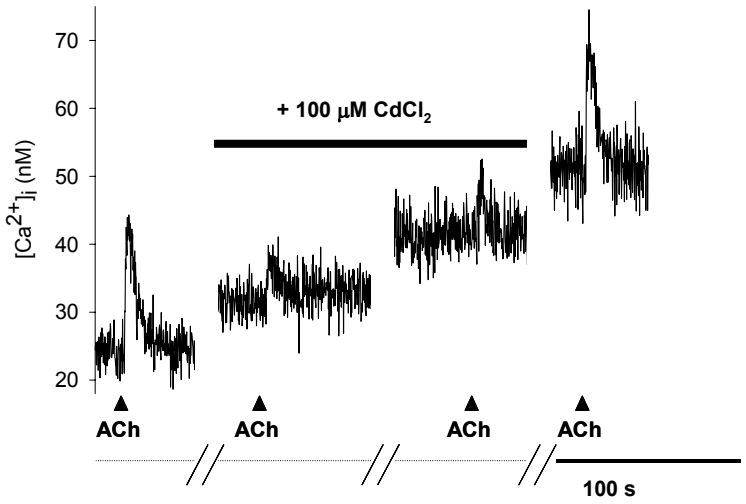

Figure 27: $CdCl_2$ appears to diminish mAChR-induced $[Ca^{2+}]_i$ transients

$[Ca^{2+}]_i$ transients in response to focal application of 500 µM ACh obtained in the absence (control) and presence of 100 µM $CdCl_2$ in the bath solution.
The bath solution also contained 3 µM mecamylamine to inhibit nAChR.

Further suspecting an interaction of Cd^{2+} ions with fura-2, spectrophotometric measurements were carried out using solutions with 0 nM $[Ca^{2+}]_s$ (EGTA solution) or > 0.1 mM $[Ca^{2+}]_s$ (Ca^{2+} -EGTA solution) in the presence or absence of 100 µM Cd^{2+}.

In analogy to the experiments described in chapter 3.1.1.1, it was firstly examined whether 100 µM $CdCl_2$ alters the absorbance of solutions in the absence of fura-2. As shown in figure 28A, *Cd^{2+}* basically *affected the absorbance* all solutions *to a minor, but constant degree over the whole wavelength range under investigation.*

Secondly, the effects of $CdCl_2$ on the absorbance of solutions supplemented with 10 µM fura-2 were examined. As shown in figure 28B, the presence of *$CdCl_2$ did basically not affect the absorbance of the fura-2 containing Ca^{2+} -EGTA solution*. However, it *affected the absorbance of the fura-2 containing (Ca^{2+} -free) EGTA solution*, with *increased values for excitation wavelengths < 355 nm* and *decreased values for excitations wavelength > 355 nm.*

Finally, it was examined whether $CdCl_2$ affects the absorption characteristics of fura-2 itself after any non-specific effect of $CdCl_2$ on solutions in general (in the absence of the dye) had been eliminated by subtracting the absorbance of the dye-free solutions from those of dye-containing (10 µM fura-2) solutions. As shown in figure 28C, the resulting *absorbance curves were only identical in the absence and presence of $CdCl_2$ for the Ca^{2+} -EGTA solutions*. In contrast, *$CdCl_2$ enhanced the absorbance of the virtually Ca^{2+} -free EGTA solutions for wavelengths < 355 nm, while the absorbance for wavelengths > 355 nm was decreased*, showing that *$CdCl_2$ interacts with fura-2 under these conditions.*

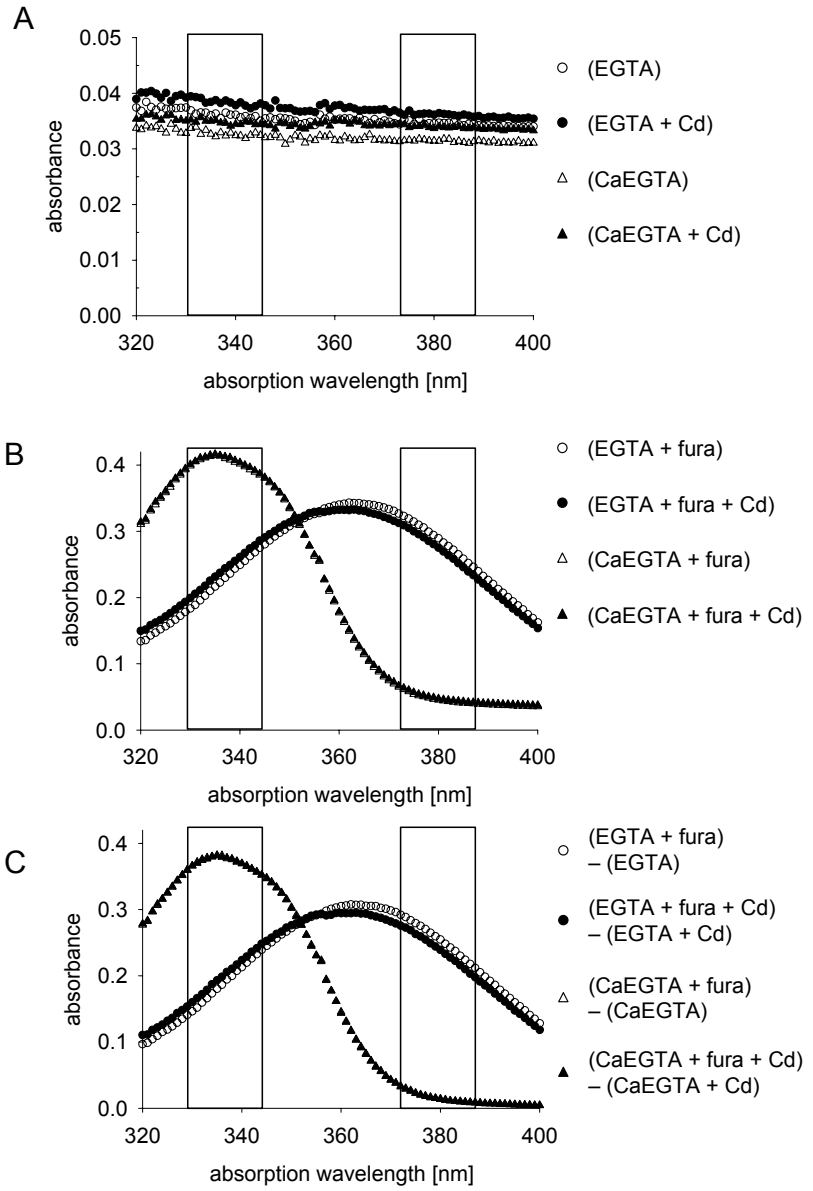

Figure 28: Effects of $CdCl_2$ (Cd) on the absorption spectra of Ca^{2+} -free or Ca^{2+} -containing solutions in the absence or presence of fura-2 pentapotassium salt

Vertical bars indicate the full width at half maximum (FWHM) of the excitation light obtained by the use of typical excitation filters or monochromators in fura-2 experiments (for filter spectra see e.g. Omega Optical, Inc., http://www.omegafilters.com).

A: Absorption spectra of EGTA and Ca^{2+} -EGTA solutions in the absence of fura-2 and the presence of 0 (control) or 100 μM $CdCl_2$.

$CdCl_2$ marginally increased the absorbance in Ca^{2+} -free and Ca^{2+} -containing solutions.

B: Absorption spectra of EGTA and Ca^{2+} -EGTA solutions containing 10 μM fura-2, and 0 (control) or 100 μM $CdCl_2$.

The absorbance of Ca^{2+} -EGTA solutions containing fura-2 was virtually unaffected by the presence of $CdCl_2$. In contrast, absorbance was markedly altered when fura-2 containing solutions were based on (Ca^{2+} -free) EGTA solutions.

C: Absorbtion spectra obtained by subtracting the absorption curves of solutions containing no fura-2 (see A) from the corresponding curves of solutions containing 10 μM fura-2 pentapotassium salt (see B).

The subtraction eliminates unspecific absorbance effects of $CdCl_2$ on solutions in general from possible effects on fura-2 itself. Absorbance in Ca^{2+} -free solutions was increased at excitation wavelengths < 355 nm and reduced at excitation wavelengths > 355 nm with $CdCl_2$ present as indicated by the arrows.

Further experiments using $CdCl_2$ were abandoned as the interaction of the divalent cation Cd^{2+} with fura-2 was also likely to confound the assessment of the contribution of Ca_v to the $[Ca^{2+}]_i$ transients following nAChR activation. Alternatively, control experiments using the peptide toxin ω-conotoxin GVIA were carried out. ω-conotoxin GVIA specifically blocks N-type Ca_v in a virtually irreversible manner (recovery > 1 hr, see Boland et al., 1994; Feng et al., 2001) and a maximally effective concentration (300 nM) of ω-conotoxin GVIA inhibits ~ 70 % of the voltage-gated Ca^{2+} -currents in rat intracardiac neurons (see chapter 1.4.2). Given that (i) a remainder of ~ 30 % of the voltage-gated Ca^{2+} -currents cannot be blocked by ω-conotoxin GVIA in intracardiac neurons and (ii) voltage-gated sodium channels may activate unblocked Ca_v by intensifying the depolarization initiated by nAChR activation, a high concentration (1 μM) of tetrodotoxin (TTX) to block voltage-gated sodium channels was used together with an almost maximally effective concentration (100 nM) of the expensive ω-conotoxin GVIA (Xu & Adams, 1992b).

As shown in figure 29, *100 nM ω-conotoxin GVIA and 1 μM TTX reduced $[Ca^{2+}]_i$ transients* evoked by the focal application of 500 μM ACh in the presence of 1 μM atropine by 69 % from 26 ± 5 nM to 8 ± 2nM in fura-2 loaded intracardiac neurons ($P < 0.01$; $n = 5$). Note that the control condition is uniquely based on transients obtained prior to the wash-in of ω-conotoxin GVIA and TTX and does not include values from a washout condition as the effects of *ω-conotoxin GVIA are virtually irreversible*. The calculated magnitude of the inhibition may therefore be somewhat overestimated, as this procedure does not correct for any rundown in the cellular responses to agonist application.

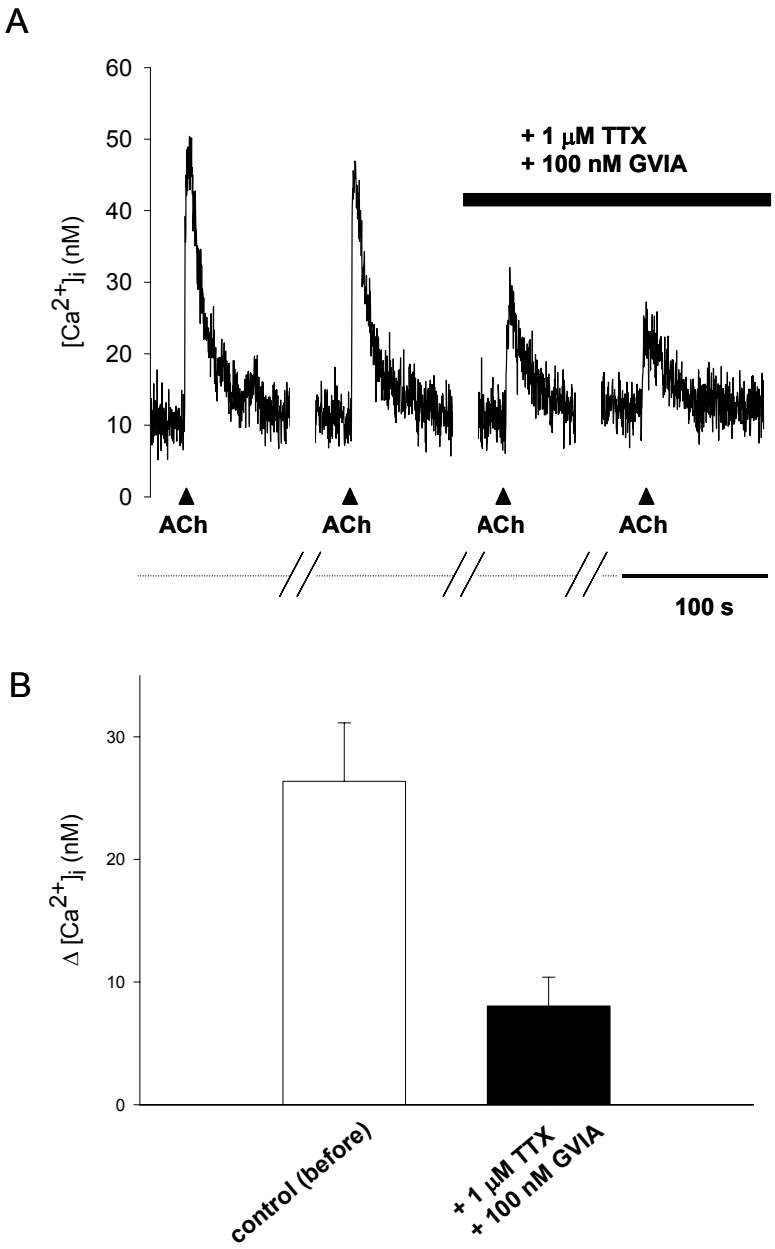

Figure 29: *nAChR-induced $[Ca^{2+}]_i$ transients in rat intracardiac neurons are inhibited by ω-conotoxin GVIA and TTX*

A: *$[Ca^{2+}]_i$ transients in response to focal application of 500 µM ACh obtained in the absence (control) and presence of 100 nM ω-conotoxin GVIA and 1 µM TTX in the bath solution.*
The bath solution also contained 1 µM atropine to inhibit mAChRs.

B: *Bar graphs of the changes in ACh-induced $[Ca^{2+}]_i$ increases by ω-conotoxin GVIA and TTX together with 1 µM atropine bath applied.*
Bath application of 100 nM ω-conotoxin GVIA and 1 µM TTX significantly reduced ACh-induced increases in $[Ca^{2+}]_i$ ($P < 0.01$, n = 5).

Taken together, the control experiments described above show that *voltage-gated Ca^{2+} channels contribute to the increase in $[Ca^{2+}]_i$ initiated by nAChR activation*, but the *exact magnitude of their contribution remains to be determined.*

3.2 Effects of i.v. anaesthetics on $[Ca^{2+}]_i$ transients and membrane currents in intracardiac neurons

3.2.1 Thiopental

3.2.1.1 Inhibition of nAChR-induced $[Ca^{2+}]_i$ transients

In fura-2-loaded rat intracardiac neurons, focal application of 500 μM ACh to the cell soma in the presence of the muscarinic ACh receptor antagonist, atropine (100 nM) in the bath solution, evoked a rapid, transient increase in $[Ca^{2+}]_i$ ($\Delta[Ca^{2+}]_i$) of 70 ± 5 nM above resting $[Ca^{2+}]_i$ (n = 21).

In the presence of the barbiturate, thiopental (25 μM = clinical EC_{50}; Franks & Lieb, 1994; Krasowski & Harrison, 1999; Yamakura et al., 2001), however, the *increase in $[Ca^{2+}]_i$* evoked by focal application of 500 μM ACh in the presence of atropine was *inhibited* by 42 % from 66 ± 14 nM to 38 ± 10 nM ($P < 0.01$; n = 6) as shown in figure 30A. Applying ACh in the presence of atropine and varying concentrations of thiopental obtained a *concentration-response curve. Half maximal inhibition of $\Delta[Ca^{2+}]_i$ by thiopental* occurred at *28 μM*, a value comparable to the clinical EC_{50} of thiopental, with a *Hill coefficient of 1.24*, as shown in figure 30 B.

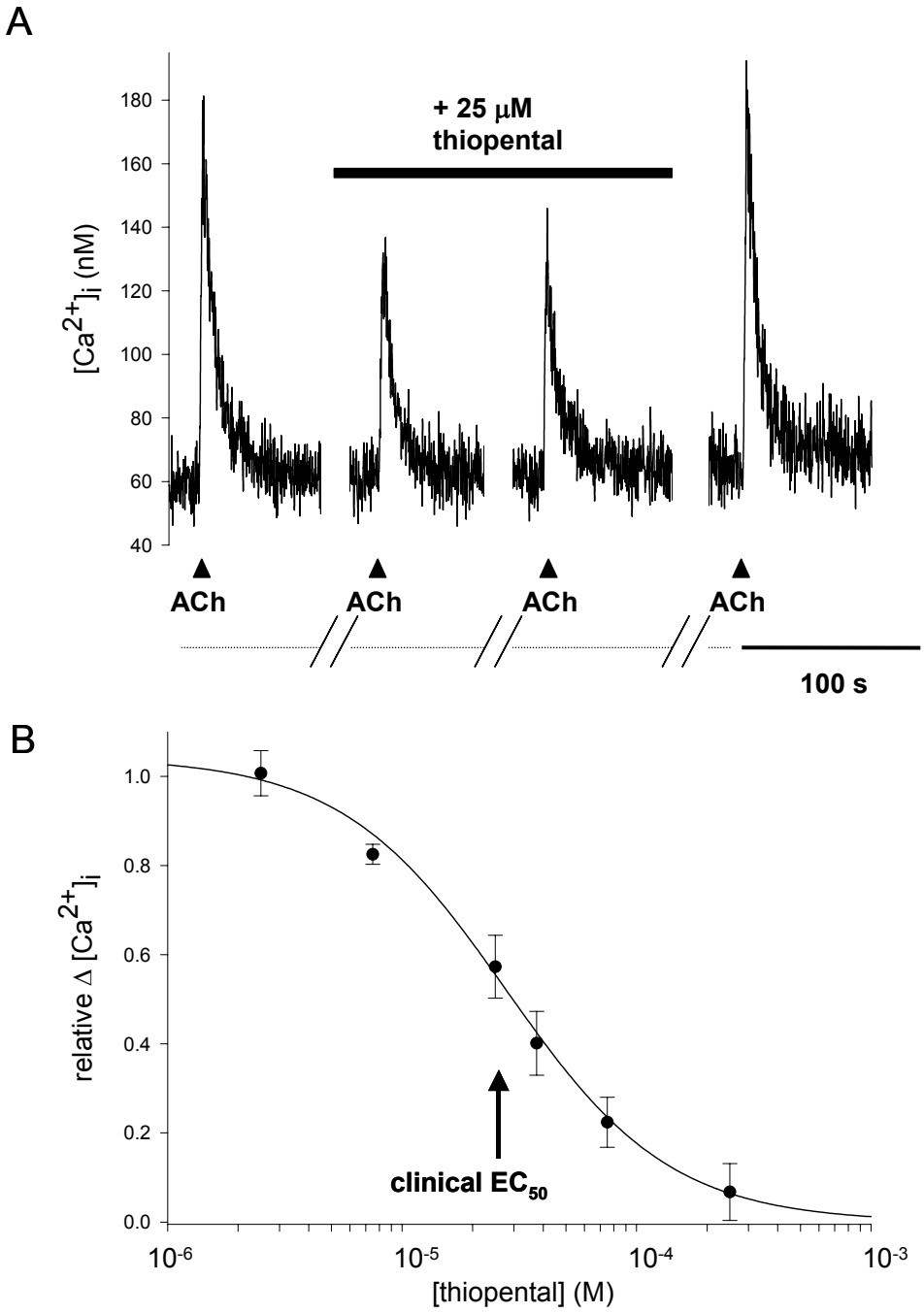

Figure 30: Clinically relevant concentrations of thiopental inhibit nAChR-mediated $[Ca^{2+}]_i$ transients in rat intracardiac neurons

A: *$[Ca^{2+}]_i$ transients in response to focal application of 500 μM ACh obtained in the absence (control) and presence of 25 μM thiopental in the bath solution.*
The bath solution also contained 100 nM atropine to inhibit mAChR.

B: *Concentration-response relationship for inhibition of ACh-induced $[Ca^{2+}]_i$ transients by thiopental in the presence of 100 nM atropine.*
Average $[Ca^{2+}]_i$ responses to ACh in the presence of thiopental were normalized to average responses obtained with agonist applications before and after superfusion with thiopental in the same cells. Data points represents the mean normalized $[Ca^{2+}]_i$ response ± S.E.M. from 2 to 7 cells. The curve of best fit to the data had a K_d = 28 μM and Hill coefficient of 1.24.

3.2.1.2 Simultaneous inhibition of nAChR-induced currents and $[Ca^{2+}]_i$ transients in voltage-clamped neurons

To exclude any contribution of a secondary influx of Ca^{2+} ions to the increase in $[Ca^{2+}]_i$ due to the involvement of voltage-dependent Ca^{2+} channels activated by nAChR-induced depolarization of the cell membrane, the influx of Ca^{2+} by nAChR activation was studied under voltage-clamp conditions. Using the perforated patch recording configuration, fura-2 loaded neurons were held at –60 mV and application of 500 µM ACh in the presence of atropine evoked peak current amplitudes and increases in peak $[Ca^{2+}]_i$ of –602 ± 195 pA and 88 ± 19 nM (n = 4) from a resting $[Ca^{2+}]_i$ of 174 ± 12 nM respectively[2]. Bath application of 25 µM thiopental reduced the peak current amplitude by 61 % to –237 ± 84 pA ($P < 0.05$; n = 4) and the $[Ca^{2+}]_i$ response by 53 % to 41 ± 10 nM ($P < 0.05$) as shown in figure 31. This result shows that a *clinically relevant concentration of thiopental inhibits nAChR-induced peak current amplitudes and simultaneous increases in $[Ca^{2+}]_i$, without any contribution of voltage-gated Ca^{2+} channels.*

[2] Interestingly, resting $[Ca^{2+}]_i$ in patched neurons was several-fold higher than in unpatched neurons. As a comparable increase in basal $[Ca^{2+}]_i$ was observed in somatotropes due to Ca^{2+} flux via stretch-activated Ca^{2+} channels that were activated by the seal-formation during patch-clamping (Robert et al., 1999), it can be speculated that these channels may also be present in rat intracardiac neurons.

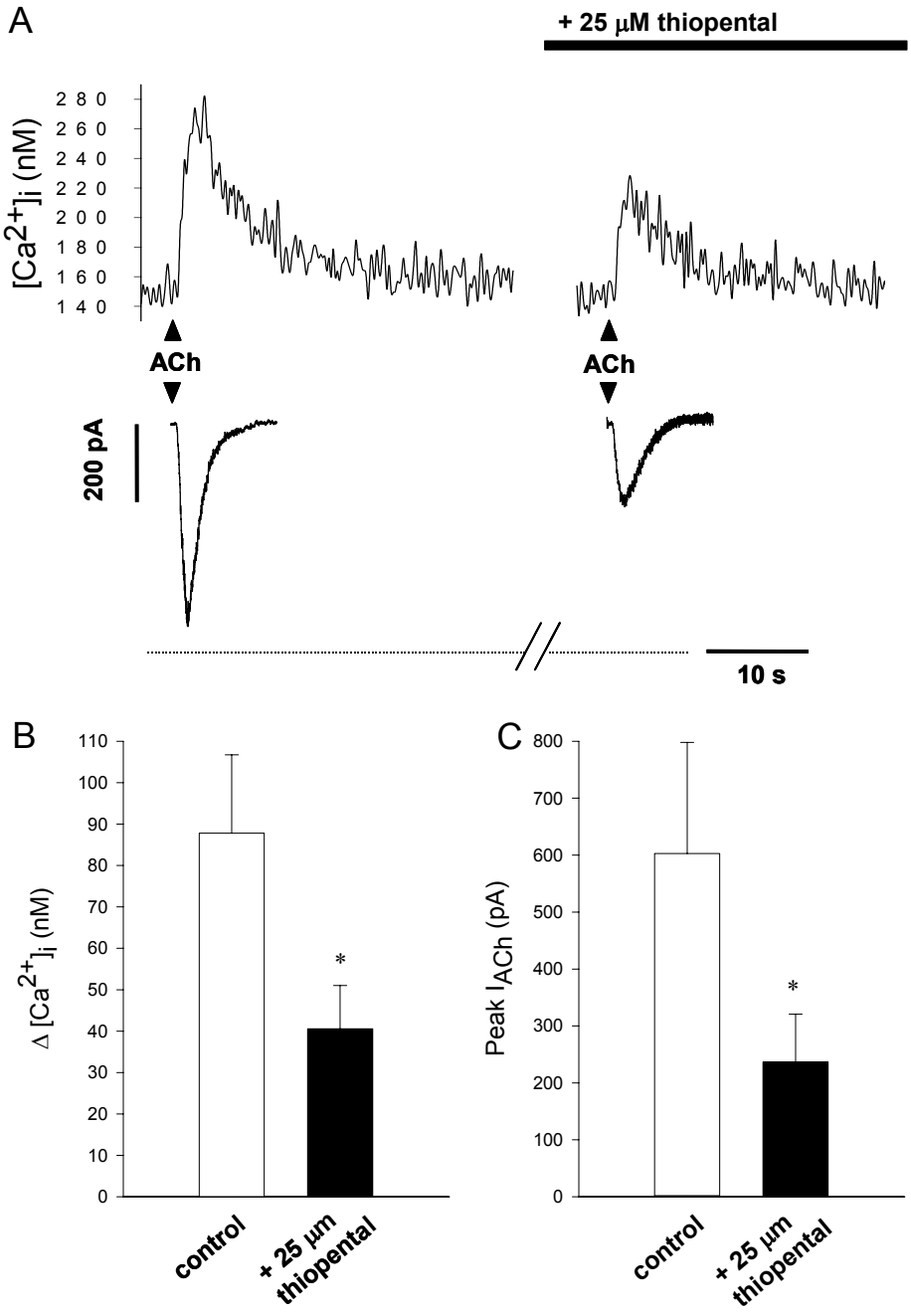

Figure 31: Inhibition of nAChR-mediated $[Ca^{2+}]_i$ transients and membrane currents (I_{ACh}) by thiopental

A: *Fura-2-loaded rat intracardiac neurons were voltage-clamped at –60 mV using the perforated patch whole-cell recording configuration.*
Traces of transient $[Ca^{2+}]_i$ and whole-cell inward currents recorded simultaneously in response to 500 µM ACh in the absence and presence of 25 µM thiopental bath applied. The bath solution also contained 100 nm atropine.

B, C: *Bar graphs of the changes in ACh-induced $[Ca^{2+}]_i$ increases and membrane currents by thiopental together with ≥ 100 nM atropine bath applied.*
Bath application of 25 µM thiopental significantly reduced ACh-induced increases in $[Ca^{2+}]_i$ ($P < 0.05$, n = 4) and peak inward current amplitude ($P < 0.05$, n = 4).

3.2.1.3 Voltage-independent inhibition of nAChR-induced currents

Further experiments were carried out using the *dialyzed-patch* recording configuration in which the pipette solution contained *2 mM BAPTA to surmount any intracellular Ca^{2+} buffers*. The ACh-evoked currents exhibited strong inward rectification and reversed close to 0 mV as described previously (Adams & Nutter, 1992; Fieber & Adams, 1991a). As shown in figure 32A and B, bath application of 25 μM thiopental reversibly inhibited nAChR-induced peak current amplitudes at negative holding potentials ranging from –120 mV to –40 mV. *Thiopental significantly inhibited peak current amplitudes* at –120mV by 38 % from –1077 ± 122 pA to –671 ± 105 pA, at –80 mV by 38 % from –732 ± 81 pA to –454 ± 70 pA and at –40 mV by 35 % from –314 ± 32 pA to –205 ± 30 pA (n = 11, $P < 0.00033$ for each holding potential). The significance criteria (α) of p = 0.001 were conservatively adjusted to p = 0.00033 for each of these three holding potentials to take the number of comparisons (= 3) into account. A linear regression of the relative peak current amplitudes and the holding potentials revealed that the slope was not significantly different from zero ($P > 0.3$), indicating that *thiopental inhibition of nAChR-induced currents* was *voltage-independent over the range of –120 to –40 mV* (see figure 32C).

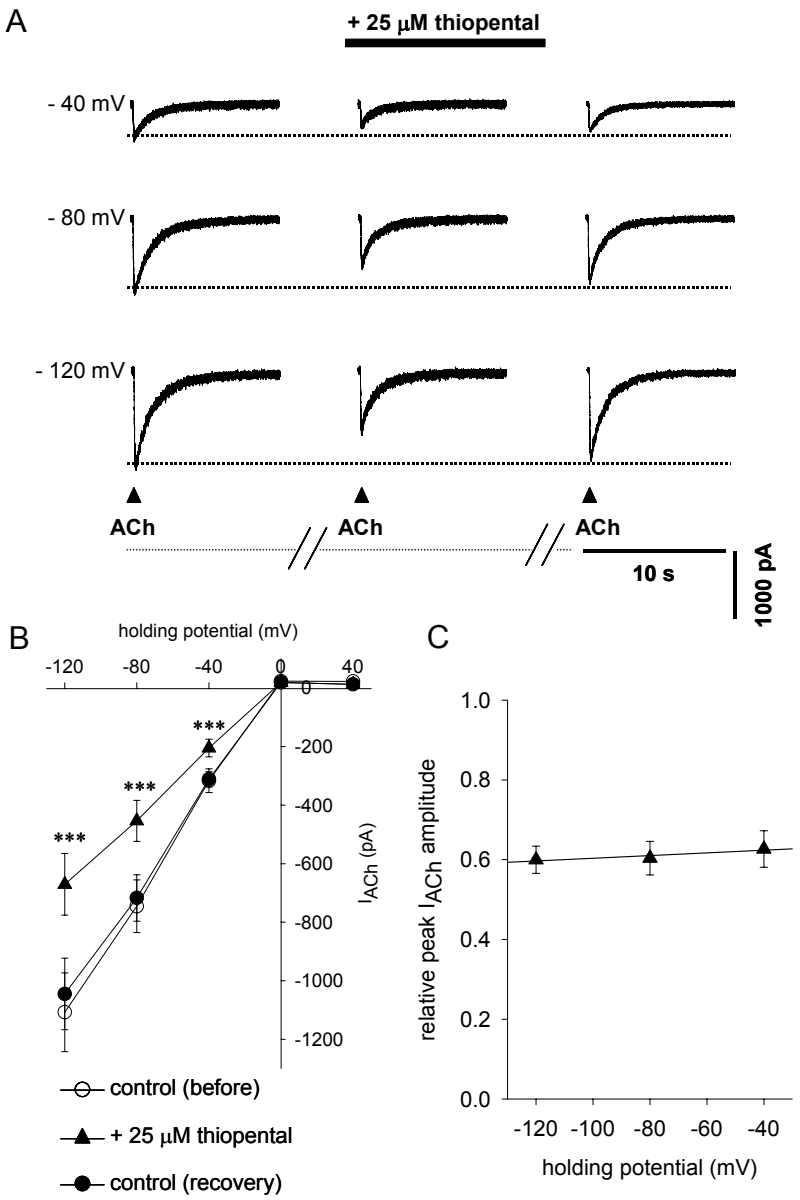

Figure 32: *Voltage-independent inhibition of nAChR-mediated membrane currents by thiopental in voltage-clamped rat intracardiac neurons*

A: *Whole-cell currents evoked by 300 μM ACh in the presence of 100 nM atropine at various membrane potentials in the absence (control) and presence of 25 μM thiopental, as indicated by the horizontal bar.* The dashed horizontal lines indicate control responses obtained by averaging the peak current amplitudes before and after superfusion with thiopental.

B: *Current-voltage relationship for peak current amplitude evoked by 300 ACh μM in the presence of 100 nM atropine.*

Data points represent mean peak current amplitudes ± SEM of 11 cells, before, during and after superfusion with 25 μM thiopental.

C: *Inhibition of ACh-induced peak current amplitudes by thiopental as a function of membrane potential in the presence of 100 nM atropine.*

Data points represent normalized mean peak current amplitudes ± SEM of 11 cells in the presence of 25 μM thiopental. Responses were normalized to average responses obtained before and after the superfusion with 25 μM thiopental in each individual cell. A linear regression of the relative peak current amplitudes and the holding potentials indicated that the slope was not significantly different from 0 ($P > 0.3$).

3.2.1.4 No inhibition of Ca^{2+} release from caffeine-sensitive Ca^{2+} stores

Recently, we have shown that Ca^{2+} influx upon nAChR activation leads to Ca^{2+}-induced Ca^{2+} release (CICR) from intracellular, ryanodine-sensitive Ca^{2+} stores in rat intracardiac neurons (Beker et al., 2003). The secondary Ca^{2+} release from intracellular Ca^{2+} stores via ryanodine receptor (RyR) channels thus amplifies the nAChR-induced increase in $[Ca^{2+}]_i$. Given that thiopental has been suggested to inhibit ryanodine-induced Ca^{2+} release from the SR of papillary muscle cells (Komai & Rusy, 1994), the effect of thiopental on RyR channels was examined in rat intracardiac neurons. Caffeine, which is known to activate RyR channels, while inhibiting IP_3 receptor channels (Ehrlich et al., 1994), was used to examine the effects of thiopental on Ca^{2+} release from ryanodine-sensitive intracellular stores. As shown in figure 33, application of *10 mM caffeine*, which is likely to induce a maximal Ca^{2+} release from ryanodine-sensitive stores, evoked *a transient, approximated, increase in $[Ca^{2+}]_i$* of 92 ± 14 nM (n = 9), which was *not significantly different from that obtained in the presence of 25 μM thiopental* (90 ± 14 nM; 98 % of control, n = 9; $P > 0.3$). These data indicate that the *clinical EC_{50} of thiopental does not inhibit RyR mediated-Ca^{2+} transients in rat intracardiac neurons.*

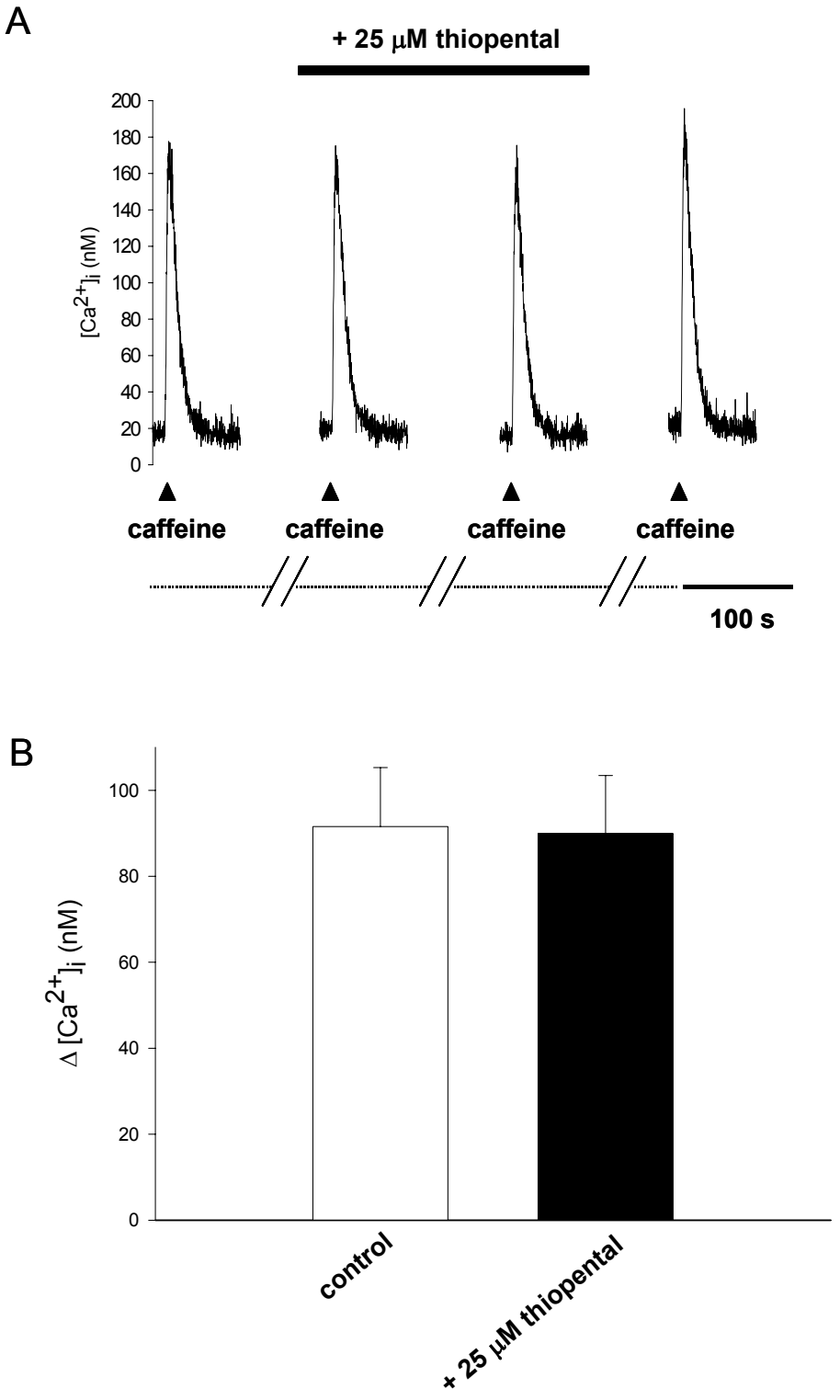

Figure 33: Caffeine-induced $[Ca^{2+}]_i$ transients are not inhibited by thiopental

A: *$[Ca^{2+}]_i$ transients evoked upon activation of ryanodine receptors by application of 10 mM caffeine* in the absence (control) and presence of 25 μM thiopental, as indicated by the horizontal bar.

B: *Bar graphs of caffeine-induced $[Ca^{2+}]_i$ increases in the absence (control) and presence of 25 μM thiopental.* Bath application of 25 μM thiopental did not significantly change caffeine-induced increases in $[Ca^{2+}]_i$ ($P > 0.3$, n = 9).

3.2.2 Pentobarbital

Bath application of the barbiturate, pentobarbital (50 μM = clinical EC_{50}; Franks & Lieb, 1994; Krasowski & Harrison, 1999; Yamakura et al., 2001), reversibly inhibited increases in $[Ca^{2+}]_i$ evoked by focal application of 500 μM ACh by 40 % from 77 ± 7 nM to 46 ± 11 nM (n = 8; $P < 0.01$) as shown in figure 34A and C.

3.2.3 Ketamine

Similarly, the dissociative anaesthetic, ketamine (10 μM = clinical EC_{50}; Krasowski & Harrison, 1999; Yamakura et al., 2001), also reversibly inhibited ACh-induced increases in $[Ca^{2+}]_i$ by 43 % from 65 ± 8 nM to 37 ± 10 nM[3] (n = 7; $P < 0.05$) as shown in figure 34B and C.

[3] Increases in $[Ca^{2+}]_i$ were reduced by 40 % to 39 ± 11 nM ($P < 0.05$) when approximations of $[Ca^{2+}]_i$ using formula (3) were based on the corrected (i.e. reduced by 4 %) R_{max} value for the ketamine condition (see chapter 3.1.1.2).

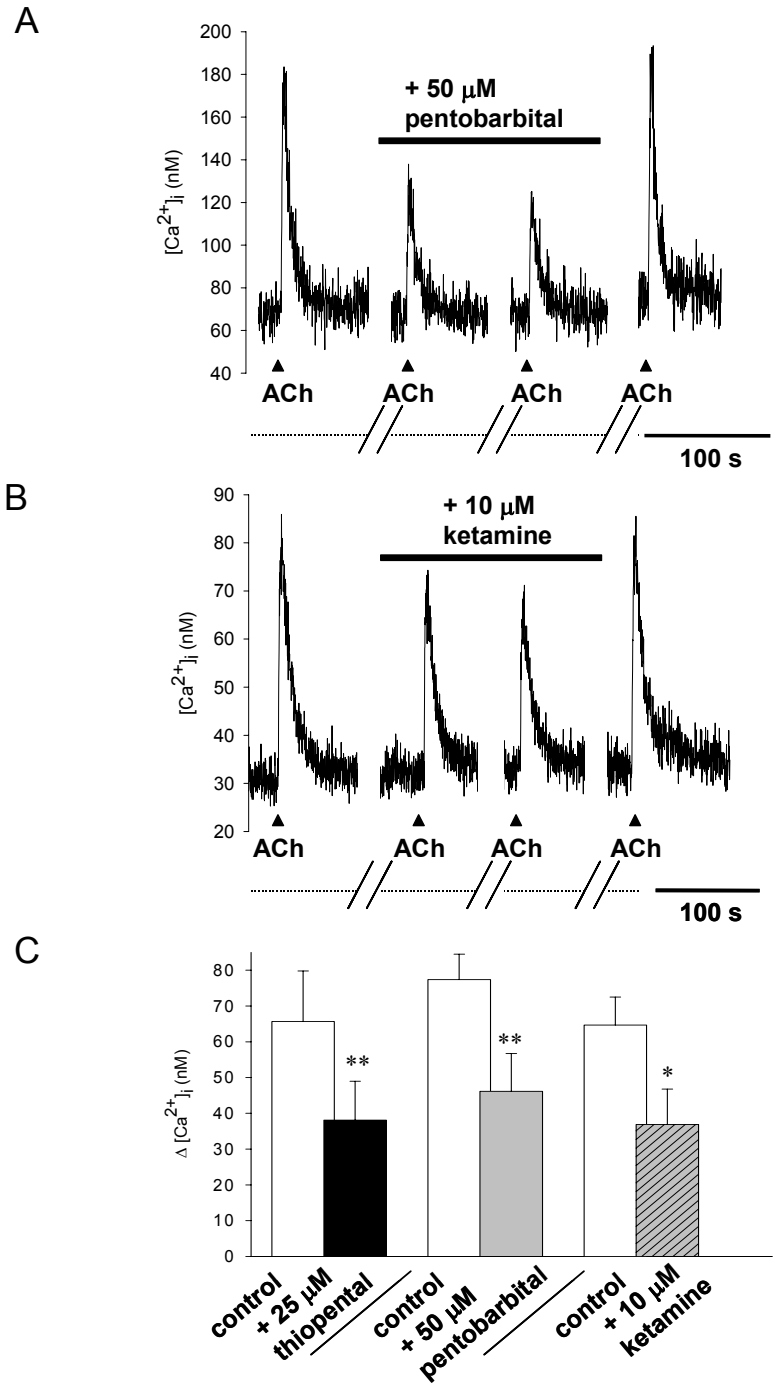

Figure 34: Clinically relevant concentrations of thiopental, ketamine and pentobarbital inhibit nAChR-mediated $[Ca^{2+}]_i$ transients

A: *$[Ca^{2+}]_i$ transients in response to focal application of 500 μM ACh obtained in the absence (control) and presence of 50 μM pentobarbital in the bath solution.*
The bath solution also contained 100 nM atropine to inhibit mAChR.

B: *$[Ca^{2+}]_i$ responses to 500 μM ACh focally applied in the presence of 100 nM atropine obtained in the absence (control) and presence of 10 μM ketamine in the bath solution.*

C: *Bar graph of Δ $[Ca^{2+}]_i$ in response to ACh (control), ACh + 25 μM thiopental (n = 6), 50 μM pentobarbital (n = 8), and 10 μM ketamine (n = 7).*
Atropine (100 nM) was present in all bath solutions to inhibit mAChR.

4 DISCUSSION

4.1 Assessment of fura-2 quenching by i.v. anaesthetics

As various chemical agents, including lipophilic solutions (Muschol, 1999; Roe et al., 1990) were shown to interfere with fura-2 measurements, we have assessed possible interactions of the very lipophilic anaesthetics thiopental, pentobarbital and ketamine with fura-2.

Firstly, using spectrophotometry, the absorbance characteristics of clinically relevant concentrations of i.v. anaesthetics were examined in the presence and absence of fura-2. As the barbiturates thiopental and its metabolite pentobarbital are chemically identical with respect to all but one of their atoms (Büch & Büch, 2001; Chan et al, 1985; Charney et al, 2001, Evers & Crowder, 2001), thiopental as the major, and clinically more relevant representative of the barbiturates was tested, as well as the chemically distinct dissociative anaesthetic ketamine.

It was shown that (i) both *25 µM thiopental and 10 µM ketamine marginally increase the absorbance of (Ca^{2+}) -EGTA solutions in an unspecific manner (also in the absence of fura-2).* This could lead to slightly diminished excitation intensities and subsequently reduced emission intensities for fura-2. However, as both Ca^{2+} -free and Ca^{2+} -containing solutions were affected similarly, these changes should affect peak and resting values of $[Ca^{2+}]_i$ transients in fura-2 loaded neurons similarly, while the calculated $\Delta [Ca^{2+}]_i$ values, on which the statistical tests are based, should not be affected by the presence of the i.v. anaesthetics. In addition, ratiometric dyes such as fura-2 are less vulnerable to changes in excitation intensities than single wavelength dyes such as fluo-4, given that both excitation wavelengths of the dual-excitation dye are more or less affected similarly.

(ii) The *ketamine-induced increase in absorbance* was *uniform over the whole excitation spectrum examined*, while the *thiopental–induced increase was more pronounced at wavelengths < 330 nm*. This can be *neglected on an actual ratiometric set-up* due to the narrow FWHM of the excitation light of the 340 nm bandpass filter or the corresponding monochromator setting.

(iii) Both, the *thiopental* or *ketamine–induced increases in absorbance* are *only a fraction of the total absorbance examined in the presence of fura-2*, again indicating that the magnitude of this effect is likely to be negligible.

(iv) Most importantly, *neither 25 μM thiopental nor 10 μM ketamine displayed a direct interaction with the dye* as virtually no specific changes of the absorbance characteristics of fura-2 (following subtraction of the unspecific, not dye-related effects) could be detected in the presence of the anaesthetics.

Taken together, these data clearly show that virtually *no anaesthetic-induced interference with the* absorbance and thus *excitation characteristics of fura-2* occurs at clinically relevant concentrations of the anaesthetics tested, suggesting that the absorbance properties of fura-2 allow for the administration of moderate doses of these anaesthetics in fura-2 experiments.

Furthermore, as not only the excitation, but also the emission characteristics of dyes can be affected by the presence of chemical agents, further *control experiments* were carried out *on the actual ratiometric imaging set-up*. Similar values for K_d, R_{min} and R_{max} and S_{f2}/S_{b2} were obtained in standard calibration solutions in the absence (control) or presence of clinically relevant concentrations of the barbiturates thiopental or pentobarbital, respectively, clearly showing that *fura-2 experiments can faithfully be carried out in the presence of these barbiturates*.

For the dissociative anaesthetic, *ketamine, R_{max} values* were *marginally*, but significantly *different from control conditions*. However, statistical tests *using R_{max} values that had been corrected for the presence of ketamine* yielded *similar results in experiments with fura-2 loaded cells,* indicating that the *mayor conclusions remain unaffected* (see chapter 3.2.3) – despite possible inaccuracies regarding the assessment of $[Ca^{2+}]_i$ in the presence of ketamine.

Finally, *resting $[Ca^{2+}]_i$ in fura-2 loaded rat intracardiac neurons* were *similar in the presence and absence of the anaesthetics* indicating that driving forces for Ca^{2+} ions were not affected by the anaesthetics.

4.2 Voltage-gated Ca^{2+} -channels contribute to nAChR-induced $[Ca^{2+}]_i$ transients

Further experiments using *Ca^{2+} -channels blockers cadmium* and *ω-conotoxin GVIA* have revealed that voltage-gated Ca^{2+} channels contribute to the increases in $[Ca^{2+}]_i$ following nAChR activation, but the exact extend of this contribution could not be assessed.

The voltage-gated Ca^{2+} -channel blocker *$CdCl_2$ appeared to strongly and reversibly inhibit nAChR induced increases in $[Ca^{2+}]_i$*. Note that this observed inhibition is unlikely to be due to a block of nAChR channels, given that the EC_{50} for the $CdCl_2$ induced block

of nAChR in rat intracardiac neurons is ~ 500 μM (Nutter & Adams, 1995) and thus about five-fold higher than the $CdCl_2$ concentration used in the present experiment. The astonishing finding, however, was that *mAChR induced increases in $[Ca^{2+}]_i$ in the presence of mecamylamine were similarly inhibited*. One explanation for the latter finding would be an *incomplete block of nAChR* by 3 μM mecamylamine and activation of voltage-gated Ca^{2+} channels following membrane depolarization initiated by cation flux through unblocked, activated nAChR channels. This is not unlikely, as a complete block of ACh-evoked currents could not even be obtained with mecamylamine concentrations several orders of magnitude greater than its K_d for inhibition of ACh-evoked currents in rat intracardiac neurons (37 nM; Fieber & Adams, 1991a). In line with that, and also in rat intracardiac neurons, Hogg et al. (1999) have determined the residual nAChR evoked current in the presence of 1 μM mecamylamine as about 12 %. In addition, several subunit combinations of nAChR channels, when expressed in *Xenopus* oocytes, including the very Ca^{2+} permeable α7 homomeric channel, have been shown to be relatively insensitive to mecamylamine (Chavez-Noriega et al., 1997).

However, alternative explanations for these results do arise from *multiple (unwanted) cadmium effects* aside from a block of voltage-gate Ca^{2+} -channels that are likely to confound fluorimetric $[Ca^{2+}]_i$ measurements.

Cadmium's major setback for fura-2 experiments is its direct *interaction with the dye*. Most importantly, in line with previous studies, our photospectrometer results demonstrate that *Cd^{2+} ions change the absorbance of unsaturated fura-2 in a similar manner like Ca^{2+}* (Hinkle et al., 1992; Marchi et al., 2000), with increased absorbance for excitation wavelengths below the isosbestic point (~355 nm) and reduced absorbance above it. Assuming that Cd^{2+} penetrates the cell, its interaction with intracellularly trapped fura-2 thus would increase fluorescence ratios and erroneously suggest increases in $[Ca^{2+}]_i$. However, there is some *controversy* concerning the *magnitude of fura-2 quenching in living cells*. Marchi and co-workers argue that the presence of heavy metal ions does not interfere with fluorescent Ca^{2+} measurements in living cells, as cytosolic metal ligands such as reduced glutathione diminish dye quenching considerably, but other groups use fura-2 quenching by Cd^{2+} as a method to measure Cd^{2+} fluxes inside cells (Hinkle et al., 1992; Usai et al., 1999). The crux of the matter, however, is that basically nothing is known about the *pathways of Cd^{2+} entry into intracardiac neurons*. In other cell types, including neurons, voltage-gated Ca^{2+} channels have been suggested to be a major entry pathway for Cd^{2+} ions (Hinkle et al., 1987; Hinkle et al., 1992), but Ca^{2+} -permeable receptor-

operated channels (ROC) and other Ca^{2+} entry pathways have been implied, too (Usai et al., 1999). Taken together, as cadmium ions are known to (i) quench fura-2 and (ii) are thought to enter excitable cells, they are likely to disturb fura-2 measurements also in rat intracardiac neurons.

A second crucial, cadmium-associated point is its *perturbation of the Ca^{2+} homeostasis of cells*. Most importantly, intracellular cadmium has been shown to increase $[Ca^{2+}]_i$ (Benters et al., 1997). Several factors are likely to contribute to cadmium-induced rises in $[Ca^{2+}]_i$, including cadmium binding to calmodulin and other cytosolic *Ca^{2+} -binding proteins* (Richard et al, 1986; Vig & Nath, 1991), inhibition of *Ca^{2+} -ATPases* (Hechtenberg & Beyersmann, 1991; Zhang et al., 1990), and a *perturbation of the IP_3 metabolism (*Benters et al., 1997). In particular, Benters and co-workers (1997) observed a cadmium-induced transient increase in the intracellular IP_3 concentration that peaked about 5 min following the beginning of the cadmium exposure. Increases in the intracellular IP_3 concentrations were followed by increases in $[Ca^{2+}]_i$ that reached a peak value about 15 min following the exposure to cadmium. A similar perturbation of the IP_3 mechanism in our preparation could alternatively explain the observed inhibition of mAChR induced $[Ca^{2+}]_i$ transients by cadmium ions, given that activation of mAChR in rat intracardiac neurons mobilizes Ca^{2+} from intracellular stores in a PLC – and thus most likely IP_3 – dependent manner, as we were recently able to show (Beker et al., 2003). In addition, the relatively slow increase in $[Ca^{2+}]_i$ following exposure to cadmium as observed in the study of Benters et al. (1997) may – at least in part – explain why resting $[Ca^{2+}]_i$ even appeared to increase during washout of cadmium. The increases in resting F_{340}/F_{380} observed in our experiments using $CdCl_2$ can therefore not only be due to fura-2 quenching by cadmium, but may at least in part reflect *true (cadmium-related) increases in $[Ca^{2+}]_i$*, indicating that driving forces for Ca^{2+} ions may be altered following cadmium application.

Taken together, there are still major *difficulties in interpreting ratiometric $[Ca^{2+}]_i$ measurements in the presence of cadmium*, which do not allow an unequivocal decision whether voltage-gated Ca^{2+} channels contribute to nAChR induced increases in $[Ca^{2+}]_i$.

Alternative control experiments were based on the use of the N-type voltage-gated Ca^{2+}-channel blocker ω-conotoxin GVIA (Boland et al., 1994; Feng et al., 2001) together with the voltage-gated sodium channel blocker TTX. nAChR induced $[Ca^{2+}]_i$ transients were inhibited in the presence of TTX and the peptide toxin *ω-conotoxin GVIA*. While these results clearly show that *voltage-gated Ca^{2+} channels contribute to nAChR*

induced $[Ca^{2+}]_i$ transients, the calculated percentage of inhibition (~ 70 %) does not reflect the contribution of Ca^{2+} influx via voltage-gated Ca^{2+} channels to the nAChR induced signal in the experiments with the anaesthetics. Firstly, this calculation is likely to be an *overestimation of the contribution of N-type voltage-gated Ca^{2+} channels*, as the conotoxin/TTX condition is compared with responses before the wash-in of these drugs a control condition. Thus, the estimation may be confounded by rundown of the nAChR-induced responses during the time course of the experiment. The problem here is that the effects of *ω-conotoxin GVIA* are virtually *irreversible* which means that a rundown of the observed cellular responses cannot be detected using the reversibility criteria of the washout condition. Secondly, Ca^{2+} release from *ryanodine-sensitive stores* has been shown to contribute to nAChR induced increases in $[Ca^{2+}]_i$ (Beker et al. 2003) and the magnitude of this contribution may vary with the size of the Ca^{2+} influx. Finally, a higher atropine concentration (1 μM) was used in the conotoxin experiments than in all anaesthetics experiments in unclamped cells (100 nM). This is crucial, as *high concentrations of atropine* can alter the size of (neuronal) nAChR induced currents (Zwart & Vijverberg, 1997), and thus possibly also the relative contribution of Ca^{2+} influx via nAChR channels to the nAChR induced increase in $[Ca^{2+}]_i$.

4.3 I.v. anaesthetics inhibit nAChR-induced $[Ca^{2+}]_i$ transients

We have shown that the *activation of nAChR* channels in fura-2 loaded rat intracardiac neurons induces a *transient increase in $[Ca^{2+}]_i$*, which can be *inhibited by clinically relevant concentrations of i.v. anaesthetics*. Thiopental (25 μM), inhibited nAChR-induced increases in $[Ca^{2+}]_i$ by 42 % and a similar inhibition was observed with pentobarbital (50 μM; 40 % inhibition) and with the dissociative anaesthetic, ketamine (10 μM; 43 % inhibition). These results are consistent with previously reported studies using oocyte expression systems in which i.v. anaesthetics, including barbiturates and ketamine, have been shown to inhibit neuronal nAChR-mediated currents (see Krasowski & Harrison, 2000; Yamakura et al., 2001). On a molecular and cellular level, this corresponds with the clinical observation indicating that no specific chemical group is required to produce the effects that occur during general anaesthesia (see Franks & Lieb, 1994). Given that the resting $[Ca^{2+}]_i$ was similar in the absence and the presence of the i.v. anaesthetics, indicating that *concentration gradients for Ca^{2+} were unaffected*, then changes in the driving force for Ca^{2+} cannot account for the inhibition of ACh-induced $[Ca^{2+}]_i$ transients

observed in the presence of the i.v. anaesthetics. Taken together, these results clearly show that clinically relevant concentrations of *i.v. anaesthetics* can *modulate intracellular Ca^{2+} signals* in response to nAChR activation and thus possibly modify various cellular, Ca^{2+}-dependent functions, ranging from neuronal excitability to neurotransmitter secretion in intracardiac ganglia. Bath application of the i.v. anaesthetics prior to ACh application is likely to *simulate the situation* that occurs *during* the *maintenance of general anaesthesia* whereby the *receptor and anaesthetic are at equilibrium* (Downie et al., 2000). Our data demonstrate that bath application of clinically relevant concentrations of i.v. anaesthetics in intact, unclamped cells inhibit nAChR-induced Ca^{2+} transients. These data strongly suggest that *similar effects* may occur *when intracardiac neurons* are *exposed to cholinergic stimulation in the presence of i.v. anaesthetics during anaesthesia.*

The *concentration-response curve* for the thiopental inhibition of nAChR-induced increases in $[Ca^{2+}]_i$ had a Hill coefficient of 1.24 and a half maximal inhibition, IC_{50} of 28 μM, which is close to the clinical EC_{50} of thiopental, indicating that the nAChR may represent an *important molecular target* of clinically relevant concentrations of thiopental.

4.4 Thiopental inhibits nAChR- induced currents and $[Ca^{2+}]_i$ transients in voltage-clamped neurons

4.4.1 Thiopental simultaneously inhibits nAChR-induced currents and $[Ca^{2+}]_i$ transients

Voltage-gated Ca^{2+} channels have been shown to be relatively insensitive to clinically relevant concentrations of general anaesthetics although a few exceptions have been reported (Franks & Lieb, 1994; 1998; Lynch & Pancrazio, 1994; Study, 1994). Under voltage-clamp conditions, ACh-induced transient increases in $[Ca^{2+}]_i$ concomitant with rapid inward currents were inhibited in the presence of 25 μM thiopental. These data demonstrate that, (i) *i.v. anaesthetic block of nAChR-induced Ca^{2+} transients in rat intracardiac neurons occurs without any contribution of voltage-gated Ca^{2+} channels*, and (ii) a *common mechanism* underlies the *simultaneous inhibition of nAChR-induced inward currents* and *$[Ca^{2+}]_i$ transients by an i.v. anaesthetic*, that is *block of Ca^{2+} influx through nAChRs*. Inhibition of ACh-evoked inward currents by thiopental has also been described in PC12 cells (Andoh et al. 1997) and for nAChRs exogenously expressed in *Xenopus* oocytes (Coates et al., 2001; Downie et al., 2000).

4.4.2 Voltage-independent block of nAChR-induced currents by thiopental

Under voltage clamp conditions, thiopental inhibited nAChR-mediated currents in rat intracardiac neurons in a voltage-independent manner at membrane potentials ranging from –120 to – 40 mV, consistent with that reported previously for thiopental inhibition of nAChRs in PC12 cells (Andoh et al. 1997) and human α7 homomeric nAChR-channels expressed in *Xenopus* oocytes (Coates et al., 2001). The *voltage-independence of the thiopental inhibition* does *not exclude an action of thiopental inside the pore of the nAChR channel* (Andoh et al., 1997), as ~ 35 % of the thiopental molecules are likely to be present in the non-dissociated – and thus uncharged – state under our experimental conditions. This can be estimated based on the pKa value for thiopental (= 7.6; see Büch & Büch, 2001; Wellhöner, 1988), the pH value of our solutions (= 7.34; see chapter 2.5) and using the equation (see e.g. Wellhöner et al., 1988)

$$n_b = 1/(1+10^{(pKa - pH)}) \qquad (5)$$

where n_b is the fraction of the (basic) drug that is present in the non-dissociated state. Thiopental block of nAChR-mediated currents was also observed in dialyzed patch experiments in which the pipette solution dictates the cytoplasmic composition, indicating that the *mechanism underlying the observed inhibition is not dependent on diffusible intracellular second messenger pathways*. In contrast, the involvement of diffusible intracellular second messengers in mediating the inhibition of receptor-channels by anaesthetics in *Xenopus* oocytes cannot be entirely eliminated (Downie et al., 2000). In particular, the pipette solution containing the rapid Ca^{2+} chelator, BAPTA, is likely to (i) surmount any endogenous intracellular Ca^{2+}-buffer, (ii) to ensure a stable resting $[Ca^{2+}]_i$ and (iii) to substantially suppress CICR. Therefore, it is *unlikely* that the *inhibition of nAChR-induced currents observed in the presence of thiopental* is due to a *reduced driving force for* Ca^{2+} caused either by reduced intracellular Ca^{2+} buffer capacities or increased CICR responses from internal stores. Thiopental inhibition of nAChR induced currents in rat intracardiac neurons is most likely due to a *direct action of thiopental on nAChR channels* as proposed previously in studies using oocyte expression systems (Coates et al., 2001; Downie et al., 2000).

4.5 Thiopental does not inhibit Ca^{2+} release from caffeine-sensitive Ca^{2+} stores

Given that CICR via the activation of RyR has been shown to contribute to nAChR-induced Ca^{2+} transients in rat intracardiac neurons (Beker et al., 2003), the effects of thiopental on RyR-induced CICR were examined upon activation of RyR with caffeine. As millimolar concentrations of caffeine are known to interact with fura-2 and to cause a red shift in the excitation spectra along with a reduced dynamic range of the dye (Muschol, et al. 1999; Uttenweiler et al., 1995), caffeine-induced increases in $[Ca^{2+}]_i$ should be treated as approximations and are likely to be underestimated. Despite that, it was clearly shown that *clinically relevant concentrations of thiopental* had *no effect on caffeine-induced increases in* $[Ca^{2+}]_i$, indicating that *thiopental is unlikely to inhibit CICR from internal stores by inhibiting RyR channels*. It remains to be determined, whether thiopental potentiation of Ca^{2+} release from ryanodine-sensitive Ca^{2+} stores may occur, as reported previously for high concentrations of volatile anaesthetics on the Ca^{2+}-release from the SR in skeletal muscle (Kunst et al., 1999, 2000).

5 CONCLUSION AND OUTLOOK

We have shown that clinically relevant concentrations of i.v. anaesthetics modulate Ca^{2+} homeostasis in intracardiac neurons by inhibiting ACh-induced currents and $[Ca^{2+}]_i$ transients. The *inhibition of ACh-induced $[Ca^{2+}]_i$ transients by thiopental* is due to a *direct interaction with nAChR channels* to inhibit Ca^{2+} influx and *not* a consequence of *block of voltage-dependent Ca^{2+} channels or inhibition of Ca^{2+} release* following RyR activation.

Given that ACh is the primary neurotransmitter mediating parasympathetic (vagal) regulation of the heart and the presence of functional nAChR channels in intracardiac postganglionic neurons, *clinically relevant concentrations of i.v. anaesthetics may modulate cardiac parameters during anaesthesia* by *binding to postsynaptic nAChRs and depressing ganglionic transmission.*

A direct effect of i.v. anaesthetics on nAChR channels in mammalian intrinsic cardiac neurons has not previously been taken into account when interpreting changes in heart rate and cardiac output during anaesthesia.

As nAChR can also be found presynaptically (MacDermott et al., 1999) as well as in sympathetic ganglia, it will be interesting to find out if i.v. anaesthetics similarly target nAChR in these regions.

Further studies would greatly benefit from conclusive *in vivo data* regarding the *cardiovascular effects of stereoisomers* of the anaesthetics studied. Once such data is available the effects of the stereoisomers could be studied in detail in intracardiac ganglia and other relevant target tissues to further pinpoint the origin of such clinical side effects.

The present study has investigated the effects of thiopental on the RyR that were activated by very high concentrations of caffeine, to ensure that the inhibition of nAChR induced Ca^{2+} signals was not actually due to an inhibition of RyR channels. However, the use of very high concentrations of caffeine – while providing stable signals with a good signal to noise ratio – may not allow to detect any potentiation of caffeine induced Ca^{2+} release from ryanodine-sensitive stores.

A better understanding of the cellular Ca^{2+} homeostasis during anaesthesia, however, will ultimately require an *in-depth study of the effects of clinically relevant concentrations of anaesthetics on intracellular Ca^{2+} -release channels*. In skeletal muscle, e.g. previous studies have shown that only anaesthetic concentrations several fold higher than those of clinical relevance lead to Ca^{2+} release from intracellular stores (Kunst et al., 1999, 2000). Yet, with the advancement of *confocal fluorescence microscopy*, it has become possible to

examine *local Ca^{2+} release events* from single intracellular Ca^{2+} release channels or clusters thereof. Interestingly, Uttenweiler et al. (2003) were recently able to show that clinically relevant concentrations of halothane induced such local Ca^{2+} release events from the SR of skeletal muscle, indicating that the *RyR* may have to be considered as *a distinct molecular target of general anaesthetics*. Thus, it would be highly interesting to *test clinically relevant concentrations of anaesthetics on local Ca^{2+} release* events caused by intracellular Ca^{2+} release channels *in neurons*, applying high-resolution *confocal microscopy*. Yet, the Ca^{2+} release events occurring in neurons are still at the very detection limit of confocal microscopy, even though a few reports of elementary Ca^{2+} release events from intracellular stores in neurons do exist (Koizumi et al., 1999; Melamed-Book et al., 1999). However, in analogy with the techniques used in muscle research, it may be possible to *chemically skin neurons* and thus be able to *create favourable conditions for* a reliable occurrence and *detection of local Ca^{2+} -release events in neurons*.

Our photospectrometer studies have indicated that fura-2 experiments are feasible in the presence of clinically relevant concentrations of thiopental and ketamine. However, one should be *cautious with very high concentrations* of these *anaesthetics*, given that the effects of these drugs on the *absorption characteristics of solutions in general*, as well as *on fura-2* are *likely to intensify with increasing concentrations* of the anaesthetics. Similar concerns may hold true for the emission characteristics of fura-2 and other Ca^{2+} indicators. Taken together, these are possible sources of artefacts that other researchers of the field should clearly have in mind when using Ca^{2+} indicators in the presence of (high concentrations of) lipophilic anaesthetics.

Another *possible source of artefacts in physiological experiments* in general may be related to the *use of Cd^{2+}*: Our preliminary experiments with Cd^{2+} suggests that Cd^{2+} ions can be very effective voltage-gated Ca^{2+} channel blockers, but *may enter the cytosol, where they may cause adverse effects* such as the perturbation of the Ca^{2+} pumps, or the IP3 mechanism (see chapter 4.2). While the extend of such effects may be tolerable in brief experiments – a long exposure to Cd^{2+} could aggravate these experimental problems.

Based on these preliminary results, it would also be very interesting to *investigate possible entry pathways of Cd^{2+} ions into neurons*. The combined use of fura-2 photometry together with patch-clamping is a particularly promising approach to the problem: Voltage-clamped fura-2 loaded neurons could be exposed to extracellular recording solutions with varying Ca^{2+} and Cd^{2+} concentrations, while cells are exposed to certain voltage-protocols (in combination with specific agonists) to specifically activate

presumed Cd^{2+} permeable channels. Using the dialyzed-patch configuration with fura-2 present in the patch-pipette and in the absence of extracellular and intracellular Ca^{2+} (together with well defined Mg^{2+} concentrations) may create a condition under which fura-2 mainly acts as a Cd^{2+} indicator.

The results of the present investigation lead to the important questions of the involvement of *stretch-activated Ca^{2+} permeable channels in rat intracardiac neurons*, given that (i) an increase in resting $[Ca^{2+}]_i$ was found in somatotropes due to Ca^{2+} flux via stretch-activated channels that were activated by the patch procedure and (ii) resting $[Ca^{2+}]_i$ was also several fold increased in clamped- neurons when compared with unclamped neurons of the present study (see chapter 3.2.1.2). The presence of *stretch-activated Ca^{2+} channels* may be *functionally significant*, as intracardiac neurons are likely to be exposed to mechanical forces that could activate such mechano-sensitive channels due to the pumping motion of the heart.

Finally, an intriguing possibility for *pharmaceutical research* that comes to mind when looking at nAChR subtypes would be to *take advantage of the different pharmaceutical profiles* that are related to the different subunit composition of *central vs. peripheral neuronal nAChR*. These differences could be used to *develop drugs that mainly target the CNS nAChR but not their PNS relatives or vice versa* to substantially reduce adverse side effects of such channel-modulating drugs and rat intracardiac neurons could provide a particularly interesting target tissue to test the effects of such drugs on peripheral neurons.

6 REFERENCES

Adams, D.J. & Nutter, T.J. (1992). Calcium permeability and modulation of nicotinic acetylcholine receptor-channels in rat parasympathetic neurons. *Journal of Physiology (Paris)* **86**, 67-76.

Adams, D.J., Dwyer, T.M. & Hille, B. (1980). The permeability of the endplate channels to monovalent and divalent metal cations. *Journal of General Physiology* **75**, 493-510.

Adams, H.A. & Werner, C. (1997). Vom Razemat zum Eutomer: (S)- Ketamine. *Anaesthesist* **46**, 1026-1042.

Aidley, D.J. (1998). *The physiology of excitable cells*. Cambridge: Cambridge University Press.

Akine, A., Suzuka, H., Hayashida, Y. & Kato, Y. (2001). Effects of ketamine and propofol on autonomic cardiovascular function in chronically instrumented rats. *Autonomic Neuroscience: Basics and Clinical* **87**, 201-208.

Alvarez, J. & Montero, M. (2002). Measuring [Ca^{2+}] in the endoplasmic reticulum with aequorin. *Cell Calcium* **32**, 251-260.

Andoh, T., Furuya, R., Oka, K., Hattori, S., Watanabe, I., Kamiya, Y. & Okumura, F. (1997). Differential effects of thiopental on neuronal nicotinic acetylcholine receptors and P2X purinergic receptors in PC12 cells. *Anesthesiology* **86**, 1199-1209.

Anis, N.A., Berry, S.C., Burton, N.R. & Lodge, D. (1983). The dissociative anaesthetics, ketamine and phencyclidine, selectively reduce excitation of central mammalian neurones by N-methyl-aspartate. *British Journal of Pharmacology* **79**, 565-575.

Antoni, H. (1996). Erregungsphysiologie des Herzens. In R.F. Schmidt & G. Thews (Eds.), *Physiologie des Menschen* (pp. 472-497). Berlin: Springer.

Aono, H., Hirakawa, M., Unruh, G.K., Kindscher, J.D. & Goto, H. (2001). Anesthetic induction agents, sympathetic nerve activity and baroreflex sensitivity: A study in rabbits comparing thiopental, propofol and etomidate. *Acta Med Okayama* **55**, 197-203.

Arias, H.R. McCardy, E.A., Bayer, E.Z., Gallagher, M.J. & Blanton, M.P. (2002). Allosterically linked non-competitive antagonist binding sites in the resting nicotinic acetylcholine receptor ion channel. *Archives of Biochemistry and Biophysics* **403**, 121-131.

Arias, H.R. McCardy, E.A., Gallagher, M.J. & Blanton, M.P. (2000). Interaction of

barbiturate analogs with the Torpedo californica nicotinic acetylcholine receptor ion channel. *Molecular Pharmacology* **60**, 497-506.

Armour, J.A. & Hopkins, D.A. (1990a). Activity of canine in situ left atrial ganglion neurons. *American Journal of Physiology* **259**, H 1207-1215.

Armour, J.A. & Hopkins, D.A. (1990b). Activity of in vivo canine ventricular neurons. *American Journal of Physiology* **258**, H 326-H336.

Armour, J.A. (1999). Myocardial ischaemia and the cardiac nervous system. *Cardiovascular Research* **41**, 41-54.

Armour, J.A., Murphy, D.A., Yuan, B-X., McDonald, S & Hopkins, D.A. (1997). Gross and microscopic anatomy of the human intrinsic cardiac nervous system. *The Anatomical Record* **247**, 289-298.

Armstrong, C., Edwards, R., Jan, L., Kaback, R., Kühlbrandt, W. Miller, C., Sanes, J. & Unwin, N. (2002). Membrane transport of small molecules and the electrical properties of membranes. In B. Alberts, A. Johnson, J. Lewis, M. Raff, K. Roberts & P. Walter (Eds.) *The molecular biology of the cell* (pp. 615-657). New York: Garland Science.

Azari, D.M. & Cork, R.C. (1993). Comparative myocardial depressive effects of propofol and thiopental. *Anesthesia* & *Analgesia* **77**, 324-329.

Babcock, D.F. & Hille, B. (1998). Mitochondrial oversight of cellular Ca^{2+} signaling. *Current Opinion in Neurobiology* **8**, 398-404.

Bakowski, D. & Parekh, A.B. (2002). Permeation through store-operated CRAC channels in divalent-free solution: potential problems and implications for putative CRAC channel genes. *Cell Calcium* **32**, 379-391.

Bålfors, E., Höggmark, S., Nyhman, H., Rydvall, A. & Reiz, S. (1983). Droperidol inhibits the effects of ketamine on central hemodynamics and myocardial oxygen consumption in patients with generalized atherosclerotic disease. *Anestesia* & *Analgesia* **62**, 193-197.

Baluk, P. & Gabella, G. (1990). Some parasympathetic neurons in the guinea-pig heart express aspects of the catecholaminergic phenotype in vivo. *Cell and Tissue Research* **261**, 275-285.

Becker, K.E. Jr. (1978). Plasma levels of thiopental necessary for anesthesia. *Anesthesiology* **49**, 192-196.

Beker, F., Weber, M., Fink, R.H.A. & Adams, D.J. (2003). Muscarinic and nicotinic ACh receptor activation differentially mobilize Ca^{2+} in rat intracardiac neurons.

Journal of Neurophysiology **90**, 1956-1964.

Benet, L.Z., Øie, S. & Schwartz, J.B. (1996). Design and optimization of dosage regimens; pharmacokinetic data. In J.G. Hardman, L.E. Limbird, P.B. Molinoff, R.W. Ruddon & A.G. Gillman (Eds.), *Goodman* & *Gilman's The pharmacological basis of therapeutics* (pp. 1707-1792). New York: McGraw-Hill.

Benters, J., Flögel, U., Schäfer, T., Leibfritz, D., Hechtenberg, S. & Beyersmann, D. (1997). Study of the interactions of cadmium and zinc ions with cellular calcium homeostasis using ^{19}F-NMR spectroscopy. *Biochemical Journal* **322**, 793-799.

Berne, R.M. & Levy, M.N. (1998). The cardiovascular system. In R.M. Berne, M.N. Levy, B.M. Koeppen & B.A. Stanton (Eds.), *Physiology* (pp. 317-513). St. Louis: Mosby.

Berridge, M.J. (1997). Annual Review Prize Lecture: Elementary and global aspects of calcium signalling. *Journal of Physiology* **499**, 291-306.

Berridge, M.J. (1998). Neuronal calcium signaling. *Neuron* **21**, 13-26.

Berridge, M.J., Bootman, M.D. & Lipp, P. (1998). Calcium – a life and death signal. *Nature* **395**, 645-648.

Berridge, M.J., Bootman, M.D. & Roderick, H.L. (2003). Calcium signaling: Dynamics, homeostasis and remodelling. *Nature Reviews Molecular Cell Biology* **4**, 517-529.

Berridge, M.J., Lipp, P. & Bootman, M.D. (2000). The versatility and universality of calcium signalling. *Nature Reviews Molecular Cell Biology* **1**, 11-21.

Beutner, G., Sharma, V.K., Giovannucci, D.R., Yule, D.I., Sheu, S-S. (2001). Identification of a ryanodine receptor in rat heart mitochondria. *Journal of Biological Chemistry* **276**, 21482-21488.

Bibevski, S., Zhou, Y., McIntosh, J.M., Zigmond, R.E. & Dunlap, M.E. (2000). Functional nicotinic acetylcholine receptors that mediate ganglionic transmission in cardiac parasympathetic neurons. *Journal of Neuroscience* **20**, 5076-5082.

Blake, D.W. & Korner, P.I. (1981). Role of baroreceptor reflexes in the hemodynamic and heart rate responses to althesin, ketamine and thiopentone anesthesia. *Journal of the Autonomic Nervous System* **3**, 55-70.

Boland, L.M., Morrill, J.A. & Bean, B.P. (1994). Omega-conotoxin block of N-type calcium channels in frog and rat sympathetic neurons. *Journal of Neuroscience* **14**, 5011-5027.

Bootman, M.D., Thomas, D., Tovey, S.C., Berridge, M.J. & Lipp, P. (2000). Nuclear calcium signalling. *Cellular and Molecular Life Sciences* **57**, 371-378.

Brini, M. (2003). Ca^{2+} signalling in mitochondria: mechanism and role in physiology and pathology. *Cell Calcium* **34**, 399-405.

Bristow, J.D., Prys-Roberts, C. Fisher, A. Pickering, T.G. & Sleight, P. (1969). Effects of anesthesia on baroreflex control of heart rate in man. *Anesthesiology* **31**, 422-428.

Büch, H.P. & Büch, U. (2001). Narkotika, Narkose. In W. Forth, D. Henschler, W. Rummel, U. Förstermann & K. Starke (Eds.), *Allgemeine und spezielle Pharmakologie und Toxikologie* (pp. 277-297). München: Urban & Fischer.

Burch, P.G. & Stanski, D.R. (1983). The role of metabolism and protein binding in thiopental anesthesia. *Anesthesiology* **58**, 146-152.

Butler, C.K., Smith, M., Cardinal, R., Murphy, D.A., Hopkins, D.A. & Armour, J.A. (1990). Cardiac responses to electrical stimulation of discrete loci in canine atrial and ventricular ganglionated plexi. *American Journal of Physiology* **259**, H1365-H1373.

Byrne, A.J., Healey, T.E.J. & Tomlinson, D.R. (1979). The effects of ketamine on noradrenergic transmission and the response to noradrenaline in rat smooth muscle. *British Journal of Pharmacology* **67**, 462.

Castro, N.G. & Albuquerque, E.X. (1995). α-bungarotoxin-sensitive hippocampal nicotinic acetylcholine receptor channel has a high calcium permeability. *Biophysical Journal* **68**, 516-524.

Catterall, W.A. (2000). Structure and regulation of voltage-gated Ca^{2+} channels. *Annual Review of Cell and Developmental Biology* **16**, 521-555.

Chan, H.N., Morgan, D.J., Crankshaw, D.P. & Boyd, M.D. (1985). Pentobarbitone formation during thiopentone infusion. *Anaesthesia* **40**, 1155-1159.

Charney, D.S., Mihic, S.J. & Harris, R.A. (2001). Hypnotics and sedatives. In J.G. Hardman, L.E. Limbird & A.G. Gillman (Eds.), *Goodman & Gilman's The pharmacological basis of therapeutics* (pp. 399-427). New York: McGraw-Hill.

Chavez-Noriega, L.E., Crona, J.H., Washburgn, M.S., Urrutia, A., Elliot, K.J. & Johnson, E.C. (1997). Pharmacological characterization of recombinant human neuronal nicotinic Acetylcholine receptors hα2β2, hα2β4, hα3β2, hα3β4, hα4β2, hα4β4 and hα7 expressed in Xenopus oocytes. *Journal of Pharmacology and Experimental Therapeutics* **280**, 346-356.

Christensen, H.D. & Lee, I.S. (1973). Anesthetic potency and acute toxicity of optically active disubstituted barbituric acids. *Toxicology and Applied Pharmacology* **26**, 495-503.

Christensen, J.H., Andreasen, F. & Jansen, J.A. (1982). Pharmacokinetics and pharmacodynamics of thiopentone. *Anaesthesia* **37**, 398-404.

Clanachan, A.S. & McGrath, J.C. (1976). Effects of ketamine on the peripheral autonomic system of the rat. *British Journal of Pharmacology* **58**, 247-252.

Clergue, F. Auroy, I., Pequignot, F., Jougla, E., Lienhart, A. & Laxenaire, M-C. (1999). French survey of anesthesia in 1996. *Anesthesiology* **91**, 1509-1520.

Coates, K.M. & Flood, P. (2001). Ketamine and its preservative, benzethonium chloride, both inhibit human recombinant α7 and α4β2 neuronal nicotinic acetylcholine receptors in Xenopus oocytes. *British Journal of Pharmacology* **134**, 871-879.

Coates, K.M., Mather, L.E., Johnson, R. & Flood, P. (2001). Thiopental is a competitive inhibitor of the human α7 nicotinic acetylcholine receptor. *Anesthesia & Analgesia* **92**, 930-933.

Costa, A.C.S., Patrick, J.W. & Dani, J.A. (1994). Improved technique for studying ion channels expressed in Xenopus oocytes, including fast superfusion. *Biophysical Journal* **67**, 395-401.

Couturier, S., Bernard, D., Matter, J.M., Hernandez, M.C., Bertrand, S., Millar, N., Valera, S., Barkas, T., & Ballivet, M. (1990). A neuronal nicotinic acetylcholine receptor subunit (alpha 7) is developmentally regulated and forms homo-oligomeric channel blocked by alpha-BTX. *Neuron* **5**, 847-856.

Cuevas, J. & Adams, D.J. (1994). Local anaesthetic blockade of neuronal nicotinic ACh receptor-channels in rat parasympathetic ganglion cells. *British Journal of Pharmacology* **111**, 663-672.

Cuevas, J. & Adams, D.J. (2000). Substance P preferentially inhibits large conductance nicotinic ACh receptor channels in rat intracardiac ganglion neurons. *Journal of Neurophysiology* **84**, 1961-1970.

Cuevas, J. & Berg, D.K. (1998). Mammalian nicotinic receptors with α7 subunits that slowly desensitize and rapidly recover from α –bungarotoxin blockade. *Journal of Neuroscience* **18**, 10335-10344.

de Armendi, A.J., Tonner, P.H., Bugge, B. & Miller, K.W. (1993). Barbiturate action is dependent on the conformational state of the acetylcholine receptor. *Anesthesiology* **79**, 1033-1041.

Després, G., Veissier, I. & Boissy, A. (2002). Effects of autonomic blockers on heart rate variability in calves: Evaluation of sympatho-vagal balance. *Physiological Research* **51**, 347-353.

Diaz, F.A., Bianco, J.A., Bello, A., Beer, N., Velarde, H., Izquierdo, J.P. & Jaen, R.

(1976). Effects of ketamine on cardiovascular function. *British Journal of Anaesthesia* **48**, 941-946.

Dickinson, R., White, I., Lieb, W.R. & Franks, N.P. (2000). Stereoselective loss of righting reflex in rats by isoflurane. *Anesthesiology* **93**, 837-843.

Dilger, J.P. (2002). The effect of general anaesthetics on ligand-gated ion channels. *British Journal of Pharmacology* **89**, 41-51.

Dilger, J.P., Boguslavsky, R., Barann, M., Katz, T. & Vidal, A.M. (1997). Mechanisms of barbiturate inhibition of acetylcholine receptor channels. *Journal of General Physiology* **109**, 401-414.

Doenicke, A., Angster, R., Mayer, M., Adams, H.A., Grillenberger, G. & Nebauer, A.E. (1992). Die Wirkung von S-(+) -Ketamin auf Katecholamine und Cortisol im Serum. Vergleich zum Ketamin-Razemat. *Anaesthesist* **41**, 597-603.

Domino, E.F., Chodoff, P. & Corssen, G. (1965). Pharmacologic effects of Cl-581, a new dissociative anaesthetic, in man. *Clinical Pharmacology* & *Therapeutics* **6**, 696-699.

Dowdy, E.G. & Kaya, K. (1968). Studies of the mechanism of cardiovascular responses to CI-581. *Anesthesiology* **29**, 931-943.

Downie, D.L., Franks, N.P. & Lieb, W.R. (2000). Effects of thiopental on optical isomers on nicotinic acetylcholine receptors. *Anesthesiology* **93**, 774-783.

Ehrlich, B.E., Kaftan, E., Bezprozvannaya, S., and Bezprozvanny, I. (1994). The pharmacology of intracellular Ca^{2+}-release channels. *Trends in Pharmacological Sciences* **15**, 145-149.

Ehrnebo, M. & Odar-Cederlöf, I. (1977). Distribution of pentobarbital and diphenylhydantoin between plasma and cells in blood: Effect of salicylic acid, temperature and total drug concentration. *European Journal of clinical Pharmacology* **11**, 37-42.

Elgoyhen, A.B., Vetter, D.E., Katz, E., Rothlin, C.V., Heinemann, S.F. & Boulter, J. (2001). α10: A determinant of cholinergic receptor function in mammalian vestibular and cochlear mechanosensory hair cells. *Proceedings of the National Academy of Sciences of the USA* **98**, 3501-3506.

Ertel, E.A., Campbell, K.P., Harpold, M.M., Hofmann, F., Mori, Y., Perez-Reyes, E., Schwartz, A., Snutch, T.P., Tanabe, T., Birnbaumer, L., Tsien, R.W. & Catterall, W.A. (2000). Nomenclature of voltage-gated calcium channels. *Neuron* **25**, 533-535.

Evers, A.S. & Crowder, C.M. (2001). General anesthetics. In J.G. Hardman, L.E. Limbird & A.G. Gillman (Eds.), *Goodman* & *Gilman's The pharmacological basis of*

therapeutics (pp. 337-365). New York: McGraw-Hill.

Feltz, A. & Trautmann, A. (1982). Desensitization at the frog neuromuscular junction: a biphasic process. *Journal of Physiology* **322**, 257-272.

Feng, Z-P., Hamid, J., Doering, C., Bosey, G.M., Snutch, T.P. & Zamponi, G.W. (2001). Residue gly^{1326} of the N-type calcium channel α_{1B} subunit controls reversibility of ω-conotoxin GVIA and MVIIA block. *Journal of Biological Chemistry* **276**, 15728-15735,

Ferrari, D., Pinton, P., Szabadkai, G., Chami, M., Campanella, M., Pozzan, T. & Rizzuto, R. (2002). Endoplasmic reticulum, Bcl-2 and Ca^{2+} handling in apoptosis. *Cell Calcium* **32**, 413-420.

Fichtl, B. (2001). Pharmakokinetische Daten. In W. Forth, D. Henschler, W. Rummel, U. Förstermann & K. Starke (Eds.), *Allgemeine und spezielle Pharmakologie und Toxikologie* (pp. 95-110). München: Urban & Fischer.

Fieber, L. A. & Adams, D. J. (1991a). Acetylcholine-evoked currents in cultured neurons dissociated from rat parasympathetic cardiac ganglia. *Journal of Physiology* **434**, 215-237.

Fieber, L. A. & Adams, D. J. (1991b). Adenosine triphosphate-evoked currents in cultured neurones dissociated from rat parasympathetic cardiac ganglia. *Journal of Physiology* **434**, 239-256.

Fill, M. & Copello, J.A. (2002). Ryanodine receptor calcium release channels. *Physiological Reviews* **82**, 893-922.

Filner, B.E. & Karliner, J.S. (1976). Alterations of normal left ventricular performance by general anesthesia. *Anesthesiology* **45**, 610-621.

Fink, R.H.A. & Veigel, C. (1996). Calcium uptake and release modulated by counter-ion conductances in the sarcoplasmic reticulum of skeletal muscle. *Acta Physiologica Scandinavica* **156**, 387-396.

Flood, P. & Krasowski, M.D. (2000). Intravenous anesthetics differentially modulate ligand-gated ion channels. *Anesthesiology* **92**, 1418-1425.

Flood, P. & Role, L.W. (1998). Neuronal nicotinic acetylcholine receptor modulation by general anesthetics. *Toxicology Letters* **100-101**, 149-153.

Fragen, R.J. & Avram, M.J. (2000). Barbiturates. In RD. Miller (Ed.), *Anesthesia. Volume 1* (5th ed, pp. 209-227). Philadelphia: Churchill Livingstone.

Frankl, W.S. & Poole-Wilson, P.A. (1981). Effects of thiopental on tension development, action potential and exchange of calcium and potassium in rabbit

ventricular myocardium. *Journal of Cardiovascular Pharmacology* **3**, 554-565.

Franks, N.P. & Lieb, W.R. (1984). Do general anaesthetics act by competitive binding to specific receptors? *Nature* **310**, 599-601.

Franks, N.P. & Lieb, W.R. (1994). Molecular and cellular mechanisms of general anaesthesia. *Nature* **367**, 607-614.

Franks, N.P. & Lieb, W.R. (1998). Which molecular targets are most relevant to general anaesthesia? *Toxicology Letters* **100-1001**, 1-8.

Fucile, S., Renzi, M., Lax, P. & Eusebi, F. (2003). Fractional Ca^{2+} current through human $\alpha 7$ nicotinic acetylcholine receptors. *Cell Calcium* **34**, 205-209.

Furuya, R., Oka, K., Watanabe, I., Kamiya, Y., Itoh, H. & Andoh, T. (1999). The effects of ketamine and propofol on neuronal nicotinic acetylcholine receptors and P_{2x} purinoceptors in PC12 cells. *Anesthesia* & *Analgesia* **88**, 174-180.

Gage, P.W. & McKinnon, D. (1985). Effects of pentobarbital on acetylcholine-activated channels in mammalian muscle. *British Journal of Pharmacology* **85**, 229-235.

Gelissen, H.P., Epema, A.H., Henning, R.H., Krijnen, J., Hennis, P.J. & den Hertog, A. (1996). Inotropic effects of propofol, thiopental, midazolam, etomidate and ketamine on isolated human atrial muscle. *Anesthesiology* **84**, 397-403.

Gill, S.S., Pulido, O.M., Mueller, R.W. & McGuire, P.F. (1998). Molecular and immunohistochemical characterization of the inotropic glutamate receptors in the rat heart. *Brain Research Bulletin* **46**, 429-434.

Graf, B.M. & Martin, E. (1998). Stereoisomerie in der Anästhesie. Theoretische Grundlagen und klinische Bedeutung. *Anaesthesist* **47**, 172-183.

Graf, B.M., Vicenci, M. N., Martin, E., Bosnjak, Z.J. & Sowe, D.F. (1995). Ketamine has stereospecific effects in the isolated perfused Guinea pig heart. *Anesthesiology* **82**, 1426-1435.

Grynkiewicz, G, Poenie, M. & Tsien, R. Y. (1985). A new generation of Ca^{2+} indicators with greatly improved fluorescence properties. *Journal of Biological Chemistry 260*, 3440-3450.

Hajnóczky, G., Csordás, G. & Yi, M. (2002). Old players in a new role: mitochondria--associated membranes, VDAC, and ryanodine receptors as contributors to calcium signal propagation from endoplasmic reticulum to the mitochondria. *Cell Calcium* **32**, 363-377.

Haley, T.J. & Gidley, J.T. (1970). Pharmacological comparison of R(+), S(–) and racemic secobarbital in mice. *European Journal of Pharmacology* **9**, 358-361.

Haley, T.J. & Gidley, J.T. (1976). Pharmacological comparison of R(+), S(–) and racemic thiopentone in mice. *European Journal of Pharmacology* **36**, 211-214.

Hall, A.C., Lieb, W.R. & Franks, N.P. (1994). Stereoselective and non-stereoselective actions of isoflurane on the $GABA_A$ receptor. *British Journal of Pharmacology* **112**, 906-910.

Halliwill, J.R. & Billman, G.E. (1992). Effect of general anesthesia on cardiac vagal tone. *American Journal of Physiology* **262**, H1719-H1724.

Hamill, O.P., Marty, A., Neher, E., Sakmann, B. & Sigworth, F.J. (1981). Improved patch-clamp techniques for high-resolution current recording from cells and cell-free membrane patches. *Pfluegers Archives. European Journal of Physiology*, **391**, 85-100.

Hechtenberg, S. & Beyersmann, D. (1991). Inhibition of sarcoplasmic reticulum Ca^{2+}-ATPase activity by cadmium, lead and mercury. *Enzyme* **45**, 109-115.

Herrmann-Frank, A., Luttgau, H.C. & Stephenson, D.G. (1999). Caffeine and excitation-contraction coupling in skeletal muscle: a stimulatory story. *Journal of Muscle Research and Cell Motility* **20**, 223-227.

Hill, G.E., Wong, K.C., Shaw, C.L., Sentker, C.R. & Blatnick, R.A. (1978). Interactions of ketamine with vasoactive amines at normothermia and hypothermia in the isolated rabbit heart. *Anesthesiology* **48**, 315-319.

Hille, B. (2001). *Ion channels of excitable membranes*. Sunderland, MA: Sinauer Associates.

Hinkle, P.M., Kinsella, P.A. & Osterhoudt, K.C. (1987). Cadmium uptake and toxicity via voltage-gated calcium channels. *Journal of Biological Chemistry* **262**, 16333-16337.

Hinkle, P.M., Shanshala, E.D. & Nelson, E.J. (1992). Measurement of intracellular cadmium with fluorescent dyes. Further evidence for the role of calcium channels in cadmium uptake. *Journal of Biological Chemistry* **267**, 25553-25559.

Hogg, R.C., Mirand, L.P., Craik, D.J., Lewis, R.J., Alewood, P.F., & Adams, D.J. (1999). Single amino acid substitutions in α-conotoxin PnIA shift selectivity for subtypes of the mammalian neuronal nicotinic acetylcholine receptor. *Journal of Biological Chemistry* **274**, 36559-36564.

Horackova, M., Armour, JA. & Byczko, Z. (1999). Distribution of intrinsic cardiac neurons in whole-mount guinea pig atria identified by multiple neurochemical coding. A confocal microscopy study. *Cell Tissue Research, 297,* 409-421.

Horn R. & Marty A. (1988). Muscarinic activation of ionic currents measured by a new whole-cell recording method. *Journal of General Physiology* **92**, 145-152.

Horwitz, L.D. (1977). Effects of intravenous anesthetic agents on left ventricular

function in dogs. *American Journal of Physiology* **232**, H44-H48.

Huang, M.H., Smith, F.M. & Armour, J.A. (1993). Modulation of in situ canine intrinsic cardiac neuronal activity by nicotinic, muscarinic, and β-adrenergic agonists. *American Journal of Physiology* **265**, R659-R669.

Idvall, J., Ahlgren, I., Aronsen, K.F. & Stenberg, P. (1979). Ketamine infusions: Pharmacokinetics and clinical effects. *British Journal of Anaesthesia* **51**, 1167-1173.

Inoue, K. & Arndt, J.O. (1982). Efferent vagal discharge and heart rate in response to methohexitone, althesin, ketamine and droperidol on peripheral vagal transmission. *British Journal of Anaesthesia* **61**, 456-461.

Inoue, K. & König, L.A. (1988). Effects of methohexitone, althesin, ketamine and etomidate in cats. *British Journal of Anaesthesia* **54**, 1105-1116.

Irnaten, M., Wang, J., Venkatesan, P., Evans, C., Chang, K.S.K., Andresen, M.C. & Mendelowitz, D. (2002). Ketamine inhibits presynaptic and postsynaptic nicotinic excitation of identified cardiac parasympathetic neurons in Nucleus Ambiguus. *Anesthesiology* **96**, 2002, 667-674.

Ivankovich, A.D., Miletich, D.J., Reimann, C., Albrecht, R.F. & Zahed, B. (1974). Cardiovascular effects of centrally administered ketamine in goats. *Anesthesia & Analgesia* **53**, 924-933.

Iversen, S., Iversen, L. & Saper, CB. (2000). The autonomic nervous system and the hypothalamus. In ER. Kandel, JH. Schwartz & TM Jessel (Eds.), *Principals of Neural Science* (4th ed, pp. 960-981). New York: Elsevier.

Jacobson, I., Pocock, G. & Richards, C.D. (1991). Effects of pentobarbitone on the properties of nicotinic channels of chromaffin cells. *European Journal of Pharmacology* **202**, 331-339.

Johnstone, M. (1976). The cardiovascular effects of ketamine in man. *Anaesthesia* **31**, 873-882.

Jugdutt, B.I., Rogers, M.C., Hutchins, G.M. & Becker, L.C. (1986). Increased myocardial infarct size by thiopental after coronary occlusion in the dog. *American Heart Journal* **112**, 485-494.

Just, A., Faulhaber, J. & Ehmke, H. (2000). Autonomic cardiovascular control in conscious mice. *American Journal of Physiology/Regulatory, Integrative and Comparative Physiology* **29**, R2214-2221.

Kamiya, Y., Andoh, T., Watanabe, I., Higashi, T. & Itoh, H. (2001). Inhibitory effects of barbiturates on nicotinic acetylcholine receptors in rat central nervous system

neurons. *Anesthesiology* **94**, 694-704.

Kandel, E.R. & Siegelbaum, S.A. (2000). Ion channels. In ER. Kandel, JH. Schwartz & TM Jessel (Eds.), *Principals of Neural Science* (4th ed, pp. 187-206). New York: Elsevier.

Kao, J.P.Y. (1994). Practical aspects of measuring [Ca^{2+}] with fluorescent indicators. In R. Nuccitelli (Ed.), *Methods in cell biology. Volume 40. A practical guide to the study of calcium in living cells* (pp. 155-181). San Diego: Academic Press.

Kemp, J.A. & McKernan, R.M. (2002). NMDA receptor pathways as drug targets. *Nature Neuroscience* **5**, 1039-1042.

Kissin, I., Motomura, S., Aultman, D.F. & Reves, J.G. (1983). Inotropic and anesthetic potencies of etomidate and thiopental in dogs. *Anesthesia* & *Analgesia* **62**, 961-965.

Koblin, D.D., Chortkoff, B.S., Laster, M.S., Eger, E.I. 2nd, Halsey, M.J. & Ionescu, P. (1994). Polyhalogenated and perfluorinated compounds that disobey the Meyer-Overton hypothesis. *Anesthesia* & *Analgesia* **79**; 1043-1048.

Koizumi, S., Bootman, M.D., Bobanovic, L.K., Schell, M.J., Berridge, M.J. & Lipp, P. (1999). Characterization of elementary Ca^{2+} release signals in NGF-differentiated PC12 cells and hippocampal neurons. *Neurons* **22**, 125-137.

Komai, H. & Rusy, B.F. (1984). Differences in the myocardial depressant action of thiopental and halothane. *Anesthesia* & *Analgesia* **63**, 313-318.

Komai, H. & Rusy, B.F. (1994). Effect of thiopental on Ca^{2+} release from sarcoplasmic reticulum in intact myocardium. *Anesthesiology* **81**, 946-952.

Krasowski, M.D. & Harrison, N.L. (1999). General anaesthetic actions on ligand-gated ion channels. *Cellular and Molecular Life Sciences* **55**, 1278-1303.

Kunst, G., Graf, B.M., Schreiner, M., Martin, E. & Fink, R.H.A. (1999). Differential effects of sevoflurane, isoflurane and halothane on Ca^{2+} release from sarcoplasmic reticulum of skeletal muscle. *Anesthesiology* **91**, 176-186.

Kunst, G., Stucke, A.G., Graf, B.M., M., Martin, E. & Fink, R.H.A. (2000). Desflurane induces only minor Ca^{2+} release from the sarcoplasmic reticulum of mammalian skeletal muscle. *Anesthesiology* **93**, 832-836.

Lankowicz, J.R. (1983). *Principles of fluorescence spectroscopy*. New York: Plenum Press.

Larsen, R. (2002). *Anästhesie*. München: Urban & Fischer.

Le Novère, N., Corringer, P-J. & Changeux, J-P. (2002). The diversity of the subunit composition of nAChR: Evolutionary origins, physiologic and pharmacologic consequences. *Journal of Neurobiology* **53**, 447-456.

Leger, J., Croll, RP. & Smith, FM. (1999). Regional distribution and intrinsic innervation of intrinsic cardiac neurons in the Guinea pig. *Journal of Comparative Neurology* **407***,* 303-317.

Leonard, R.J., Labarca, C.G., Charnet, P., Davidson, N. & Lester, H.A. (1988). Evidence that the M2 membrane-spanning region lines the ion channel pore of the nicotinic receptor. *Nature* **243**, 1578-1580.

Lewis, T.M., Harkness, P.C., Colquhoun, D., & Millar, N.S. (1997). The ion channel properties of a rat recombinant nicotinic receptor are dependent on the host cell type. *Journal of Physiology* **505**, 299-306.

Liao, J.C., Koehntop, D.E. & Buckley, J.J. (1979). Dual effects of ketamine on peripheral vasculature. *Anesthesiology* **51**, S116.

Lieb, C.C. & Mulinos, M.G. (1929). Some further observations on sodium-iso-amyl-ethyl-barbiturate as a laboratory anesthetic. *Proceedings of the Society for Experimental Biology and Medicine* **26**, 709-711.

Liu D-M. & Adams, D.J. (2001). Ionic selectivity of native ATP-activated (P2X) receptor channels in dissociated neurons from rat parasympathetic ganglia. *Journal of Physiology* **534**, 423-435.

Liu, D-M., Cuevas, J. & Adams, D.J. (2000a). VIP and PACAP potentiation of nicotinic ACh-evoked currents in rat parasympathetic neurons is mediated by G-protein activation. *European Journal of Neuroscience,* **12**, 2243-2251.

Liu, D-M., Katnik, C., Stafford, M. & Adams, D.J. (2000b). PY2 purinoceptor activation mobilizes intracellular Ca^{2+} and induces a membrane current in rat intracardiac neurones. *Journal of Physiology* **526**, 287-298.

Lodge, D., Anis, N.A. & Burton, N.R. (1982). Effects of optical isomers of ketamine on excitation of cat and rat spinal neurones by amino acids and acetylcholine. *Neuroscience Letters* **29**, 281-286.

Lynch, C. 3rd & Pancrazio, J. (1994). Snails, spiders and stereospecificity - is there a role for calcium channels in anesthetic mechanisms? *Anesthesiology* **81**, 1-5.

MacDermott, A., Role, L.W. & Siegelbaum , S.A. (1999). Presynaptic ionotropic receptors and the control of transmitter release. *Annual Reviews in Neuroscience* **22**, 443-485.

Manders, W.T. & Vatner, S.F. (1976). Effects of sodium pentobarbital anesthesia on left ventricular function and distribution of cardiac output in dogs, with particular reference to the mechanism for tachycardia. *Circulation Research* **39**, 512-527.

Manhood, V., Byrne, A.J., Healey, T.E.J. & Hussain, S.Z. (1980). Effect of ketamine on transmission in sympathetic ganglia. *British Journal of Anaesthesia* **52**, 371-375.

Marchi, B., Burlando, B., Panfili, I. & Viarengo, A. (2000). Interference of heavy metal cations with fluorescent Ca^{2+} probes does not affect Ca^{2+} measurements in living cells. *Cell Calcium* **28**, 225-231.

Marietta, M.P., Way, W. Castagnoli, N.Jr. & Trevor, A.J. (1977). On the pharmacology of ketamine enantiomorphs in the rat. *Journal of Pharmacology and Experimental Therapeutics* **202**, 157-165.

Marty, A. & Neher, E. (1995). Tight-seal whole-cell recording. In B. Sakmann & E. Neher (Eds.), *Single-channel recording* (pp. 31-52). New York: Plenum Press.

Mawe, G.M., Talmawe, E.K., Lee, K.P. & Parsons, R.L. (1996). Expression of choline acetyltransferase immunoreactivity in guinea pig cardiac ganglia. *Cell and Tissue Research* **285**, 281-286.

Mayer, M.L., & Westbrook, G.L. (1987). Permeation and block of N-methyl-D-aspartic acid receptor channels by divalent cations in mouse cultured central neurons. *Journal of Physiology* **394**, 501-527.

McGehee D. S. (1999). Molecular diversity of neuronal nicotinic acetylcholine receptors. *Annals of the New York Academy of Sciences* **868**, 565-577.

McPherson, P.S. & Campbell, K.P. (1993a). Characterization of the major brain form of the ryanodine receptor/Ca^{2+} release channel. *Journal of Biological Chemistry* **268**, 19785-19790.

McPherson, P.S. & Campbell, K.P. (1993b). The ryanodine receptor/Ca^{2+} release channel. *Journal of Biological Chemistry* **268**, 13765-13768.

Melamed-Book, N., Kachalsky, S.G., Kaiserman, I. & Rahamimoff, R. (1999). Neuronal calcium sparks and intracellular calcium noise. *Proceedings of the National Academy of Sciences of the USA* **96**, 15217-15221.

Meldolesi, J. & Pozzan, T (1998). The endoplasmic reticulum Ca^{2+} store: a view from the lumen. *Trends in Biochemical Sciences* **23**, 10-14.

Michelmore, S., Croskery, K., Nozulak, J., Hoyer, D., Longato, R., Weber, A., Bouhelal, R. & Feuerbach, D. (2002). Study of the calcium dynamics of the human $\alpha4\beta2$, $\alpha3\beta4$ and $\alpha1\beta1\gamma\delta$ nicotinic acetylcholine receptors. *Naunyn-Schmiedeberg's Archives in Pharmacology* **366**, 235-245.

Miletich, D.J., Ivankovic, A.D., Albrecht, R.F., Zahed, B. & Ilahi, A.A. (1973). The effect of ketamine on catecholamine metabolism in the isolated perfused rat heart.

Anesthesiology **39**, 271-277.

Milocco, I., Löf, B.A., William-Olsson, G. & Appelgren, L.K. (1985). Haemodynamic stability during anaesthesia induction and sternotomy in patients with ischaemic heart disease. *Acta Anaesthesiologica Scandinavica* **29**, 465-473.

Miyazawa, A., Fujiyoshi, Y., Stowell, M. & Unwin, N. (1999). Nicotinic acetylcholine receptor at 4.6 Å resolution: Transverse tunnels in the channel wall. *Journal of Molecular Biology* **288**, 765-786.

Moravec, M. & Moravec, J. (1989). Adrenergic neurons and short proprioceptive feedback loops involved in the integration of cardiac function in the rat heart. *Cell and Tissue Research* **258**, 381-385.

Moreno Davila, H. (1999). Molecular and functional diversity of voltage-gated calcium channels. *Annals of the New York Academy of Sciences* **868**, 102-117.

Morrison, J.L., Walker, H.A. & Richardson, A.P. (1950). The effect of pentobarbital on the response of cardiovascular system of dogs to epinephrine, acetylcholine and tilting. *Archives Internationales de Pharmacodynamie et de Thérapie* **82**, 53-62.

Most, P., Remppis, A., Pleger, S.T., Löffler, E., Ehlermann, P., Bernotat, J., Kleuss, C., Heierhorst, J., Ruiz, P., Witt, H., Karczewski, P., Mao, L., Rockman, H.A., Duncan, S.J., Katus, H.A. & Koch, W.J. (2003). Transgeneic overexpression of the Ca^{2+} binding protein S100A1 in the heart leads to increased in vivo myocardial contractile performance. *Journal of Biological Chemistry* **278**, 33809-33817.

Most, P., Remppis, A., Weber, C., Bernotat, J., Ehlermann, P., Pleger, S.T., Kirsch, W., Weber, M., Uttenweiler, D., Smith, G.L., Katus, H.A. & Fink, R.H.A. (2003). The C terminus (amino acids 75-94) and the linker region (amino acids 42-54) of the Ca^{2+} binding protein S100A1 differentially enhance sarcoplasmic Ca^{2+} release in murine skinned skeletal muscle fibers. *Journal of Biological Chemistry* **278**, 26356-26364.

Mousa, W.F., Enoki, T. & Fukuda, K. (2000). Thiopental induces contraction of rat aortic smooth muscle through Ca^{2+} release from the sarcoplasmic reticulum. *Anesthesia* & *Analgesia* **91**, 62-67.

Murthy, V.S., Zagar, M.E., Vollmer, R.R. & Schmidt, D.H. (1982). Pentobarbital-induced changes in vagal tone and reflex vagal activity in rabbits. *European Journal of Pharmacology* **84**, 41-50.

Muschol, M, Dasgupta, B.R. & Salzberg, B.M. (1999). Caffeine interaction with fluorescent calcium indicator dyes. *Biophysical Journal* **77**, 577-586.

Mutschler, E., Geisslinger, G., Kroemer, H.K. & Schäfer-Korting, M. (2001). *Arzneimittelwirkungen. Lehrbuch der Pharmakologie und Toxikologie*. Stuttgart: Wissenschaftliche Verlags-Gesellschaft.

Naguib, M., Hammond, D.L. 3rd, Schmid, P.G., Baker, M.T., Cutkomp, J. Queral, L. & Smith, T. (2003). Pharmacological effects of intravenous melatonin: comparative studies with thiopental and propofol. *British Journal of Anaesthesia* **90**, 504-507.

Nedergaard, O.A. (1973). Cocaine-like effect of ketamine on vascular adrenergic neurones. *European Journal of Pharmacology* **23**, 153-161.

Nicholls, J.D., Martin, A.R., Wallace, B.G. & Fuchs, P.A. (2001). *From neuron to brain*. Sunderland: Sinauer Associates.

Nilius, B., Hess, P., Lansman, J.B. & Tsien, R.W. (1985). A novel type of cardiac calcium channel in ventricular cells. *Nature* **316**, 443-446.

Nishimura, K., Kitamura, Y., Hamal, R., Kitamura, E. & Fujimori, M. (1973). Pharmacological studies of ketamine hydrochloride in the cardiovascular system. *Osaka City Medical Journal* **19**, 17-26.

Nowycky, M.C., Fox, A.P. & Tsien, R.W. (1985). Three types of neuronal calcium channel with different calcium agonist sensitivity. *Nature* **316**, 440-443.

Numberger, M. & Draguhn, A. (1996). *Patch-Clamp Technik*. Heidelberg: Spektrum, Akademischer Verlag.

Nutter, T.J. & Adams, D.J. (1995). Monovalent and divalent cation permeability and block of neuronal nicotinic receptor channels in rat parasympathetic ganglia. *Journal of General Physiology* **105**, 701-723.

O'Leary, D., Rossi, N.F. & Churchill, P.C. (1997). Substantial cardiac parasympathetic activity exits during heavy dynamic exercise in dogs. *American Journal of Physiology/Heart and Circulatory Physiology* **273**, H2135-H2140.

Ochoa, E.L., Chattopadhyay, A. & McNamee, M.G. (1989). Desensitization of the nicotinic acetylcholine receptor: Molecular mechanisms and effects of modulators. *Cellular and Molecular Neurobiology* **9**, 191-178.

Ortells, M.O. & Lunt, G.G. (1995). Evolutionary history of the ligand-gated ion channel superfamily of receptors. *Trends in Neurosciences* **18**, 121-127.

Pagel, P.S., Kampine, J.P. Schmeling, W.T. & Warltier, D.C. (1992). Ketamine depresses myocardial contractility as evaluated by the preload recruitable stroke work relationship in chronically instrumented dogs with autonomic nervous blockade. *Anesthesiology* **76**, 564-572.

Palecek, J., Lips, M.B. & Keller, B.U. (1999). Calcium dynamics and buffering in motoneurones of the mouse spinal cord. *Journal of Physiology* **520**, 485-502.

Park, W.K. & Lynch, C. 3rd (1992). Propofol and thiopental depression of myocardial contractility. A comparative study of mechanical and electrophysiological effects in isolated guinea pig ventricular muscle. *Anesthesia* & *Analgesia* **74**, 384-394.

Pauza, D.H., Skripka, V., Pauziene, N. & Stropus, R. (2000). Morphology, distribution, and variability of the epicardiac neural ganglionated subplexuses in the human heart. *The Anatomical Record* **259**, 353-382.

Peiss, C.N. & Manning, J.W. (1964). Effects of sodium pentobarbital on electrical and reflex activation of the cardiovascular system. *Circulation Research* **14**, 228-235.

Pfenninger, E., Baier, S., Claus, S. & Hege, G. (1994). Untersuchung zu psychometrischen Veränderungen sowie zur analgetischen Wirkung und kardiovaskulären Nebenwirkungen von Ketamin-Razemat versus S-(+)-Ketamin in subanästhetischer Dosierung. *Anaesthesist* **43**, S68-S75.

Poth, K., Nutter, T. J., Cuevas, J., Parker, M. J., Adams, D. J. & Luetje, C. W. (1997). Heterogeneity of nicotinic receptor class and subunit mRNA expression among individual parasympathetic neurons from rat intracardiac ganglia. *Journal of Neuroscience* **17**, 586- 596.

Powley, TL. (1999). Central control of autonomic functions. In M.J. Zigmond, F.E. Bloom, SC. Landis, JL. Roberts & LR. Squire (Eds.), *Fundamental Neuroscience* (pp. 1027-1050). San Diego: Academic Press.

Price, H.L., Conner, E.H., Elder, J.D. & Dripps, R.D. (1952). Effect of sodium thiopental on circulatory response to positive pressure inflation of the lung. *Journal of Applied Physiology* **4**, 629-635.

Price, H.L., Kovnat, P.J., Safer, J.N., Conner, E.H. & Price, M.L. (1960). The uptake of thiopental by body tissues and its relation to the duration of narcosis. *Clinical Pharmacology* & *Therapeutics* **1**, 16-22.

Putney, J.W. Jr. (2003). Capacitive calcium entry in the nervous system. *Cell Calcium* **34**, 339-344.

Quick, M.W. & Lester, R.A.J. (2002). Desensitization of neuronal nicotinic receptors. *Journal of Neurobiology* **53**, 457-478.

Raaflaub, J. (1970). Über die Beziehung zwischen der Lipidlöslichkeit von Pharmaka und ihrem pharmakokinetischen Verhalten. *Experientia* **26**, 457-476.

Rae, J., Cooper, K., Gates, P. & Watsky, M. (1991). Low access resistance perforated

patch recordings using amphotericin B. *Journal of Neuroscience Methods* **37**, 15-26.

Rathouz, M.M. & Berg, D.K. (1994). Synaptic-type acetylcholine receptors raise intracellular calcium levels in neurons by two mechanisms. *Journal of Neuroscience* **14**, 6935-6945.

Rathouz, M.M., Vijayaraghavan, S. & Berg, D.K. (1996). Elevation of intracellular calcium levels in neurons by nicotinic acetylcholine receptors. *Molecular Neurobiology* **12**, 117-131.

Reiz, S., Bålfors, E., Friedmann, A., Höggmark, S. & Peter, T. (1981). Effects of thiopentone on cardiac performance, coronary hemodynamics and myocardial oxygen consumption in chronic ischemic heart disease. *Acta Anaesthesiologica Scandinavica* **25**, 103-110.

Reves, J.G., Glass, P.S.A. & Lubarsky, D.A. (2000). Nonbarbiturate intravenous anesthetics. In R.D. Miller (Ed.), *Anesthesia. Volume 1* (5th ed, pp. 228-272). Philadelphia: Churchill Livingstone.

Reves, J.G., Hill, S. & Berkowitz, D. (1999). Pharmacology of Intravenous Anesthetic Induction Drugs. In J.A. Kaplan, D.L. Reich & S.N. Konstadt (Eds.), *Cardiac Anesthesia* (4th ed, pp. 611-634). Philadelphia: WB Saunders Company.

Richard, G., Federolf, G. & Habermann, E. (1986). Affinity of heavy metal ions to intracellular Ca^{2+} binding proteins. *Biochemical Pharmacology* **35**, 1331-1335

Robert, C., Tseeb, V., Kordon, C. & Hammond, C. (1999). Patch-clamp induced perturbations of $[Ca^{2+}]_I$ activity in somatotropes. *Neuroendocrinology* **70**, 343-352.

Roe, M.W., Lemasters, J.J. & Herman, B. (1990). Assessment of fura-2 for measurements of cytosolic free calcium. *Cell Calcium* **11**, 63-73.

Rogers, M. & Dani, J.A. (1995). Comparison of quantitative calcium flux through NMDA, ATP, and ACh receptor channels. *Biophysical Journal* **68**, 501-506.

Rogers, M., Colquhoun, L.M., Patrick, J.W. & Dani, J.A. (1997). Calcium influx through predominantly independent purinergic ATP and nicotinic acetylcholine receptors. *Journal of Neurophysiology* **77**, 1407-1417.

Role, L.W. & Berg, D.K. (1996). Nicotinic receptors in the development and modulation of CNS synapses. *Neuron* **16**, 1077-1085.

Rossi, D. & Sorrentino, V. (2002). Molecular genetics of ryanodine receptors Ca^{2+} -release channels. *Cell Calcium* **32**, 307-319.

Sakmann, B., Patlak, J. & Neher, E. (1980). Single acetylcholine-activated channels show burst-kinetics in presence of desensitizing concentrations of agonist. *Nature*

286, 71-73.

Salt, P.J., Barnes, P.K. & Beswick, F.J. (1979). Inhibition of neuronal and extraneuronal uptake of noradrenaline by ketamine in the isolated perfused rat heart. *British Journal of Anaesthesia* **51**, 835-838.

Saper, C.B. (2000). Brain stem, reflexive behavior, and the cranial nerves. In E.R. Kandel, J.H. Schwartz & T.M Jessel (Eds.), *Principals of Neural Science* (4th ed, pp. 873-888). New York: Elsevier.

Sasaki, T., Andoh, T., Watanabe, I., Kamiya, Y., Itoh, H., Higashi, T. & Matsuura, T. (2000). Nonstereoselective inhibition of neuronal nicotinic acetylcholine receptors by ketamine isomers. *Anesthesia* & *Analgesia* **91**, 741-748.

Savege, T.M., Colvin, M.P., Weaver, E.J.M., Bond, C., Drake, J. & Inniss, R. (1976). A Comparison of some cardiorespiratory effects of althesin and ketamine when used for induction of anaesthesia in patients with cardiac disease. *British Journal of Anaesthesia* **48**, 1071-1081.

Scheffer, G.J., Ten Vodre, B.J., Karemaker, J.M., Ros, H.H. & De Lange, J.J. (1993). Effects of thiopentone, etomidate and propofol on beat-to-beat cardiovascular signals in man. *Anaesthesia* **48**, 849-855.

Scheller, M., Bufler, J., Hertle, I., Schneck, H.J., Franke, C. & Kochs, E. (1996). Ketamine blocks currents through mammalian nicotinic acetylcholine receptor channels by interaction with both the open and closed state. *Anesthesia* & *Analgesia* **83**, 830-836.

Schmidt, R.F. (1992). *Physiologie* (Memorix spezial). Weinheim: VCH.

Schofield, P.R., Darlison, M.G., Fujita, N., Burt, D.R., Stephenson, F.A., Rodriguez, H., Rhee, L.M., Ramachandran, J., Reale, V., Glencorse, T.A., Seeburg, P.H. & Barnard, E.A. (1987). Sequence and functional expression of the $GABA_A$ receptor shows a ligand-gated receptor super-family. *Nature* **328**, 221-227.

Schwartz, D.A. & Horwitz, L.D. (1975). Effects of ketamine on left ventricular performance. *Journal of Pharmacology and Experimental Therapeutics* **194**, 410-414.

Seabrook, G.R., Fieber, L.A. & Adams, D.J. (1990). Neurotransmission in neonatal rat intracardiac ganglia in situ. *American Journal of Physiology* **259**, H997-H1005.

Seguela, P., Wadiche, J., Dineley-Miller, K., Dani, J.A. & Patrick, J.W. (1993). Molecular cloning, functional properties, and distribution of rat brain alpha 7: a nicotinic cation channel highly permeable to calcium. *Journal of Neuroscience* **13**, 596-604.

Seltzer, J.L., Gerson, J.I. & Allen, F.B. (1980). Comparison of the cardiovascular effects

of bolus v. incremental administration of thiopentone. *British Journal of Anaesthesia* **52**, 527-530.

Shafer, G.D., Underwood, F.J. & Gaynor, E.P. (1929). The action of amytal in impairing vagus cardiac inhibitory effects, and of ether in increasing the respiratory rate after its depression by amytal. *American Journal of Physiology* **91**, 461-466.

Sharma, M.R., Jeyakumar, L.H., Fleischer, S. & Wagenknecht, T. (2000). Three-dimensional structure of ryanodine receptor isoform three in two-conformational states as visualized by cryoelectron microscopy. *Journal of Biological Chemistry* **275**, 9485-9491.

Sharma, M.R., Penczek, P., Grassucci, R., Xin, H-B., Fleischer, S. & Wagenknecht, T. (1998). Cryoelectron microscopy and image analysis of the cardiac ryanodine receptor. *Journal of Biological Chemistry* **273**, 18429-18434.

Shimokawa, A., Kunitake, T., Takasaki, M. & Kannan, H. (1998). Differential effects of anesthetics on sympathetic nerve activity and arterial baroreceptor reflex in chronically instrumented rats. *Journal of the Autonomic Nervous System* **72**, 46-54.

Sigworth, F.J. (1995). Electronic design of the patch clamp. In B. Sakmann & E. Neher (Eds.), *Single-channel recording* (pp. 95-127). New York: Plenum Press.

Sivilotti, L.G., McNeil, D.K., Lewis, T.M., Nassar, M.A., Schoepfer, R. & Colquhoun, D. (1997). Recombinant nicotinic receptors, expressed in Xenopus oocytes, do not resemble native rat sympathetic ganglion receptors in single-channel behaviour. *Journal of Physiology* **500**, 123-138.

Skovsted, P., Price, M.L. & Price, H.L. (1970). The effects of short-acting barbiturates on arterial pressure, preganglionic sympathetic activity and barostatic reflexes. *Anesthesiology* **33**, 10-18.

Slavikova, J., Goldstein, M. & Dahlström, A. (1993). The postnatal development of tyrosine hydroxylase immunoreactive nerves in rat atrium, studied with immunofluorescence and confocal laser scanning microscopy. *Journal of the Autonomic Nervous System* **43**, 159-170.

Smith, A.B. & Adams, D.J. (1999). Met-enkephalin-induced mobilization of intracellular Ca^{2+} in rat intracardiac ganglionic neurones. *Neuroscience Letters* **264**, 105-108.

Sonntag, H., Hellberg, K., Schenk, H-D., Donath, U. Regensburger, D., Kettler, D., Duchanova, H. & Larsen, R. (1975). Effects of thiopental (Trapanal®) on coronary blood flow and myocardial metabolism in man. *Acta Anaesthesiologica*

Scandinavica **19**, 69-78.

Stanley, T.H. (1973). Blood-pressure and pulse-rate responses to ketamine during general anesthesia. *Anesthesiology* **39**, 648-649.

Steele, P.A., Gibbins, I.L. & Morris, J.L. (1996). Projections of intrinsic cardiac neurons to different targets in the guinea-pig heart. *Journal of the Autonomic Nervous System* **56**, 191-200.

Study, R.E. (1994). Isoflurane inhibits multiple voltage-gated calcium currents in hippocampus pyramidal neurons. *Anesthesiology* **81**, 104-116.

Sved, AF. (1999). Cardiovascular system. In M.J. Zigmond, F.E. Bloom, S.C. Landis, J.L. Roberts & L.R. Squire (Eds.), *Fundamental Neuroscience* (pp. 1051-1062). San Diego: Academic Press.

Tarabadkar, S., Kopriva, C.J., Screenivasan, N., Lesovich, F. & Barash, P.G. (1980). Hemodynamic impact of induction in patients with decreased cardiac reserve. *Anesthesiology* **53**, S43.

Tassonyi, E., Charpantier, E., Muller, D., Dumont, L. & Bertrand, D. (2002). The role of nicotinic acetylcholine receptors in the mechanisms of anesthesia. *Brain Research Bulletin* **57**, 133-150.

Taylor, C.W. & Laude, A.J. (2002). IP_3 receptors and their regulation by calmodulin and cytosolic Ca^{2+}. *Cell Calcium* **32**, 321-334.

Thews, G. & Vaupel, P. (1997). *Vegetative Physiologie*. Berlin: Springer.

Thummel, K.E. & Shen, D.D. (2001). Design and optimization of dosage regimens; pharmacokinetic data. In J.G. Hardman, L.E. Limbird & A.G. Gillman (Eds.), *Goodman & Gilman's The pharmacological basis of therapeutics* (pp. 1917-2023). New York: McGraw-Hill.

Tomlin, S.L., Jenkins, A., Lieb, W.R. & Franks, N.P. (1998). Stereoselective effects of etomidate optical isomers on gamma-aminobutyric acid type A receptors and animals. *Anesthesiology* **90**, 1714-1722.

Tomlin, S.L., Jenkins, A., Lieb, W.R. & Franks, N.P. (1999). Preparation of barbiturate optical isomers and their effects on $GABA_{(A)}$ receptors. *Anesthesiology* **90**, 1714-1722.

Toyoshima, C. Nakasako, M. & Ogawa, H. (2000). Crystal structure of the calcium pump of sarcoplasmic reticulum at 2.6 Å resolution. *Nature* **405**, 647-655.

Traber, D.L., Wilson, R.D. & Priano, L.L. (1968). Differentiation of the cardiovascular effects of CI-581. *Anesthesia & Analgesia* **47**, 769-778.

Trevor, A.J. & Miller, R.D. (2001). General anesthetics. In B.G. Katzung (Ed.), *Basic & clinical pharmacology* (pp. 419-435). New York: Lange Medical Books/McGraw-Hill.

Tsien, R.Y. (1980). New calcium indicators and buffers with high selectivity against magnesium and protons: Design, synthesis, and properties of prototype structures. *Biochemistry* **19**, 2396-2404.

Tsien, R.Y. (1981). A non-disruptive technique for loading calcium buffers and indicators into cells. *Nature* **290**, 527-528.

Unwin, N. (1995). Acetylcholine receptor channel imaged in the open state. *Nature* **373**, 37-43.

Unwin, N. (2000). The Croonian lecture 2000. Nicotinic acetylcholine receptors and the structural basis of fast synaptic transmission. *Philosophical Transactions: Biological Sciences. Royal Society London,* **355**, 1813-1829.

Urban, B.W. & Bleckwenn, M. (2002). Concepts and correlations relevant to general anaesthesia. *Journal of Anaesthesia* **89**, 3-16.

Usai, C., Barberis, A., Moccagatta, L. & Marchetti, C. (1999). Pathways of cadmium influx in mammalian neurons. *Journal of Neurochemistry* **72**, 2154-2161.

Uttenweiler, D., Both, M., Zink, W., Sinner, B., Martin, E., Graf, B.M. & Fink, R.H.A. (2003). Hochauflösende Fluoreszenzmikroskopie in Kombination mit mathematischer Modellierung. Erstmaliger Nachweis von subzellulären Anästhetikawirkungen auf Ca^{2+} -Sparks in situ. *Anaesthesist* **52**, 162-168.

Uttenweiler, D., Wojciechowski, R., Makabe, M., Veigel, C. & Fink, R.H.A. (1995). Combined analysis of intracellular calcium with dual excitation fluorescence photometry and imaging. *Optical Engineering* **34**, 2864-2871.

Valicenti, J.F. Jr., Newman, W.H., Bagwell, E.E., Pruett, J.K. & Robie, N.W. (1973). Myocardial contractility during induction and steady-state ketamine anesthesia. *Anesthesia* & *Analgesia* **52**, 190-194.

Van Citters, R.L., Franklin, D.L. & Rushmer, R.F. (1964). Left ventricular dynamics in dogs during anesthesia with alpha-chloralose and sodium pentobarbital. *American Journal of Cardiology* **13**, 349-354.

Vander, AJ., Sherman JH. & Luciano, DS. (1987). *Human physiology. The mechanisms of body function*. New York: McGraw-Hill.

Vernino, S., Amador, M., Luetje, C.W., Patrick, J. & Dani, J.A. (1992). Calcium modulation and high calcium permeability of neuronal nicotinic acetylcholine receptors. *Neuron* **8**, 127-134.

Vernino, S., Rogers, M., Radcliffe, K.A. & Dani, J.A. (1994). Quantitative measurement of calcium flux though muscle and neuronal nicotinic acetylcholine receptors. *Journal of Neuroscience* **14**, 5514-5524.

Vig P.G. & Nath, R. (1991). In vivo effects of cadmium on calmodulin and calmodulin related enzymes in rat brain. *Biochemistry International* **23**, 927-934.

Virtue, R.W., Alanis, J.M., Mori, M., Lafargue, R.T., Vogel, J.H.K. & Metcalf, D.R. (1967). An anesthetic agent: 2-orthochlorophenyl, 2-methylamino cyclohexanone HCl (CI 581). *Anesthesiology* **28**, 823-833.

Vogel, H. (1997). *Gerthsen Physik*. Heidelberg: Springer.

Wachtel, R.E. & Wegrzynowicz, E.S. (1992). Kinetics of nicotinic acetylcholine ion channels in the presence of intravenous anaesthetics and induction agents. *British Journal of Pharmacology* **106**, 623-627.

Wachtel, R.E. (1988). Ketamine decreases the open time of single-channel currents activated by acetylcholine. *Anesthesiology* **68**, 563-570.

Waxham, M.N. (1999). Neurotransmitter receptors. In M.J. Zigmond, F.E. Bloom, J.L. Roberts, S.C. Landis & L.R. Squire (Eds.), *Fundamental Neuroscience* (pp. 235-267). San Diego: Academic Press.

Waxman, K., Shoemaker, W.C. & Lippmann, M. (1980). Cardiovascular effects of anesthetic induction with ketamine. *Anesthesia* & *Analgesia* **59**, 355-358.

Wellhöner, H.-H. (1988). *Allgemeine und systematische Pharmakologie und Toxikologie*. Berlin: Springer.

White, P.F., Ham, J., Way, W.L. & Trevor, A.J. (1980). Pharmacology of the ketamine isomers in surgical patients. *Anesthesiology* **52**, 231-239.

White, P.F., Schüttler, J., Shafer, A., Stanski, D.R., Horai, Y. & Trevor, A.J. (1985). Comparative pharmacology of the ketamine isomers. *British Journal of Pharmacology* **57**, 197-203.

White, P.F., Way, W.L. & Trevor, A.J. (1982). Ketamine – Its pharmacology and therapeutic uses. *Anesthesiology* **56**, 119-136.

Wilson, G.G. & Karlin, A. (1998). The location of the gate in the acetylcholine receptor channel. *Neuron* **20**, 1269-1281.

Wilson, G.G. & Karlin, A. (2000). Acetylcholine receptor channel structure in the resting, open and desensitized states probed with the substituted-cysteine-accessibility method. *Proceedings of the National Academy of Sciences of the USA* **98**, 1241-1248.

Wuytack, F., Raeymaekers, L. & Missiaen, L. (2002). Molecular physiology of the SERCA and SPCA pumps. *Cell Calcium* **32**, 279-305.

Xu, Z-J. & Adams D.J. (1992a). Resting membrane potential and potassium currents in cultured parasympathetic neurons from rat intracardiac ganglia. *Journal of Physiology* **456**, 405-424.

Xu, Z-J. & Adams D.J. (1992b). Voltage-dependent sodium and calcium currents in cultured parasympathetic neurones from rat intracardiac ganglia. *Journal of Physiology* **456**, 425-441.

Xu, Z-J. & Adams D.J. (1993). α-Adrenergic modulation of ionic currents in cultured parasympathetic neurons from rat intracardiac ganglia. *Journal of Neurophysiology* **69**, 1060-1070.

Yamakura, T., Bertaccini, E, Trudell, J.R. & Harris, R.A. (2001). Anesthetics and ion channels: molecular models and sites of action. *Annual Reviews in Pharmacology and Toxicology* **41**, 23-51.

Yamakura, T., Borghese, C. & Harris, A. (2000a). A transmembrane site determines sensitivity of neuronal nicotinic acetylcholine receptors to general anesthetics. *Journal of Biological Chemistry* **275**, 40879-40886.

Yamakura, T., Chavez-Noriega, L.E. & Harris, A. (2000b). Subunit-dependent inhibition of human neuronal nicotinic acetylcholine receptors and other ligand-gated ion channels by dissociative anesthetics ketamine and dizocilpine. *Anesthesiology* **92**, 1144-1153.

Yuan, B.-X., Ardell, J.L., Hopkins, D.A. & Armour, J.A. (1993). Differential cardiac responses induced by nicotine sensitive canine atrial and ventricular neurons. *Cardiovascular Research* **27**, 760-769.

Zeilhofer, H.U., Swandulla, D., Geisslinger, G. & Brune, K. (1992). Differential effects of ketamine enantiomers on NMDA receptor currents in cultured neurons. *European Journal of Pharmacology* **213**, 155-158.

Zhang, G.H., Yamaguchi, M., Kimura, S., Higham, S. & Kraus-Friedmann, N. (1990). Effects of heavy metal on rat liver microsomal Ca^{2+} ATPase and Ca^{2+} sequestering. *Journal of Biological Chemistry* **265**, 2184-2189.

Zsigmond, E.K. (1974). Guest Discussion. *Anesthesia* & *Analgesia* **53**, 931-933.

Zsigmond, E.K., Kothary, S.P., Matsuki, A., Kelsch, R.C. & Martinez, O. (1974). Plasma free norepinephrine and epinephrine concentrations following diazepam-ketamine induction in patients undergoing cardiac surgery. *Clinical Pharmacology and*

Therapeutics **15**, 224-225.

Zwart, R. & Vijverberg, P.M. (1997). Potentiation and inhibition of neuronal nicotinic receptors by atropine: Competitive and noncompetitive effects. *Molecular Pharmacology* **52**, 886-895.

6.1 Own publications

Beker, F., Weber, M., Fink, R.H.A. & Adams, D.J. (2003). Muscarinic and nicotinic ACh receptor activation differentially mobilize Ca^{2+} in rat intracardiac neurons. *Journal of Neurophysiology* **90**, 1956-1964.

Most, P., Remppis, A., Weber, C., Bernotat, J., Ehlermann, P., Pleger, S.T., Kirsch, W., Weber, M., Uttenweiler, D., Smith, G.L., Katus, H.A. & Fink, R.H.A. (2003). The C terminus (amino acids 75-94) and the linker region (amino acids 42-54) of the Ca^{2+} binding protein S100A1 differentially enhance sarcoplasmic Ca^{2+} release in murine skinned skeletal muscle fibers. *Journal of Biological Chemistry* **278**, 26356-26364.

Weber, M., Gaul, S., Beker, F., Fink, R.H.A. & Adams, D.J.. Intravenous anaesthetics inhibit nicotinic receptor-mediated currents and Ca^{2+} transients in rat intracardiac ganglion neurons. *To be submitted.*

Abstract

Weber, M., Fink, R.H.A. & Adams, D.J. (2002). Inhibition of nicotinic receptor mediated currents and Ca^{2+} responses in rat intracardiac neurons by intravenous anaesthetics. *Proc. Aust. Neuroscience Soc* **13**, 161a.

A APPENDIX

A.1 Statistical Analysis

A.1.1 Calibration of the fura-2 signal in the presence of i.v. anaesthetics

Given that the properties of UV-lamps used in a fluorescence microscopes typically change during their life times (typically ~ 400 operating hours), calibrations on the ratiometric imaging set-up in the presence of the anaesthetics were carried out alternately with control calibrations (in the absence of the anaesthetics) to ensure that the experimental conditions with respect to the operating hours of the UV-lamp were comparable.

At first, calibrations in the presence and absence (control #1) of thiopental were done. Calibrations in the presence of either pentobarbital or ketamine were carried out at a later stage (with more operating hours of the UV-lamp) and were compared to a common, second and time matched control condition (control #2).

t-tests (two-tail) *for unpaired samples* were carried out for all the constants in equation 3 (see chapter 2.3), namely K_d, R_{min}, R_{max} and S_{f2}/S_{b2}:

A.1.1.1 Thiopental

Control condition #1 (n = 8): (Ca^{2+}) –EGTA calibration solutions & fura-2

Experimental condition (n = 8): + 25 μM thiopental

t-test for K_d:

T value	0.7522535606	P value	0.4643593662	Degrees of Freedom	14

t-test for R_{min}:

T value	0.9182842612	P value	0.3740200449	Degrees of Freedom	14

t-test for R_{max}:

T value	0.0372479221	P value	0.9708132442	Degrees of Freedom	14

t-test for S_{f2}/S_{b2}:

T value	0.0155576153	P value	0.9878068585	Degrees of Freedom	14

A.1.1.2 Pentobarbital

Control condition #2 (n = 9): (Ca^{2+}) –EGTA calibration solutions & fura-2

Experimental condition (n = 10): + 50 μM pentobarbital

t-test for K_d:

T value -0.5303514830 P value 0.6027277542 Degrees of Freedom 17

t-test for R_{min}:

T value 0.6793582904 P value 0.5060563161 Degrees of Freedom 17

t-test for R_{max}:

T value 0.4796799493 P value 0.6375681690 Degrees of Freedom 17

t-test for S_{f2}/S_{b2}:

T value -0.2673684991 P value 0.7924020947 Degrees of Freedom 17

A.1.1.3 Ketamine

Control condition #2 (n = 9): (Ca^{2+}) –EGTA calibration solutions & fura-2

Experimental condition (n = 11): + 10 μM ketamine

t-test for K_d:

T value -1.4422885561 P value 0.1663958946 Degrees of Freedom 18

t-test for R_{min}:

T value -1.9389820169 P value 0.0683442065 Degrees of Freedom 18

t-test for R_{max}:

T value 2.1748849923 P value 0.0432139035 Degrees of Freedom 18

t-test for S_{f2}/S_{b2}:

T value 1.6113836877 P value 0.1244918372 Degrees of Freedom 18

A.1.2 $[Ca^{2+}]_i$ transients in unclamped, fura-2 loaded neurons

t-tests (two tail) *for paired samples* were carried out for increases in $[Ca^{2+}]_i$ ($\Delta[Ca^{2+}]_i$) using nM values. Control conditions are based on responses obtained in the same cells, but in the absence of the antagonists (i.e. voltage-gated channel blockers or anaesthetics, respectively; see chapter 2.6).

A.1.2.1 ACh-induced responses

t-test for effects of ω-conotoxin GVIA (+ TTX) on ACh-induced $\Delta[Ca^{2+}]_i$:

Control condition: 500 μM Ach & 1 μM atropine in PSS

Experimental condition: + 100 nM ω-conotoxin GVIA & 1 μM TTX

T value 5.6468834522 P value 0.0048435733 Degrees of Freedom 4

n = 5

t-test for effects of thiopental on ACh-induced $\Delta[Ca^{2+}]_i$:

Control condition: 500 μM ACh & 100 nM atropine in PSS

Experimental condition: + 25 μM thiopental

T value 6.4995059381 P value 0.0012870977 Degrees of Freedom 5

n = 6

t-test for effects of pentobarbital on ACh-induced $\Delta[Ca^{2+}]_i$:

Control condition: 500 μM ACh & 100 nM atropine in PSS

Experimental condition: + 50 μM pentobarbital

T value 4.5699118262 P value 0.0025744035 Degrees of Freedom 7

n = 8

t-test #1 for effects of ketamine on ACh-induced $\Delta[Ca^{2+}]_i$ (uncorrected R_{max}; see chapter 3.1.1.2 and 3.2.3):

Control condition: 500 μM ACh & 100 nM atropine in PSS

Experimental condition: + 10 μM ketamine

T value 2.8191590810 P value 0.0303877426 Degrees of Freedom 6

n = 7

t-test #2 for effects of ketamine on ACh-induced $\Delta[Ca^{2+}]_i$ (corrected R_{max}; see chapter 3.1.1.2 and 3.2.3):

Control condition: 500 μM ACh & 100 nM atropine in PSS

Experimental condition: + 10 μM ketamine

T value 2.4933855001 P value 0.0469465722 Degrees of Freedom 6

n = 7

A.1.2.2 Caffeine-induced responses

t-test for effects of thiopental on caffeine-induced $\Delta[Ca^{2+}]_i$:

Control condition: 10 mM caffeine in PSS

Experimental condition: + 25 μM thiopental

T value 0.8724328954 P value 0.4083928772 Degrees of Freedom 8

n = 9

A.1.3 Combined membrane current and $[Ca^{2+}]_i$ recordings in voltage-clamped, fura-2 loaded neurons (perforated-patch)

t-tests (two tail) *for paired samples* were carried out for ACh-induced increases in $[Ca^{2+}]_i$ ($\Delta[Ca^{2+}]_i$, using nM values), as well as for baseline-adjusted, peak current amplitudes (using pA values). Control conditions are based on responses obtained in the same cells, but in the absence of thiopental (see methods, chapter 2.6).

t-test for effects of thiopental on ACh-induced $\Delta[Ca^{2+}]_i$ in cells voltage-clamped at –60 mV:

Control condition:	500 µM ACh & 0.1 or 1 µM atropine in PSS; holding potential: -60 mV
Experimental condition:	+ 25 µM thiopental

T value 4.9234481111 P value 0.0160564992 Degrees of Freedom 3

n = 4

t-test for effects of thiopental on ACh-induced peak current amplitudes in cells voltage-clamped at –60 mV:

Control condition:	500 µM ACh & 0.1 or 1 µM atropine in PSS; holding potential: -60 mV
Experimental condition:	+ 25 µM thiopental

T value -3.2684754177 P value 0.0468308643 Degrees of Freedom 3

n = 4

A.1.4 Membrane currents in voltage-clamped neurons (dialysed -patch)

t-tests (two tail) *for paired samples* were carried out for ACh-induced, baseline-adjusted peak current amplitudes (using pA values) for cells held at holding-potentials from –120 mV to –40 mV. No tests were carried out for 0 or +40 mV holding potential, as hardly any currents can be observed at these potentials due to the reversal potential and rectifying characteristics of the nAChR channel (see chapter 1.4.3). Control conditions are based on responses obtained in the same cells, but in the absence of thiopental. The shown p-values are those prior to Bonferroni-adjustment (see chapter 2.6 and 3.2.1.3).

Control condition:	300 μM ACh & 100 nM atropine in PSS;
	holding potentials: –120, –80, –40, (0, +40) mV
Experimental condition:	+ 25 μM thiopental

n = 11

t-test for effects of thiopental on ACh-induced peak current amplitudes at –120 mV:

T value	-10.7011027017	P value	0.0000008513	Degrees of Freedom	10

t-test for effects of thiopental on ACh-induced peak current amplitudes at –80 mV:

T value	-7.1993132358	P value	0.0000292851	Degrees of Freedom	10

t-test for effects of thiopental on ACh-induced peak current amplitudes at –40 mV:

T value	-8.1718566527	P value	0.0000097701	Degrees of Freedom	10

A.2 Pharmacological data on thiopental, pentobarbital, and ketamine

drug	FW	pKa	% of molecules in the non-dissociated state at pH 7.4	i.v. induction dose (mg/kg)	duration of induction dose (min)	urinary excretion (%)*	plasma protein binding (%)	clearance (ml*min^{-1} *kg^{-1})	vol. distribution (l/kg)	$t_{1/2\beta}$ (h)
thiopental	241.33	7.6[2,5]	~ 39[8]	3-5[7]	5-8[7]	< 1[1,6]	~85 ± 4[1,2,5,6]	3.9 ± 1.2[1,6]	2.3 ± 0.5[1,6]	~12.1[7]
pento-barbital	225.27	8.11[5]	~ 16[8]			20-70[5]	~61[4]	-	~0.6[3]	~30[3,5]
ketamine	237.74	7.5[5]	~ 44[8]	0.1-1.5[7]	10-15[7]	4 ± 3[1]	~12[1,2,5]	15 ± 5[1]	1.8 ± 0.7[1]	~3[7]

Values are expressed as mean (± SD).

*Excretion of *unchanged* drug

[1]Benet et al. (1996); [2]Büch & Büch (2001); [3]Fichtl (2001); [4]Franks & Lieb (1994), based on Ehrnebo & Odar-Cederlöf (1977); [5]Wellhöner (1988); [6]Thummel & Shen (2001); [7]Evers & Crowder (2001); [8]Calculation of pKa values is based on equation 5 (see chapter 4.4.2).

ACKNOWLEDGEMENTS

I am greatly indebted to a number of people who have supported me in many ways throughout my PhD project:

First of all, I would like to thank *Prof. Dr. Rainer H.A. Fink* from the University of Heidelberg, my PhD supervisor for inviting me to the lab. You have always been genuinely friendly, very supportive and extremely competent. Thanks also for allowing the atmosphere in your lab being equally relaxed, creative and fun! I'm also greatly indebted to my Australian supervisor from the University of Queensland, *Prof. Dr. David J. Adams* for the very same reasons. No wonder that the two of you are friends! ☺

From the lab in Heidelberg, I would like to say special thanks to *Friederike Beker* for the patience in teaching me the dissection of intracardiac neurons, the excellent advice on ratiometric Ca^{2+} imaging, as well as the persistent and friendly support throughout the project. I'm also very much indebted to *Martin Vogel*, his invaluable "computer wizardry" whenever I needed it, the helpful thoughts on projects and manuscripts, and for being the best office buddy I could have possibly hoped for. A great thanks also goes to *Dr. Dietmar Uttenweiler* for excellent advice, food, and fun! Other people who've always granted me their help whenever I needed it include *Martin Both*, *Simon Gaul*, *Stephan Henze*, *Dr. Wolfgang Kirsch*, *Tobias Ober*, *Jolanthe Schatterny*, *Frederick von Wegner* and last but not least the good soul of the lab: *Cornelia Weber*. (I don't have to mention, that I've enjoyed it a lot to work (and to joke!) with all of you, do I?). Another person that I'm greatly indebted to is *Rainer Förderer* from the workshop of the department: Every peace of equipment that you've built was nothing but excellent!

From the lab in Australia, I'm very thankful to *Dr. Ron C. Hogg*, *Dr. D-M. Liu* and *Dr. "Sandy" Harper* for giving me a first clue about electrophysiology, teaching me the essentials of lab work, for patience and humour! Other very friendly and always helpful people from Brissie include *Kerry Dayas Dr. Mitchell Hansen, Dr. Deanne Hryciw, Dr. Amanda Smith, Mark Stafford* and the people from the *"Prof. Kunzelmann lab"*. I would also like to thank the one and only *Takka Yasuda* for both the scientific as well as personal conversations, for the fun and most of all for the friendship.

I would also like to thank *Prof. Dr. Michael Wink* from the *Graduate Program "Biotechnology - molecular and biochemical basics"* of the DFG, and *Dr. Max Brocker* from the *German National Merrit Foundation* for both financial and superb administrative support and finally, *Prof. Dr. Nils Metzler-Nolte* for his equally superb administrative support.